DEVELOPMENT OF A MICRO AIR VEHICLE FOR METEOROLOGICAL SOUNDINGS

By

ANDREW WALSH

Bachelor of Science in Mechanical Engineering
Oklahoma State University
Stillwater, Oklahoma
2018

Bachelor of Science in Aerospace Engineering
Oklahoma State University
Stillwater, Oklahoma
2018

Submitted to the Faculty of the
Graduate College of the
Oklahoma State University
in partial fulfillment of
the requirements for
the Degree of
Master of Science
December, 2021

DEVELOPMENT OF A MICRO AIR VEHICLE

FOR METEOROLOGICAL SOUNDINGS

Thesis Approved:

Dr. Jamey D. Jacob

Thesis Advisor

Dr. Kurt P. Rouser

Dr. Brian R. Elbing

ACKNOWLEDGMENTS

I would like to thank Dr. Jacob for all of his support during my undergraduate and graduate career at Oklahoma State University. I would also like to thank Ben Loh for all the advice and support he provided throughout the time I was working on my thesis. In addition to Ben, I would also like to thank all the staff and students at USRI who helped with flight testing SPARROW, especially Levi Ross, Marc Hartman, Kyle Hickman, Muwanika Jdiobe, and AJ Burba. Also thank you to my parents Billie and Scott Walsh for supporting me during my time at Oklahoma State University. Finally, I want to extend a special thanks to Caleigh Shaw who helped and supported me throughout the process of obtaining my Master's degree.

Acknowledgments reflect the views of the author and are not endorsed by committee members or Oklahoma State University.

Name: Andrew Walsh

Date of Degree: December, 2021

Title of Study: DEVELOPMENT OF A MICRO AIR VEHICLE FOR METEOROLOGICAL SOUNDINGS

Major Field: Mechanical and Aerospace Engineering

Abstract: To have accurate forecasting models for weather systems, data must be collected on the thermodynamic structure of the Atmospheric Boundary Layer (ABL). Currently this information is gathered using weather balloons, but they are easily influenced by wind and rise through the ABL quickly, providing low vertical resolution. Additionally, the sensors on board a weather balloon are only reusable if they happen to be recovered wherever they land. Other meteorological data collection methods such as aircraft, radar, and mesonet towers are also insufficient due to being fixed in place or requiring extensive preparation time to deploy. Thus, there is a critical need to develop a low cost, easy to manufacture, gliding radiosonde which can take high resolution vertical samples and return to a ground station for reuse. This system has 2 major advantages: it allows for more data to be collected on atmospheric conditions leading to better forecasting, and it cuts down on cost over time due to its reusable nature.

TABLE OF CONTENTS

Chapter Page

Chapter Page

LIST OF TABLES

Table Page

LIST OF FIGURES

Figure Page

Figure Page

Figure Page

CHAPTER I

Introduction

1.1 Motivation

Recently there has been a major push towards collecting more data on the ABL by the meteorological community. Reports state that if there was a system which could collect more information on the ABL by increasing the vertical resolution of atmospheric readings, it would lead to improved weather and climate model predictions[12]. Better prediction of severe weather can not only save lives, but it can also lessen the economic impact of storms. Some reports estimate the United States GDP can vary by as much as $485 billion due to weather[17]. Because of these reasons, a long sought-after piece of the U.S. atmospheric observing systems is the ability to measure vertical profiles of wind, temperature, and moisture in the lower troposphere at high spatial and temporal resolutions. However, this is not easy because the ABL is difficult to accurately model since its properties are highly variable on mesoscale time and space scales making it significantly harder to observe[5].

One major example of the benefit of improved weather predictions are with tornadoes. In recent years, advances in forecasting technology with Doppler radar have increased both the warning time and detection of tornadoes while simultaneously lowering the false alarm rate. However, recently these advances have been leveling off as seen in fig. 1. This is largely due to an increased ability to detect smaller tornadoes as they are happening, but not necessarily predict them. Collecting more atmospheric data would help improve modeling and further improve upon these statistics[7].

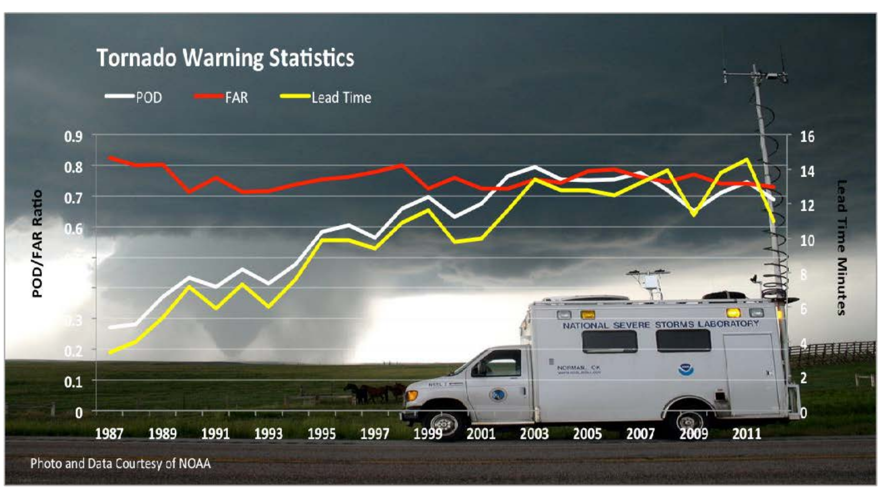

Figure 1: Changes in Tornado warning times

1.2 Background

1.2.1 Traditional Weather Sensing Methods

Across Oklahoma there is a network of 108 towers which form the Oklahoma Mesonet. These 10m tall towers are permanently stationed across the state and track parameters such as temperature, pressure, humidity, wind speed, wind direction, solar radiation, and rain accumulation. This network is integral for collecting data to make weather forecasts, but it is limited to collecting ground level data.

Mesonet Towers

Figure 2: Mesonet tower which collects environmental data every 5 minutes

Radiosonde

Weather balloons carrying radiosondes are used to collect upper atmosphere weather data for forecasting. Each day in the United States 92 sites launch 2 balloons a day at 0 UTC and 1200 UTC to get a snapshot of the atmosphere. If severe weather is to be expected, it is not uncommon for sites to launch at 0600 and 1800 to collect additional data. Each weather balloon sounding can reach altitudes of 22 miles and drift more than 180 miles over the ground. Data from these radiosondes are relayed back to the ground for processing. While it is possible to reuse a radiosonde, their uncontrolled ascent and descent combined with large drifting distances makes recovery logistics difficult. According to the national weather service only 1 in 5 radiosondes are recovered. With a cost of roughly $170 each, this means about 10 million dollars of radiosondes are lost each year in the United States alone. In addition, each unrecovered radiosonde represents more plastic, metal, and batteries being discarded into the environment.

Figure 3: Vaisala RS92 Radiosonde

Figure 4: Weather Balloon used to collect vertical profiles of environmental data

Dropsonde

Dropsondes essentially function the same as radiosondes, but with a reversed CONOPS. Typically, they are deployed from a manned aircraft such as a Lockheed WP-3D Orion. Once deployed, they float down to the ground under parachute in an uncontrolled manner. The major advantage of dropsondes over radiosondes is the ability for a single team to easily deploy them in a grid over areas without easy ground access such as an ocean environment. Data is collected on the dropsonde and sent back to the aircraft with a telemetry radio. It is also much more difficult to maintain a constant vertical velocity with dropsondes than it is with radiosondes attached to a weather balloon.

Figure 5: Vaisala RD41 Dropsonde

Figure 6: Lockheed WP-3D Orion used to deploy dropsondes

1.3 Goals and Objectives

The primary research question is: what is the best reusable system for sampling the atmospheric boundary layer? A major part of this question is evaluating how this data is currently collected and seeing if there is a better way of doing it. Current aircraft are largely deployed from either the ground or from an expensive mothership. Could such a system effectively return to a point on the ground for reuse which in turn would provide a lower cost solution than weather balloons? And could such a system be made safe so that if it failed during operation, it would not injure anyone? Would such a system even be able to collect scientifically accurate data? The primary goal of this research is to answer these questions through the development of the SPARROW vehicle.

Thus, following goals statement was created. Develop a reusable system that can be deployed from a rocket for a rapid atmospheric sampling mission. The data collected by this system must be comparable or better than what a weather balloon radiosonde system can achieve.

From this statement the following list of objectives were made:

- Benchmark specifications for a profiling mission based on current use of weather balloons
- Develop a micro air vehicle for atmospheric profiling
- Evaluate atmospheric sensors integrated into micro air vehicle
- Evaluate micro air vehicle flight

CHAPTER II

Literature Review and Previous Work

2.1 Unmanned Sensing Systems

Using UAS to take atmospheric measurements is not a new idea. There are currently a multitude of vehicles that were either design or modified for weather missions. They each have their strengths, but none of them fully solve the problem outlined above. To achieve the goal of mass adoption, it is important to consider simplicity, ease of use, and reliability of the design.

2.1.1 Small Ground Deployed Systems

MARIA

Figure 7: OSU's MARIA designed to be flown into storms for data collection.

The Oklahoma State University MARIA UAS is an integrated platform designed to collect atmospheric data near storm fronts. MARIA flies outfitted with a 5-hole probe, Tropospheric Airborne Meteorological Data Reporting sensor, hot-wire sensor, and IR camera. Additionally, MARIA has the capability to release multiple dropsondes to sample pressure, temperature, humidity, wind vector, and GPS for collecting vertical information on the ABL. It is a highly capable vehicle, but it requires a pilot to be present and has a service ceiling of 6,000 feet.

Coptersonde

Figure 8: OU's Coptersonde UAS

The OU Coptersonde is currently being developed as a fully autonomous system to aid in developing a 3D mesonet. The goal is to be able to deploy these to mesonet sites and have them autonomously take readings of the ABL. Work is being done to have the system takeoff, land, charge, and avoid manned aircraft without human intervention. If operational, this system would be a huge step toward improved forecasting, but it would still be limited to altitudes of 2000m AGL[5].

Black Swift S0

Figure 9: Black Swift S0 UAS

The Black Swift S0 was designed specifically for atmospheric profiling. It features a nose which acts as a 5-hole probe and has integrated temperature, pressure, and humidity sensors which come already calibrated. It weighs 3.5 lbs. and has a wingspan of 55 inches with the capability of up to 90 minutes of flight. The S0 has demonstrated through missions that a UAS is capable of atmospheric profiling[23].

2.1.2 Small Tube/Air Deployed Systems

Raytheon Coyote

Figure 10: Raytheon's Coyote UAS used by NOAA for collecting data inside hurricanes.

The Raytheon Coyote is a 1m long UAV which is also designed to be deployed from a sonobuoy system. However, it has a weight of 13 lbs. which limits the vehicles that it can be deployed from. Currently the Coyote is deployed from NOAA's WP-3D Orion into hurricanes to collect meteorological data[6].

Prioria Maveric

Figure 11: Prioria Maveric UAS

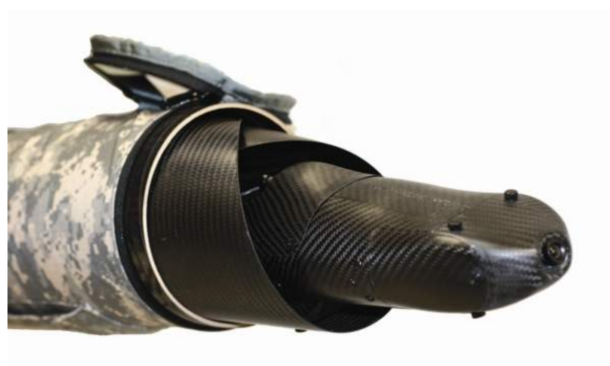

Figure 12: Folded Prioria Maveric UAS

The Prioria Maveric is a tube stowed UAS manufactured in the early 2000's. It was designed to fit in a tube for easy transport by soldiers on the battlefield. The wings on the Maveric are unique in that they are carbon fiber while still being able to roll up. This is accomplished through a complex layup process. Prioria claimed that by having a flexible wing it was more resilient to wind gusts. The Maveric weighs 2.6 lbs. and has a wingspan of 30 inches[11].

Return Glider Radiosonde

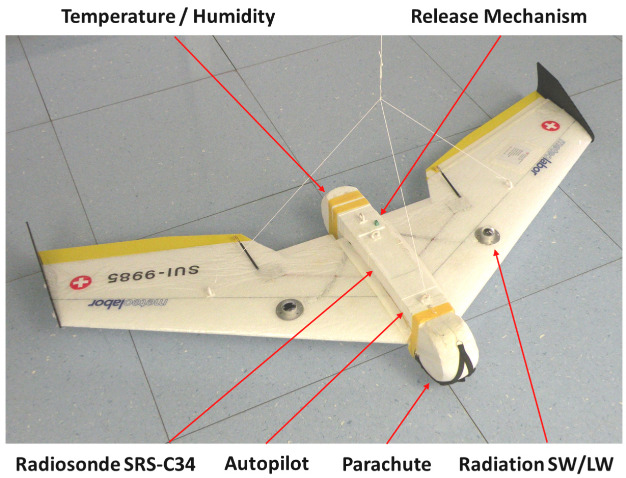

Figure 13: Return Glider Radiosonde used to collect weather data.

The Return Glider Radiosonde (RGR) glider is a foam glider designed to function as a returnable radiosonde. Its mission is to be lifted by balloon and then glide down while collecting atmospheric data. The RGR has completed missions at altitudes up to 24 km and is controlled with a Pixhawk flight computer. It weighs 11 lbs. and has a wingspan of 55 inches.[16]

2.1.3 Micro Ground Deployed Systems

Tornado Rocket

Figure 14: A small Estes rocket used to deliver an atmospheric data collection system into developing tornadoes.

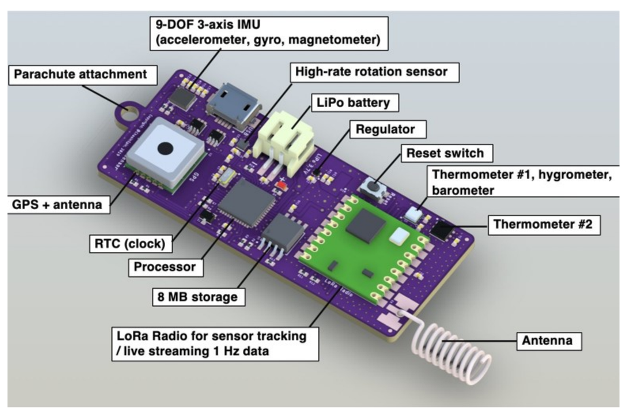

Figure 15: A DAQ designed by the team working with Reed Timmer to collect data from inside tornadoes.

Reed Timmer, a storm chaser, has developed a rocket which can be launched into a tornado to collect atmospheric data. The system consists of a small Estes rocket outfitted with a custom data collection system. This rocket is launched into the "notch" of developing tornadoes where it is hopefully sucked into the system to collect data. On one occasion the tornado rocket was taken up to an altitude of 34,000 feet. The major downside to this system is it is hard to recover. Due to weight constraints only limited telemetry is possible, so once it is in the storm system there is a certain element of luck that it lands where a person will find it.

University of Florida MAV

Figure 16: University of Florida MAV

The University of Florida MAV is designed to be as lightweight and small as possible. It is a powered aircraft which is hand launched from the ground. It features a unique flexible wing which helps passively stabilize it during flight[4]. The MAV weighs 0.7 lbs. and has a wingspan of 0.7 inches with a cruise speed of 33 ft/s[2].

2.1.4 Micro Tube/Air Deployed Systems

NRL CICADA

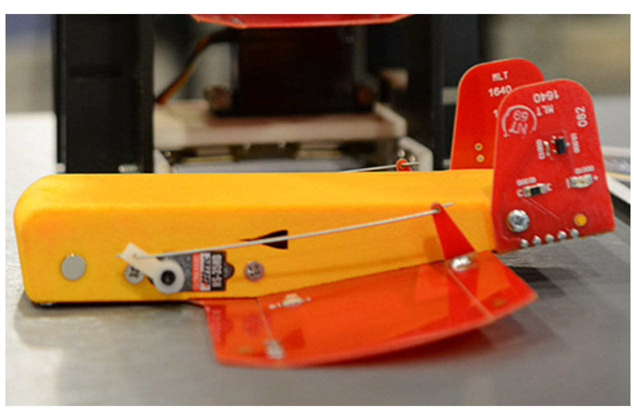

Figure 17: NRL's CICADA designed as a high packing density MAV designed to rapidly seed an area with sensor nodes.

The U.S. NRL has developed a flying sensor package known as the CICADA as seen in fig. 17. This design consists of FR4 PCB aerodynamic surfaces with a 3D printed fuselage. It was designed to be cheap, easily produced, and achieve a high packing density when stowed. These operational requirements come from DARPA's MAV program where the goal was to deploy as many sensor nodes over a distributed area as possible. The NRL chose to make the CICADA be deployable from a sonobuoy canister which significantly limits the form factor of the vehicle[9].

Testing has been done by NASA to evaluate the CICADA's performance as a meteorological sampling device. In their tests, 112 CICADAs were deployed from a series of quadcopters approximately 335m AGL. Of the 112 CICADAs deployed, 60 provided trustworthy telemetry and 12 orbited as expected. The 54% trustworthy telemetry rate can be explained by the limited range of the CICADA's radios, and the low orbiting rate is explained by how CICADAs are deployed. They stack on top of each other in such a way that when stowed half of the CICADAs are always upside down. When deployed, the upside-down vehicles have a harder time recovering into a stable flight. The onboard autopilot also only has options for clockwise or counterclockwise orbits. If a CICADA recovers into the wrong direction of orbit, it must take additional time to correct itself. This recovery process took approximately 150m for the vehicles that did recover. Besides needing a high altitude to recover, another major problem noted with the CICADA was the short battery life. While in idle mode the vehicles battery lasted approximately 2 hours, and in-flight mode the battery lasted approximately 30 minutes[1]. The CICADA is a promising platform, but there is room for improvement.

3D Microflier

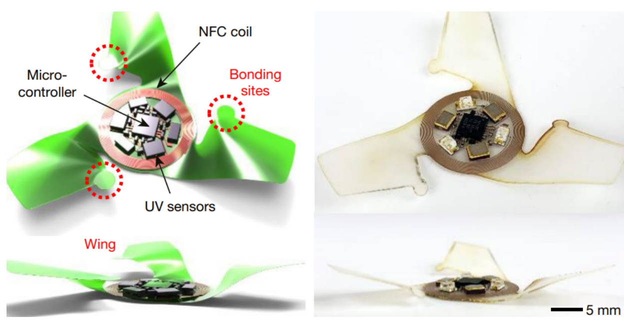

Figure 18: 3D Microflier

The 3D microflier was developed as a collaboration of multiple universities. It is a passive system which spins while falling to slow itself down, but does not feature a way to control it. Each vehicle weighs 0.00044 lbs. and is 2 inches in diameter. It is capable of carrying a payload to detect solar radiation[20].

OSU Glidersonde

Figure 19: OSU's Glidersonde UAS designed to be deployed from a rocket for rapid data collection.

A similar system was also developed at Oklahoma State University in 2016 known as the Glidersonde. The main difference is this vehicle was designed to be deployed from a rocket. It has proven viability in testing but is complex to manufacture as it requires the layup of composite materials[13].

2.2 OSU's Concurrent Research

2.2.1 Wind Estimation

Figure 20: An example of a 5-hole probe integrated onto a Nano Talon

Currently if an aircraft wants to collect wind data there are limited options. One such method is to use a pitot probe to collect airspeed data which can be fused with IMU data from an autopilot to estimate wind speed and direction, but work is still being done to validate the accuracy of these readings for scientific use. Direct sensing can be used in the place of the previously mentioned sensor fusion techniques, but they have their own problems. A TAMDAR-Edge was used on OSU's MARIA aircraft, but it is far from a lightweight system. The sensor alone was approximately 16oz which can be difficult to integrate on small UAS. It is also expensive which makes flights into weather of interest higher risk. It is also possible to use a standalone 5-hole probe which weighs less, but once again they are expensive. To solve this problem OSU's USRI is developing a 3D printable 5-hole probe which is a more cost-effective way of collecting wind speed and direction data. The 3D printed 5-hole probe can be seen above in fig. 20.[14]

2.3 Benchmarking

Table 1: Benchmarking data for aircraft with similar sizing or missions

Platform	GTOW (lb)	Span (in)	Endurance (min)	Payload (lb)	Cruise Velocity (ft/s)
CICADA mk5	0.154	4.5	30		51
MARIA	35	84	420	10	93
Coyote	13	57.9	60	2	101
Glider Sonde	0.55	24			35
RGR	11	55.11		6.61	62
UF Surveillance MAV	0.7	12		0.05	33
BAT	2.6	58	60 (goal)		98
3D Microflier	0.00044	2		0.0004	
Prioria Maveric	2.6	30	45		42

CHAPTER III

Design Methodology

3.1 Mission Outline

Currently there is a gap in weather sensing systems where low cost, powered flight, and rapidly/precisely deployable overlap. This is where SPARROW (Soaring Payload Autonomously Recording Rapidly Originating Weather) will be proposed to fill the gap. SPARROW is designed such that it can be stowed and deployed from the standard 4-inch tube used for mid power rockets. This provides the capability to launch the rocket at a point of interest to any altitude of interest within seconds. At apogee, the SPARROW is deployed and on-board sensors begin to collect in situ data. Having the capability to collect such specific data on demand is valuable to increasing forecasting capabilities. Such a system is necessary because weather rapidly evolves as it moves, and storms can pop up and then disappear before traditional ground based aircraft can be deployed.

The other advantage to the top-down mission approach described above is increased endurance. Since the vehicle is being propelled to altitude by a separate vehicle, SPARROW can spend more time in the air collecting useful data compared to a ground launched vehicle which has to climb to altitude on its own power. This more than doubles the mission time for the vehicle.

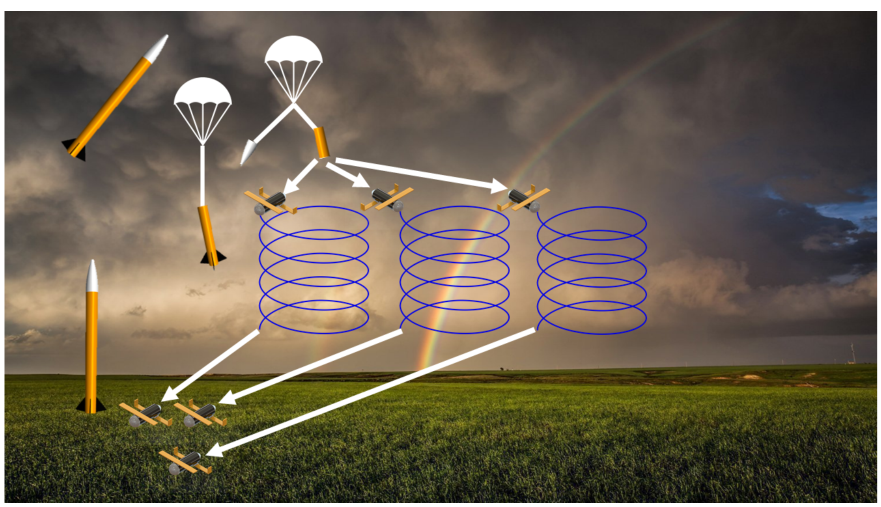

Figure 21: Rocket deployed concept of operations for SPARROW. The system can deploy one vehicle at a time or multiple vehicles at once.

Secondly, there is overlap between SPARROW's capabilities and a radiosonde. As previously discussed, radiosondes are uncontrollable and hard to recover. Thus, there is a possibility SPARROW can act as a radiosonde replacement. Currently it is not legal to release a controlled payload from a weather balloon, however Oklahoma State University's Unmanned Systems Research Institute believes the best chance of overcoming this regulatory hurdle is with a system which weighs less than 0.55 lbs. Previous research has shown vehicles in this category have a significantly lower likelihood of causing harm to an individual if it strikes them [9]. Additionally, vehicles weighing less than 0.55 lbs. fall below the threshold for needing to be registered with the FAA. This makes rapid prototyping and testing easier, and it is believed that eventual regulatory approval will also be easier. Of the previously mentioned vehicles, only the CICADA, 3D microflier, University of Florida MAV, OSU Glidersonde, and Tornado rocket meet these criteria. All of these vehicles suffer from either not being designed to carry a meteorological payload, not being easily recovered or controlled, or low reliability of deployment.

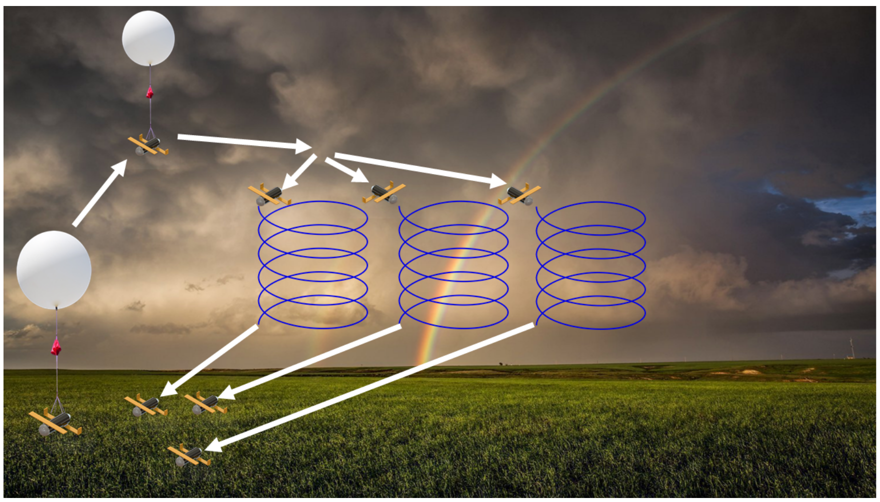

Figure 22: Weather balloon concept of operations for SPARROW. The system can deploy one vehicle at a time or multiple vehicles at once.

Table 2: Comparison of benchmarked vehicles to SPARROW

	3D microflier	Cicada	Glidersonde	UF MAV	Tornado Rocket	SPARROW
Wingspan (in)	2	4.5	24	12	N/A	18
Weight (lb)	0.00044	0.154	0.55	0.7	0.25	0.55
< 0.55 lb	yes	yes	yes	no	no	yes
Powered flight	no	no	no	yes	no	yes
Tube deployable	yes	yes	yes	no	N/A	yes
Reliable flight	no	no	no	yes	no	yes
Weather payload	no	yes	yes	no	yes	yes
Autonomous flight	no	yes	no	yes	no	yes

3.2 Design Requirements

3.2.1 Data Collection Benchmarking

Before beginning the aircraft design process, the capabilities of current radiosondes and dropsondes were benchmarked and put into tables 3 and 4 [15, 25, 26].

Table 3: Operational attributes of current radiosondes and dropsondes

Device	Vertical Speed (ft/s)	Time aloft (min)	Battery life (min)	Weight (oz)
RS92-SGP Radiosonde	15-19	120 (110k feet)	135	10.2
iMet-1-ABxn Radiosonde	15-19	120 (110k feet)	>120	9.17
RD41 Dropsonde	92 (40k ft), 38 (SL)	7 (20k ft)	120	12.3
NRD41 Dropsonde	72 (40k ft), 36 (SL)	14 (40k ft)	NA	5.8

Table 4: Measurement capabilities of current radiosondes and dropsondes

Device	Sample Rate (Hz)	Temperature response time	Humidity response time
RS92-SGP Radiosonde	1	0.5s (1000 hPa)	0.4s (25 C)
iMet-1-ABxn Radiosonde	1	2s (1000 hPa)	2s (25 C)
RD41 Dropsonde	2	0.5s (1000 hPa)	0.3s (20 C)
NRD41 Dropsonde	2	0.5s (1000 hPa)	0.3s (20 C)

In addition to the above benchmarking, it was important to understand what the windspeed is at different altitudes to ensure the vehicle is able to function without excessive drifting. To accomplish this weather balloon sounding data was downloaded for both the UTC0000 and UTC1200 launches at the Norman Oklahoma site for each day of the year in 2020. Each month was then averaged together for each sounding to produce tables 5 and 6 below. The fastest average windspeed for each altitude was then highlighted to be used as a design reference.

Table 5: Average wind speeds in mph for each month in 2020 for the UTC 0000 balloon launches out of the Norman Oklahoma balloon launch site

	0k ft	2.5k ft	5k ft	10k ft	17k ft	24k ft	30k ft	34k ft	38k ft	44k ft	51k feet
Jan	1.0	3.8	11.8	28.4	44.8	56.2	69.3	83.2	88.5	78.4	54.6
Feb	2.6	7.1	9.9	30.9	52.4	67.6	88.1	101.7	99.2	81.6	59.5
March	2.2	6.7	13.2	31.0	56.1	67.7	92.7	103.7	113.7	97.0	66.2
April	1.7	3.8	8.6	26.2	46.0	60.3	81.2	94.4	99.6	86.3	61.8
May	3.8	5.4	3.9	21.9	29.6	32.1	31.3	31.5	36.7	40.0	27.5
June	7.6	14.0	15.7	4.7	9.2	13.2	17.0	22.1	31.1	33.8	15.9
July	6.5	10.9	10.7	7.0	11.9	14.9	15.4	17.2	20.3	18.0	3.5
Aug	5.1	6.8	3.7	12.4	20.2	20.9	25.9	25.8	26.6	25.0	11.0
Sept	2.7	3.6	3.3	2.6	6.9	11.2	23.6	36.4	47.2	42.2	22.3
Oct	2.6	5.9	10.1	22.2	29.5	34.3	40.8	48.5	53.5	55.7	41.2
Nov	3.9	11.0	17.3	25.2	39.5	47.1	61.6	73.8	75.5	73.4	51.8
Dec	1.9	3.6	11.2	21.0	30.4	39.1	49.9	58.5	70.3	66.2	49.6

Table 6: Average wind speeds in mph for each month in 2020 for the UTC 1200 balloon launches out of the Norman Oklahoma balloon launch site

	0k ft	2.5k ft	5k ft	10k ft	17k ft	24k ft	30k ft	34k ft	38k ft	44k ft	51k feet
Jan	1.3	8.8	15.9	25.7	47.8	60.3	73.3	82.8	90.7	74.4	52.3
Feb	1.1	6.4	15.2	28.2	49.0	63.4	83.5	94.4	95.8	80.6	59.1
March	1.4	6.7	21.4	29.4	56.0	71.3	89.9	101.2	110.3	96.6	65.9
April	0.9	6.3	10.8	22.9	47.7	61.7	89.5	99.0	106.9	84.2	57.1
May	1.4	8.1	11.5	16.5	22.2	23.4	31.2	42.2	43.8	41.0	26.5
June	2.7	25.5	19.8	0.5	6.4	9.3	16.9	20.8	31.6	35.8	16.8
July	2.7	20.6	13.2	5.4	5.8	9.4	17.1	22.3	18.7	11.3	1.1
Aug	1.9	17.3	10.3	7.8	16.3	19.3	20.1	24.1	28.1	24.0	10.1
Sept	0.2	6.0	4.0	2.3	4.5	10.4	20.4	32.9	38.7	38.1	17.9
Oct	1.4	6.7	13.7	15.7	27.4	35.8	44.8	49.2	54.3	54.8	43.9
Nov	2.2	17.3	16.7	22.4	31.5	44.2	66.5	74.3	74.6	67.9	50.2
Dec	0.2	8.8	13.7	21.3	33.4	40.2	55.1	62.2	71.2	68.7	46.5

Also worth noting is that the National Weather Service considers 23,000 feet to be the minimum viable altitude for a successful launch[21]. If a weather balloon does not hit this altitude a new one will be launched. For comparison to the above table, the Tempest UAS developed by the University of Colorado Boulder is designed to fly into super cell thunderstorms to collect in situ atmospheric data. During the VORTEX2 campaign, the average windspeed TEMPEST encountered during supercell intercepts was 25 mph, with a max windspeed of 58.6 mph [10].

3.2.2 Sizing Restrictions

The size and shape of the airframe is largely constrained by the need to fit inside of a rocket. SPARROW was designed around being able to fit into a 4-inch rocket airframe due to it being a reasonable tradeoff between motor expense and payload volume for a vehicle to fit in. Depending on exact rocket size and motor configurations, a 4-inch rocket is capable of reaching an apogee anywhere between 1,000 feet and 40,000 feet with off the shelf motors which would satisfy the design threshold set forth for this project. If desired, a 4-inch airframe could also be place on a larger 6 or 8-inch booster as part of a 2-stage rocket to reach even higher altitudes.

The interior diameter of a 4-inch airframe is approximately 3.86 inches which becomes the absolute maximum value a vehicle dimension can be for either width or height. However due to the nature of a rocket airframe being circular, SPARROW needed to be even smaller than this.

3.2.3 Derived Performance Goals

The derived performance parameters for the vehicle are shown in fig. 7. The objective for the operational ceiling is based on the minimum viable altitude for a weather balloon launch, and the threshold altitude is based on the average altitude for the atmospheric boundary layer. Tables 5 and 6 contain the average windspeed at different altitudes in Oklahoma and was used to derive flight speeds for SPARROW. The National Weather Service defines a gust as being at least 10 knots more than the average wind which directly correlated gusts to wind speed. Threshold and objective descent rates were taken from the lowest and highest vertical velocities from the benchmarked dropsondes and radiosondes. The objective and threshold endurances were calculated by dividing the respective ceilings by their descent rates. Weight objective and threshold values were taken from the goal of 0.55 lbs. for regulatory purposes and the heaviest dropsonde benchmark value respectively.

Table 7: Derived vehicle specific objectives

Requirement	Objective	Threshold
Operational ceiling	23,000 ft	5,000 ft
Operate in precipitation	Light (up to 0.1")	Trace (greater than 0")
Operate in high winds	60-80mph	20-40mph
Sufficient descent rate for mission	15 ft/s	38 ft/s
Sufficient endurance for mission	25.5 minutes	2.2 minutes
Weight	8.8 oz	13 oz
Data	TPH + Wind	Temperature and Humidity
Control	Autonomous	Manual
Meteorological Value	High altitude atmospheric profile	ABL profile

Table 8: Wind metrics defined for this project

Wind Category	Wind Strength (mph)
1	0-20
2	20-40
3	40-60
4	60-80

Table 9: Gust metrics defined for this project

Gust Category	Gust Strength (mph)
1	12-32
2	32-52
3	52-72
4	72-92

Table 10: Rain metrics defined for this project

Rain Category	Rain Accumulation (per hour)
1	None (0")
2	Trace (greater than 0")
3	Light (up to 0.1")
4	Moderate (0.1"-0.3")

3.3 System Design Trades

3.3.1 Vehicle Type

Based on airframe sizing limitations and benchmarking, 6 potential aircraft configurations were considered. Multirotor aircraft have been proven useful for vertical profiling at a given location as they do not require runways to take off and can be easily deployed with a single pilot. However, a major challenge for multirotor aircraft, especially small multirotors, is flying in high winds. This made it difficult to justify using one for a high-altitude sampling system. Powered parasails and 3D microfliers also suffer the same issues of being insufficient for high winds. Ultimately it was determined a powered fixed wing would be best for the given mission.

Table 11: Decision matrix showing the selection of the vehicle type

	Multirotor	Powered parasail	Glider	3D Microflier	Powered fixed wing
Wind operation	-1	-1	-1	-1	1
Efficiency of stowing	1	0	1	1	1
Controllability	1	0	1	-1	1
Clean air	-1	1	1	-1	1
Total	-1	0	2	-2	4

3.3.2 Propulsion System Considerations

Initially different types of propulsion systems were considered for the SPARROW. Gas based propulsion was ruled out due to the need to air start the vehicle without human intervention. This left unpowered gliding and electric propellers as the 2 viable options. Multiple glider-based concepts were tested, however due to the lightweight nature of the vehicle there was significant trouble overcoming wind. This left the electric motor powered propeller as the only viable option to use.

Table 12: Decision matrix showing the selection of the propulsion system

	Unpowered	Gas turbojet engine	Gas piston prop	Electric prop
Air start	1	-1	-1	1
Weight	1	-1	-1	0
Size	1	-1	-1	0
Total	3	-3	-3	1

3.3.3 Planform Type

When considering planforms for SPARROW, multiple factors were considered:

1. Efficiency of stowing - An ideal planform not only fits inside the rocket body, but is also able to fold in such a way that it does not compromise aerodynamic efficiency

2. Ease of manufacturing - An ideal planform does not require a complex manufacturing process in order to lower costs and increase repeatability

3. Control surface integration - An ideal planform is able to have control surfaces integrated into the main wing minimizing the need for extra aerodynamic surfaces. Additionally, it is ideal to have the control surfaces situated in such a way that only 2 are needed to minimize servo weight

4. Ability to have aft motor - An ideal planform does not require control surfaces to be directly at the aft of the vehicle which would interfere with motor placement

5. Ability to have aft neutral point - An ideal planform keeps the neutral point as far aft as possible to allow the vehicle to be compact

6 planforms were selected as viable candidates and were evaluated based on the above criteria:

1. Roll up delta wing
2. Fold out delta wing
3. Fixed delta wing
4. Conventional with hinge
5. Tandem with hinge
6. Canard with hinge

Table 13: Decision matrix showing the selection of the vehicle planform

	Roll up DW	Fold out DW	Fixed DW	Conventional	Tandem	Canard
Efficiency of stowing	1	1	1	0	1	0
Ease of manufacturing	-1	-1	1	1	1	1
Control surface integration	0	0	0	0	1	0
Ability to have aft motor	1	1	1	-1	1	1
Ability to have aft neutral point	1	1	1	0	1	1
Total	2	2	4	0	5	3

The roll up delta wing has the major advantage of being a simple design in that there are no moving components. However, it suffers from requiring a complex layup process to manufacture. It also does not allow for control surfaces to be directly implemented on the wing requiring additional aerodynamic surfaces on the aft end of the aircraft. This is problematic because the motor has to be mounted in the rear of the aircraft with the sensors at the front in order to ensure clean air over the sensors. Additionally with a rear mounted motor the delta wing and control surfaces would not receive the same aerodynamic benefit from having propeller air being blown directly on them that similar vehicles with this configuration get such as the University of Florida MAV. Finally, due to the planform being highly cambered there is reduced payload volume available compared to other configurations for aircraft of this size.

The fold out delta wing would be a similar planform to the roll up delta wing, but would involve some hinge mechanism to spring out a fabric wing. Aside from being easier to manufacture than a roll out wing, it suffers from all of the same downsides.

The fixed delta wing would be a configuration similar to the NRL CICADA. The major advantage is there are no moving components, but due to the restriction of needing to fit in a 4-inch tube, aerodynamics efficiency is greatly affected.

The conventional, tandem, and canard configurations were all fairly similar, but ultimately the tandem configuration was chosen as it offers a compromise between the advantages of the conventional and canard configurations. While a tandem wing isn't as efficient aerodynamically, its small footprint while stowed makes it ideal for a tube deployed system.

CHAPTER IV

Design

4.1 Preliminary Designs

SPARROW MkI Demonstrator

SPARROW was the first vehicle at the OSU USRI lab to be flown using the mRo Control Zero autopilot. In order to check the performance of the autopilot and verify the general avionics setup, the SPARROW MkI was created as a low-cost demonstration vehicle. The wingspan of the SPARROW MkI was approximately 30in and had a vtail which had elevons that were the vehicles only control surfaces. Two vehicles were manufactured, and flight tests took place at the OSU Unmanned Airfield. A DJI M600 outfitted with a dropping mechanism was used to lift the vehicle up to 1500 feet to be dropped. At an altitude of approximately 100 feet, it was noted that the downwash from the M600 had folded the wing in half at the root. A repair was attempted with popsicle sticks as reinforcement, but similar results were once again noted. The avionics were moved over to the second vehicle and similar results occurred. It was apparent that the while the MkI performed well as a hand launched glider, it was not able to handle the highly turbulent environment created by the M600.

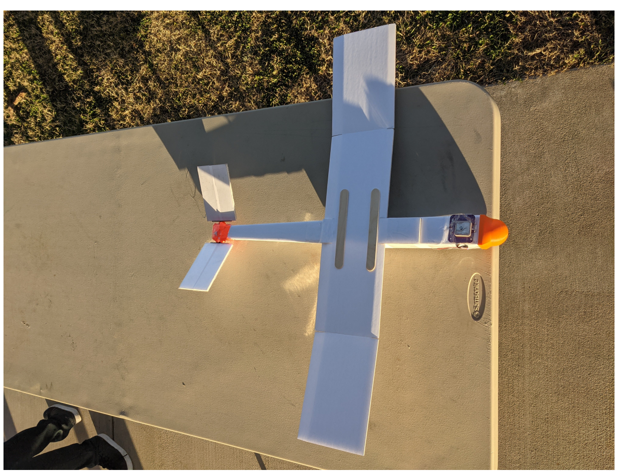

Figure 23: Top view of SPARROW MkI Demonstrator

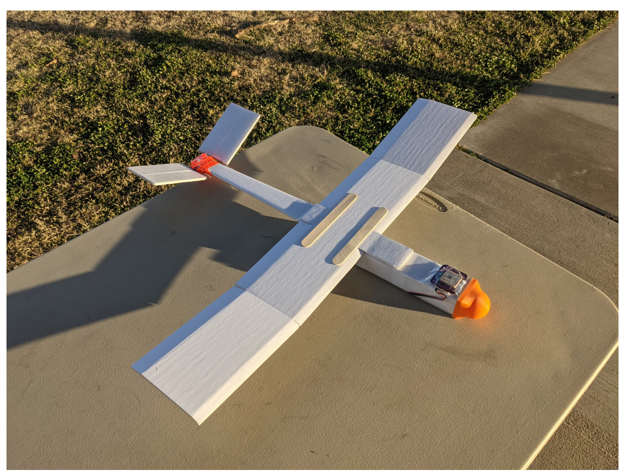

Figure 24: Side view of SPARROW MkI Demonstrator

Figure 25: SPARROW MkI Demonstrator before drop test

SPARROW MkII Demonstrator

The SPARROW MkII Demonstrator was an attempt at implementing lessons learned from the MkI vehicle. Mainly it simplified the design by going with a more traditional aircraft configuration consisting of a single elevator for pitch control and ailerons for roll control. It was powered by an Emax 1807 brushless motor driving a GF6040 prop. This flight test was done by hand launching the vehicle and a 30 second flight was achieved before the vehicle was forced to land. On this day there were 15 MPH winds which made controlling the vehicle difficult. Nonetheless it showed that the avionics were configured correctly and highlighted the need for a faster flight speed to handle windy conditions.

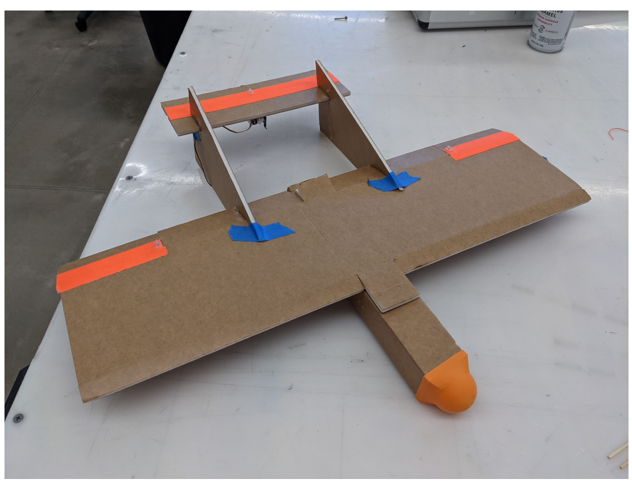

Figure 26: Side view of SPARROW MkII Demonstrator

SPARROW MkIII Prototype

SPARROW MkIII was the first iteration of the vehicle designed with the proposed mission in mind. It features a wing made from G-10/FR4 fiberglass with one copper clad side. The original intention for this is to allow sensors and autopilots to be directly integrated onto the body of the vehicle. However, this was quickly determined to be outside of the scope of this project. The fiberglass wing was also significantly too heavy while not providing enough stiffness. The body of MkIII was made using 3d printing. Figs. 27 and 28 show the progression of fuselage designs. The white fuselage was a boxy proof on concept to gain familiarity with 3d printing, and the final design tested was the orange on top which was optimized for weight reduction and length while still fitting on the bed of a Prusa Mk3s. The Mk3 design underwent a flight test by being dropped from 1500 feet using a DJI M600. As seen in fig. 30, the flight test showed some promise as it was able to achieve positive pitch, but it could not pull out before hitting the ground. As seen from the graph, the pitch angle was largely oscillatory due to the lack of rigidity in the wings. In the flight configuration tested with MkIII, the vehicle weighed approximately 0.8 lbs. which was over the requirement of 0.55lbs. The vehicle also needed lead weight as ballast in the nose to move the CG forward of the neutral point. Overall, even though the vehicle wasn't successful in flight, it provided some valuable lessons learned.

Figure 27: Top view of SPARROW MkIII fuselage design iterations from earliest (bottom) to newest (top)

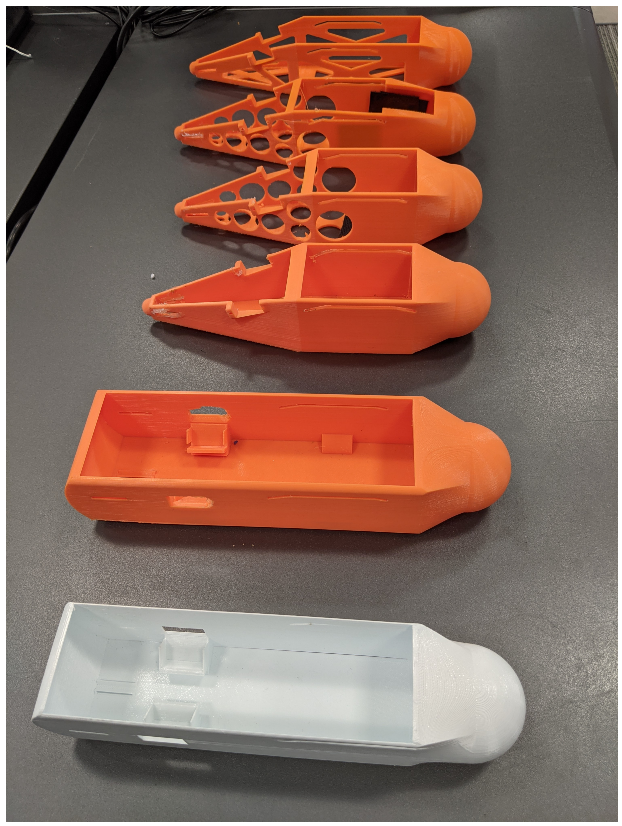

Figure 28: Side view of SPARROW MkIII fuselage design iterations from earliest (bottom) to newest (top)

Figure 29: Side view of the SPARROW MkIII

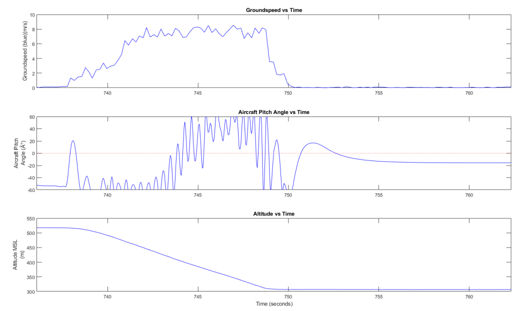

Figure 30: SPARROW MkIII Flight Test

SPARROW MkIV Prototype

SPARROW MkIV was designed in an attempt to improve on the MkIII design. It minimized the use of 3d printing in an attempt to reduce weight. The fuselage and tail were made from Hobby Lobby foamboard. Because there was no restriction on fuselage size due to 3d printing, it was able to be lengthened reducing the need for ballast weight. The tail was also moved further back in attempt to gain extra control authority. It was flight tested in the same manner as MkIII and it appeared to pull out briefly before nose diving. Upon investigation, it is believed the pushrod disconnected from the control surface mid-flight. Unfortunately, due to a failsafe, the vehicle disarmed itself while the M600 was lifting the vehicle up so no flight data was recorded.

Figure 31: Top view of SPARROW MkIV

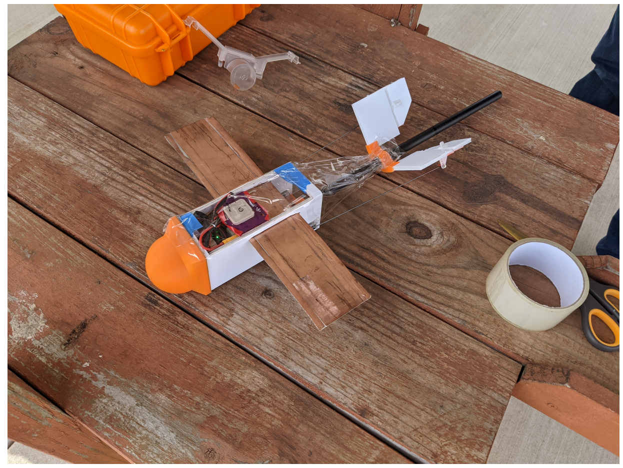

Figure 32: Side view of SPARROW MkIV

SPARROW MkV Demonstrator

The SPARROW MkV demonstrator is the culmination of work done from the Oklahoma State Argonia Cup senior design from the years of 2017 - 2021. The vehicle shown in figs. 33 & 34 was the entry for the 2021 Argonia Cup and was deployed from the rocket shown in fig. 35. This vehicle won the Argonia Cup by autonomously navigating back to a point on the ground after being deployed at 11,000 feet AGL. It is a glider which featured folding main wings with ailerons and a fixed tail with an elevator. There were no vertical control surfaces on board. The MkV demonstrator used the same avionics hardware as the final version of the SPARROW which proved it would be able to withstand the acceleration and vibrations of rocket launches.

Figure 33: Top view of rocket deployed MAV for Argonia Cup

Figure 34: Side view of rocket deployed MAV for Argonia Cup

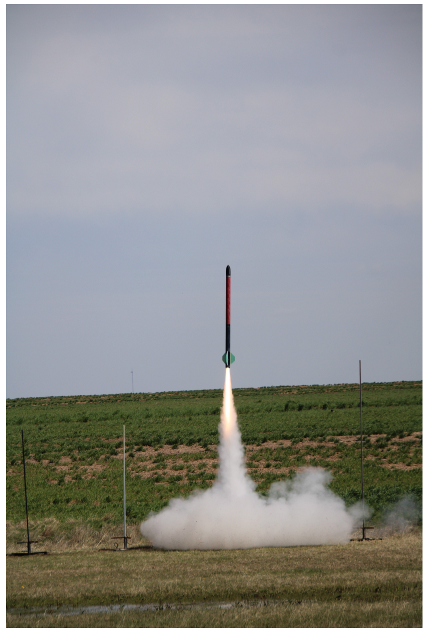

Figure 35: Rocket carrying the SPARROW MkV Demonstrator at the Argonia Cup

SPARROW MkVI Prototype

The SPARROW MkVI prototype was designed using lessons learned from all previous SPARROW revisions. The main goal of this iteration was to keep the design as simple as possible in order to produce a working vehicle. It used Flite Test foamboard as the main airframe material to reduce weight as much as possible. The wings were manufactured with bamboo skewer reinforced foamboard in the shape of a KFM airfoil. This was selected as it provided a higher operational angle of attack than a simple flat plate airfoil while also being able to take more loading. During testing the vehicle experience some failed hand launches and one instance where a motor fell off mid-flight at 60 feet altitude. Even with these crashes the wings remained unbroken as seen in fig 37. 3D printed components were only used on complex geometries such as the nose and motor mount in order to minimize weight. During drop testing the SPARROW MkVI demonstrated multiple successful flights in winds up to 30 mph. With rigidly mounted wings SPARROW Mk VI weighed less 0.5 lbs. which showed it was possible to have a vehicle at this scale fly successfully.

Figure 36: SPARROW MkVI during flight

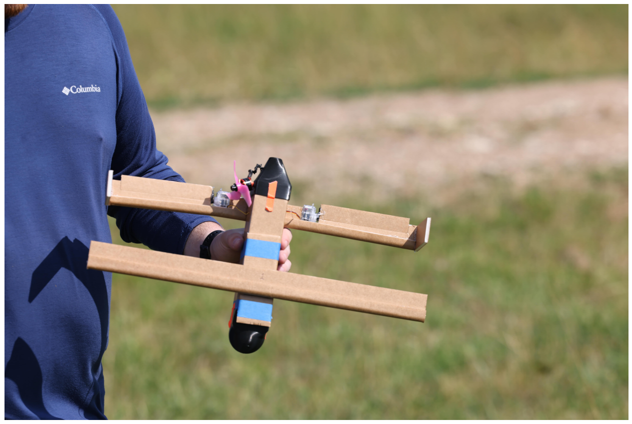

Figure 37: SPARROW MkVI after motor became detached in flight

4.2 SPARROW MkVII

SPARROW MkVII is the final iteration of the SPARROW line. It is a tandem wing aircraft designed to have folding wings allowing for tube deployment. The design process for SPARROW MkVII is outlined in the sections below.

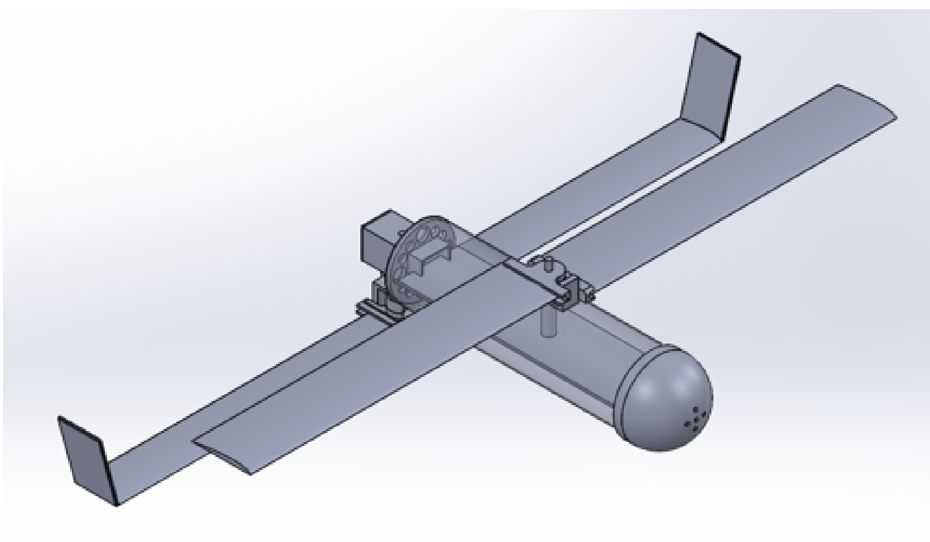

Figure 38: SPARROW MkVII rendering

4.2.1 Aerodynamics

Assumptions

Unless otherwise noted, the following assumptions were used in all calculations

1. The aircraft is in steady, level, unaccelerated flight
2. Both wings were assumed rectangular
3. Both wings were assumed to have aerodynamic centers at 25% chord

4. Wing interaction effects were neglected for the neutral point calculation
5. Aerodynamic properties of each wing were calculated independently for each wing neglecting interactions
6. Flight performance was evaluated at 5,000 feet as it is the minimum altitude required for a profiling mission
7. The effect of low temperatures at high altitude on the battery discharge was neglected

Airfoil Selection

In order to select the airfoil for SPARROW, a series of airfoils were evaluated at expected Reynolds numbers for different desired characteristics. Based on benchmarking of similar micro air vehicles, an estimated cruise Reynolds number of 40,000 was used for initial analysis. With SPARROW being designed as a vehicle which is deployed at altitude for meteorological data collection, a high $\frac{C_L^{3/2}}{C_D}$ was desired along with minimizing wing thickness to reduce vehicle weight.

It was determined a flight speed of $45\frac{ft}{s}$ would be sufficient to meet the threshold objective defined earlier. This value combined with benchmarked data and a vehicle weight of 0.55 lbs. was plugged into eqn. 4.2.1 below to get a C_L of 0.84 is required for SLUF (steady level unaccelerated flight).

$$L = \frac{1}{2}\rho V^s S C_L \tag{4.2.1}$$

Based on the above criteria, a search was performed on airfoiltools.com to find airfoils for evaluation. Five different airfoils were selected and were further evaluated using XFLR5 which is a panel method solver[27]. A sixth airfoil option was also found which is simply a 1.3% thickness 5% camber circular arc airfoil[24]. The resulting graphs can be seen in figs. 39, 40, and 41.

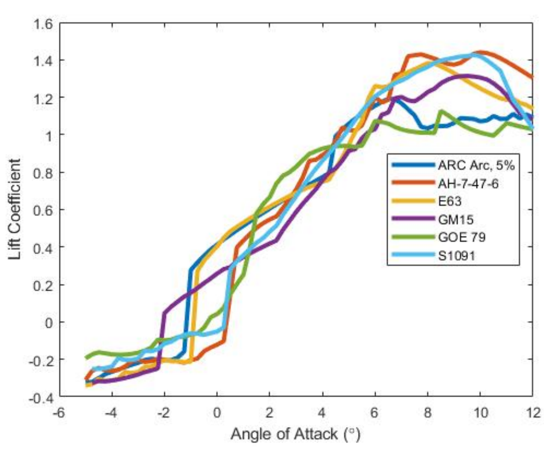

Figure 39: Graph of coefficient of lift vs angle of attack for evaluated airfoils

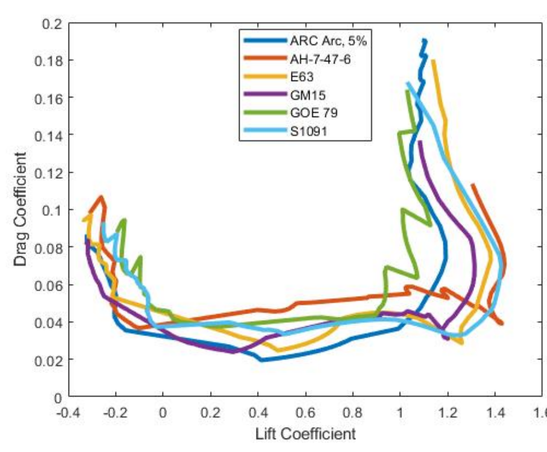

Figure 40: Graph of coefficient of drag vs lift coefficient for evaluated airfoils

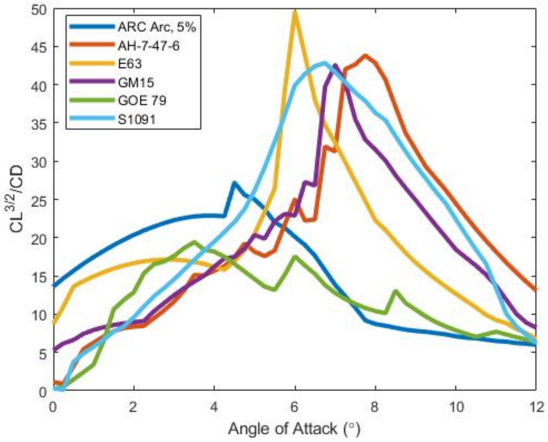

Figure 41: Graph of airfoil $Cl^{3/2}/Cd$ for evaluated airfoils

From the above graphs, it was noted that the expected airfoil performance varies non-linearly with small changes in airfoil geometry. The similarities of airfoil geometries can be seen below in fig. 42. Based on these results, it was concluded that the 5% arc airfoil would be best for SPARROW as it would be easier to reliably manufacture for repeatable results.

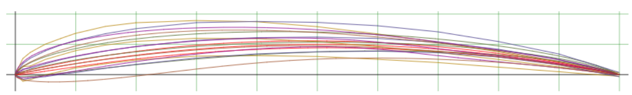

Figure 42: Graphic showing all evaluated airfoils overlaid onto each other

To check the accuracy of the XFLR5 results, the data for the arc airfoil was compared against wind tunnel data of the same airfoil[24]. As seen in figs. 43 and 44 below the 2D data showed good agreement over the angle of attack range which SPARROW is expected to fly in from 0 to 9.

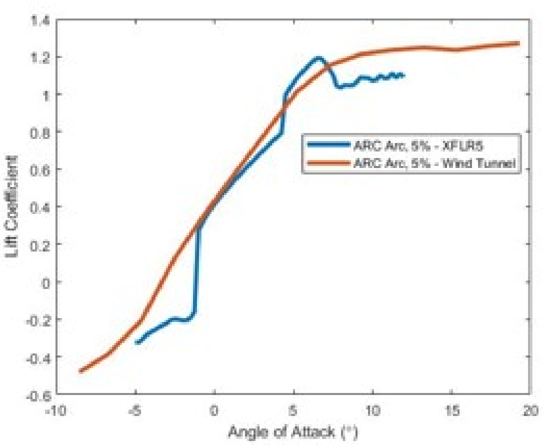

Figure 43: Graph of coefficient of lift vs angle of attack for evaluated airfoils

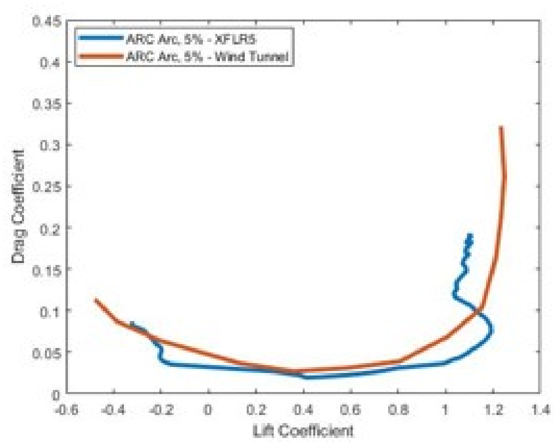

Figure 44: Graph of coefficient of drag vs lift coefficient for evaluated airfoils

Wing Sizing

The wing sizing was based on a set of constrains for the forward and aft wing. First the aft wing was considered. It needed to be located as far back as possible to allow for a further aft CG location. Additionally, the aft wing needed to have vertical stabilizers located on the ends of the wing. This meant that the wing would ideally be just long enough to extend past the nose of the aircraft when in the folded configuration. To allow this to be possible, one side of the aft wing is slightly longer than the other. Next the forward wing was considered. It was placed far enough forward that a static margin of 0.15 can be achieved.

Based on the above constraints, forward and aft wing sizing was iterated to achieve a cruise speed, endurance, and sink rate sufficient for the required performance. The image below shows 3 SPARROW vehicles with their wings folded up and stowed in a tube.

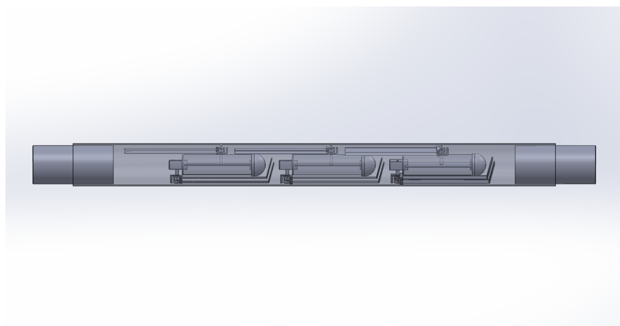

Figure 45: 3 SPARROW vehicles stowed in a common 4-inch diameter tube that is 48 inches long. Standard size tube couplers are included in image for reference.

The wings for SPARROW were then modeled in XFLR5 to evaluate 3D aerodynamic performance. A viscous model was used in the simulations for more accuracy. A picture of the wing model can be seen below in fig. 46 with the resulting L/D graph shown below. The calculated XFLR5 L/D value closely matches the value calculated using eqn. 4.2.2 with the fuselage contribution to CD0 neglected.

$$L/D = \frac{1}{2\sqrt{KC_{D0}}} \tag{4.2.2}$$

Table 14: Comparison of values between calculated L/D and XFLR prediction of L/D

	Calculated	XFLR5	Difference
L/D	11.6	11.9	2.6%

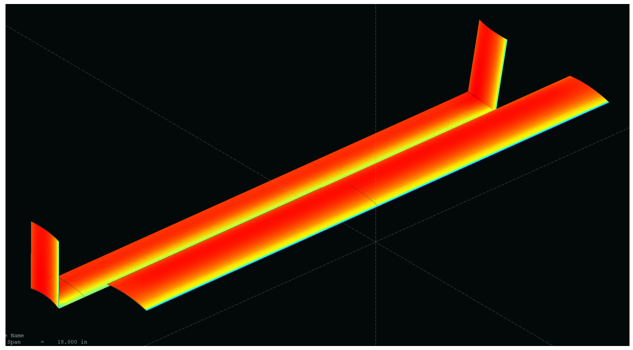

Figure 46: SPARROW wings modeled in XFLR5 for analysis

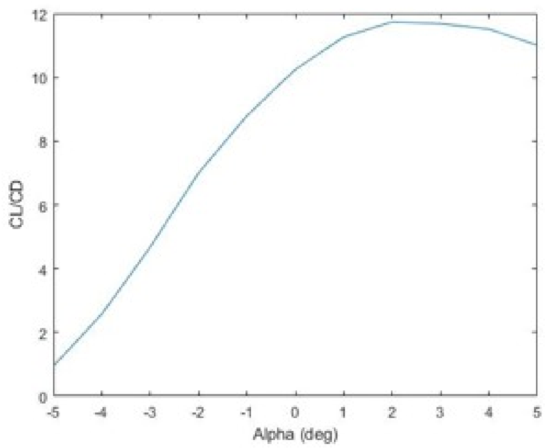

Figure 47: L/D output from XFLR5 analysis of SPARROW wings

Drag Buildup

A simple drag buildup was done using the flat plate estimation method described by Raymer[19]. This involves calculating a skin friction drag coefficient C_f and a component form factor FF which estimates the pressure drag due to viscous separation for each component. Then interference effects are accounted for using a term Q. The total drag calculated for each component is a function of each component's wetted area. The total aircraft C_{D_0} equation is defined as eqn. 4.2.3

$$C_{D_{0_{subsonic}}} = \frac{\sum C_{f_c} FF_c Q_c S_{wet_c}}{S_{ref}} \tag{4.2.3}$$

To calculate the C_f, there are two equations used. Eqn. 4.2.4 applies to laminar flow over the surface while eqn. 4.2.5 applies to turbulent flow over the surface. Typically, each of these are multiplied by a percent of chord in each regime and added together for a total value.

$$C_{f_{Laminar}} = \frac{1.328}{\sqrt{R}} \tag{4.2.4}$$

$$C_{f_{Turbulent}} = \frac{0.455}{log_{10}R^{2.58}(1 + 0.144M^2)^{0.65}} \tag{4.2.5}$$

The form factor values are calculated using eqns. 4.2.6 for the wings and 4.2.7 for the fuselage. For these terms, $\frac{x}{c}_m$ is the chordwise location of the airfoil maximum thickness point and Λ_m is the sweep of the max thickness line. For eqn. 4.2.7, f is defined by eqn. 4.2.8

$$FF_{wing} = 1 + \frac{0.6}{(\frac{x}{c})_m} * (\frac{t}{c}) + 100(\frac{t}{c})^4(1.34M^{0.18}(cos\Lambda_m)^{0.28}) \tag{4.2.6}$$

$$FF_{fuselage} = 0.9 + \frac{5}{f^{1.5}} + \frac{f}{400} \tag{4.2.7}$$

$$f = \frac{l}{d} \tag{4.2.8}$$

Benchmarked Q values which were used in the calculation can be seen below.

Table 15: Typical Q values used in drag buildup

Aircraft Component	Q Value
Fuselage	1
High Wing	1
Low Wing	1.2
Vertical Tail	1.03

An excel spreadsheet was created based on these equations and was used to find the C_{D_0} of SPARROW. This spreadsheet can be seen below in fig. 48 and the resulting total drag graph was generated as seen in fig. 49. A breakdown of individual C_{D_0} values is below in table 16

Atmospheric Properties

Cruise Alt. (ft)	5,000	ft				
M	0.010					
S	0.4	ft^2				
V	10.87	fps				
T	41.20	F				
p	1768.54	psf				
ρ	0.066135672	lbm/ft^3	0.002053903	slugs/ft^3	Color Coding	
q	0.121341397	lbf/ft^2				indicates input
μ	0.0000107	lbm/(f-s)				indicates outpu
ν	0.000161789	ft^2/s				

Aircraft Component	Wetted Area S_{WET}	Mean Chord	t/c or l/d	Mean Re	% Laminar	% Turbulent	C_f	FF	Q	C_{Do}	
Fuselage	0.40906154	0.625	3.8	41,992	10	90	0.008570	1.58448576	1	0.01388697	
Wing 1	0.49	0.146	0.029	9,809	40	60	0.012427	0.60532819	1	0.00921532	
Wing 2	0.31	0.104	0.04	6,987	40	60	0.013915	0.61315766	1.2	0.0079347	
Vertical Stabs	0.087	0.104	0.04	6,987	40	60	0.013915	0.61315766	1.03	0.00191137	
Total	1.29606154									0.03294836	**Equivalent C_{Do} Total (Friction Drag Only)**
									D	**0.0016**	**lbs**

Figure 48: Drag buildup based on flat plate approximation for SPARROW

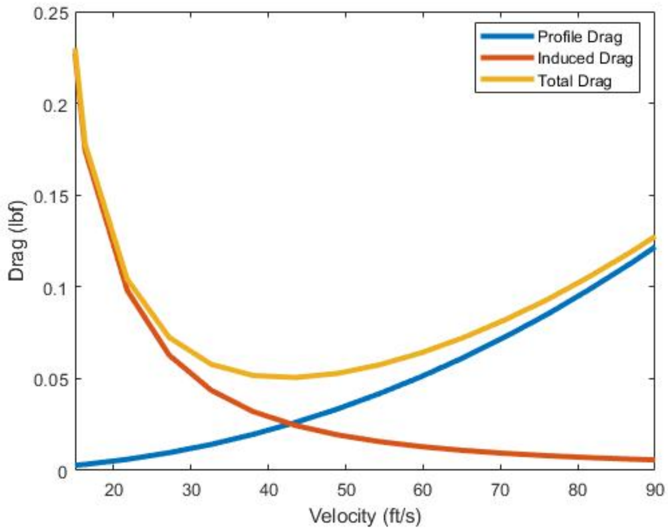

Figure 49: Total drag buildup based on induced and profile drag approximations for flight at 5,000 feet

Table 16: Breakdown of CD0 values based on component

Component	CD0
Fuselage	0.014
Forward Wing	0.012
Rear Wing	0.01
Vertical Stabilizers	0.0025
Total	0.039

Performance

The thrust and power required charts for SPARROW at different altitudes are shown below in figs. 50 and 51. These were generated using a drag buildup method combined with an eCalc approximation of 100% throttle thrust values for different altitudes. Using these charts, a max rate of climb value was able to be derived using eqn. 4.2.9.

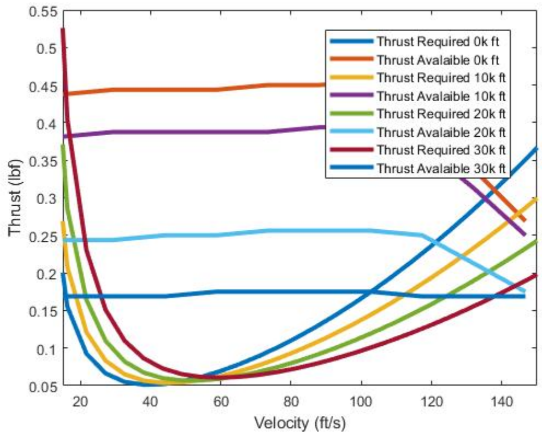

Figure 50: Graph showing thrust available and thrust required for SPARROW from 0k feet to 30k feet

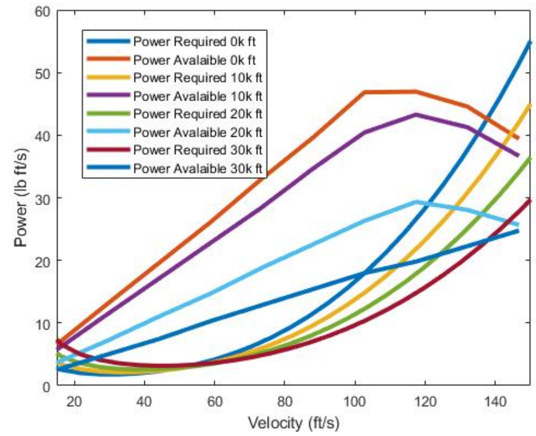

Figure 51: Graph showing power available and power required for SPARROW from 0k feet to 30k feet

$$R/C = \frac{Power_{Available} - Power_{Required}}{W} \tag{4.2.9}$$

It was assumed that SPARROW would fly at approximately 60% throttle, and based on power draw from the thrust stand testing and the W*h of the 850mAh liPo, a steady level endurance time was able to be calculates using eqn. 4.2.10.

$$E = \frac{Wh}{W} \tag{4.2.10}$$

The unpowered sink rate was approximated using a MatLAB code based on eqns. 4.2.11 and 4.2.12[3].

$$Tan(\theta) = \frac{1}{L/D_{max}} \tag{4.2.11}$$

$$V_{Sink} = \sqrt{\frac{2cos(\theta)W}{C_L S\rho}} \tag{4.2.12}$$

Table 17: SPARROW's estimated performance

Parameter	Value
Weight	0.55 lb
Aspect Ratio (front, rear)	11.6, 14.2
Wing Area (front, rear)	32.4 in^2, 21.25 in^2
Wing Span (front, rear)	18.5 in, 17 in
Vehicle L/D max	11.9
Cruise Velocity	45 ft/s
Stall Velocity	36 ft/s
Max Velocity	125 ft/s
Unpowered sink rate	4 ft/s
R/C max	38 ft/s
Endurance (60% throttle)	11.3 min

4.2.2 Fuselage Sizing

The goal of SPARROW is to be as compact as possible in order to maximize the number that can be fit into a tube. However, the fuselage still needed to be long enough for the wings to be mounted a sufficient length apart to sustain stable flight and minimize drag. Additionally, the fuselage needed to be a big enough diameter to fit all the avionics and provide enough spacing so that the meteorological sensors can be isolated from internal heat produced by the flight controller.

First eqn. 4.2.13 was plotted as a function of eqn. 4.2.14 from the drag buildup as shown in fig. 52. Based on this chart and iterations with the above constraints an ideal fuselage aspect ratio of 3.8 was selected. This resulted in a diameter of 2.5 in and a fuselage length of 9.5in.

$$FF_{fuselage} = 0.9 + \frac{5}{f^{1.5}} + \frac{f}{400} \tag{4.2.13}$$

$$f = \frac{l}{d} \tag{4.2.14}$$

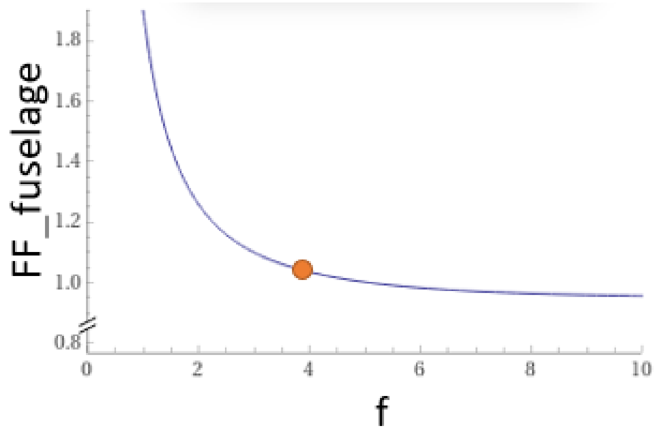

Figure 52: FF˙fuselage as a function of f

4.2.3 Stability

Static Margin

Static margin was calculated using a weighted average of wing location based on wing span. The rear wing was placed as far back on SPARROW as possible to give the largest range of CG locations possible. Once a desired CG location was established, the front wing was placed such that a static margin of 0.15 could be achieved using eqn. 4.2.15 below[18].

$$X_{NP} = \frac{X_{AC_{wing1}} C_{L_{\alpha_{wing1}}} S_{wing1} + X_{AC_{wing2}} C_{L_{\alpha_{wing2}}} S_{wing2}}{C_{L_{\alpha_{wing1}}} S_{wing1} C_{L_{\alpha_{wing2}}} S_{wing2}} \tag{4.2.15}$$

Stabilizer Sizing

The vertical stabilizers were sized based on general benchmarking guidelines outlined in Raymer's book[19]. SPARROW's mission profile most closely mimics that of a sailplane, so a vertical tail volume of 0.02 was chosen. Based on this, eqn. 4.2.16 was used to back out a stabilizer height of 2.5 inches for each of SPARROW's vertical stabilizers. The final sizing used in SPARROW MkVII is 1.25"x2.5" per stabilizer.

	Typical Values	
	Horizontal c_{HT}	Vertical c_{VT}
Sailplane	0.50	0.02
Homebuilt	0.50	0.04
General aviation—single engine	0.70	0.04
General aviation—twin engine	0.80	0.07
Agricultural	0.50	0.04
Twin turboprop	0.90	0.08
Flying boat	0.70	0.06
Jet trainer	0.70	0.06
Jet fighter	0.40	0.07–0.12*
Military cargo/bomber	1.00	0.08
Jet transport	1.00	0.09

*Long fuselage with high wing loading needs larger value.

Figure 53: Typical vertical tail volume chart[19]

$$V_v = \frac{L_v S_v}{S_{wing1} b_{wing1}} \tag{4.2.16}$$

Control Surface Sizing

Control surfaces sizing was also based on benchmarking data. Due to the short chord length, it was desired to have the elevon be as short as possible. Thus, an aileron span to wing span ratio of 0.6 was selected which resulted in an aileron chord to wing chord ratio of 0.15. Eqns. 4.2.17 and 4.2.18 were then used to get the elevon sizing shown below. It wasn't clear if the aileron sizing guidelines would apply the same to elevons, but through flight testing these values were shown to be sufficient. The final sizing used in SPARROW MkVII is 0.2"x6" per elevon.

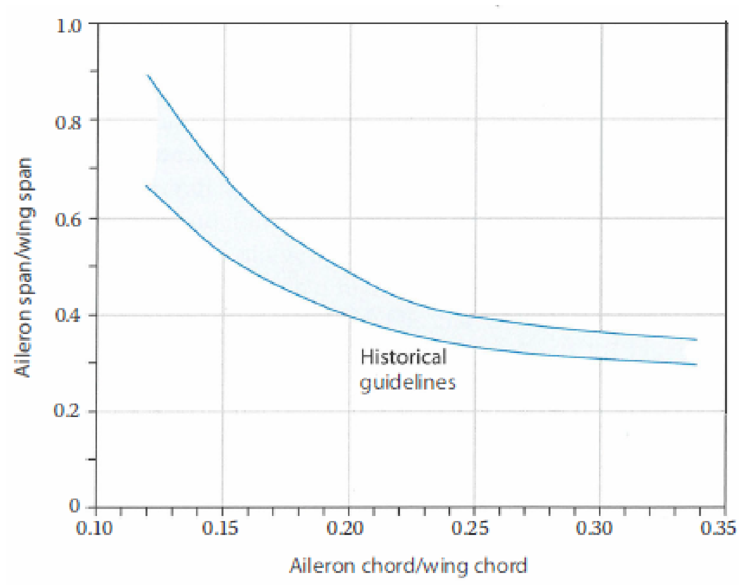

Figure 54: Aileron sizing chart[19]

$$c_{aileron} = CR_{aileron} c_{wing1} \tag{4.2.17}$$

$$b_{aileron} = SR_{aileron} \frac{b_{wing1}}{2} \tag{4.2.18}$$

4.2.4 Propulsion System

Ecalc Initial Sizing

Initial analysis was done for a propulsion system using a service called eCalc[8]. It takes inputs for plane dimensions and weights then allows for selections of different ESCs, batteries, and propellers. Several different configurations were tested, and the analysis showed the motors and propellers in table 18 would be promising configurations.

Table 18: Configurations of motors and propellers taken from ecalc and used for static thrust testing

Motor	Propeller
FPVDrone 1407 4000KV	GF 3030R 2 blade
	GF D75R 3 blade
	RMRC 4045R 2 blade
iFlight XING-E 1104 4200KV, iFlight XING-E 1103 10000KV	Beta FPV 2020 4 blade
	FPV Drone 2030 3 blade
	GF 2040 3 blade
	GF 2540 3 blade
	Beta FPV 3020 2 blade

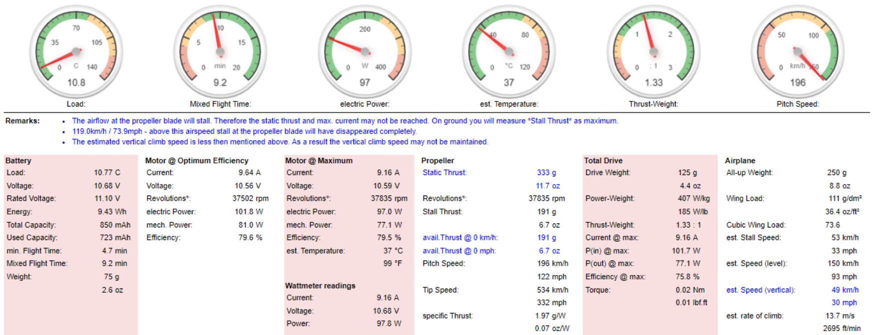

Figure 55: Sample results from Ecalc analysis of SPARROW

Motor Partial Load

Propeller	Throttle	Current (DC)	Voltage (DC)	el. Power	Efficiency	Thrust		Spec. Thrust		Pitch Speed		Speed (level)		Motor Run Time
rpm	%	A	V	W	%	g	oz	g/W	oz/W	km/h	mph	km/h	mph	(85%) min
5800	14	0.1	11.1	1.1	25.0	8	0.3	7.1	0.25	30	19	-	-	431.3
8700	21	0.2	11.1	2.2	42.0	18	0.6	7.9	0.28	45	28	-	-	214.5
11600	28	0.4	11.1	4.1	54.8	31	1.1	7.7	0.27	60	37	-	-	117.8
14500	35	0.6	11.1	6.8	63.5	49	1.7	7.2	0.25	75	47	-	-	69.9
17400	42	1.0	11.1	10.8	69.4	70	2.5	6.5	0.23	90	56	44	27	44.1
20300	50	1.5	11.0	16.3	73.3	96	3.4	5.9	0.21	105	65	81	50	29.2
23200	57	2.1	11.0	23.4	75.9	125	4.4	5.3	0.19	120	75	92	57	20.2
26100	65	3.0	11.0	32.6	77.7	159	5.6	4.9	0.17	135	84	104	64	14.5
29000	73	4.1	10.9	44.0	78.9	196	6.9	4.4	0.16	150	93	115	72	10.7
31900	82	5.4	10.9	58.0	79.7	237	8.4	4.1	0.14	165	103	127	79	8.0
34800	**90**	**7.0**	**10.8**	**74.9**	**80.2**	**282**	**9.9**	**3.8**	**0.13**	**180**	**112**	**138**	**86**	**6.2**
37700	99	8.9	10.7	94.8	80.5	331	11.7	3.5	0.12	195	121	150	93	4.8
37835	100	9.2	10.7	97.0	79.5	333	11.8	3.4	0.12	196	122	150	93	4.7

Motor Characteristic at Full Throttle

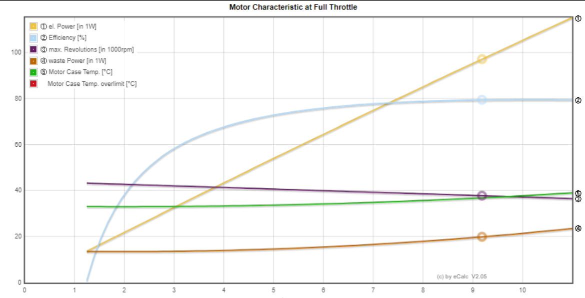

Figure 56: Sample results from Ecalc analysis of SPARROW

Experimental Testing

Static thrust stand tests were conducted for each motor and propeller combination to find the optimal real world pair. Each test was conducted using the following methodology:

1. Charge battery to 100%
2. Plug battery into thrust stand
3. Plug thrust stand into computer
4. Tare force reading
5. Run automatic throttle variance script to record data at different set points
6. Stop test either at completion of script or when a motor experience blade stall. This was defined as 3 readings at different PWM values producing the same thrust and current draw

The thrust stand used was a RCbenchmark series 1520 stand paired with the RCbenchmark software

Table 19: Specifications for RCbenchmark Series 1520 thrust stand. Actual angular speed is calculated by dividing eRPM by number of poles on motor.

Specification	Min.	Max.	Tolerance	Unit
Thrust	-5	5	0.5%	kgf
Voltage	0	35	0.5%	V
Current	0	40	1%	A
Angular Speed	0	190k	-	eRPM

Testing Results

The results of the static motor and propeller testing can be seen below.

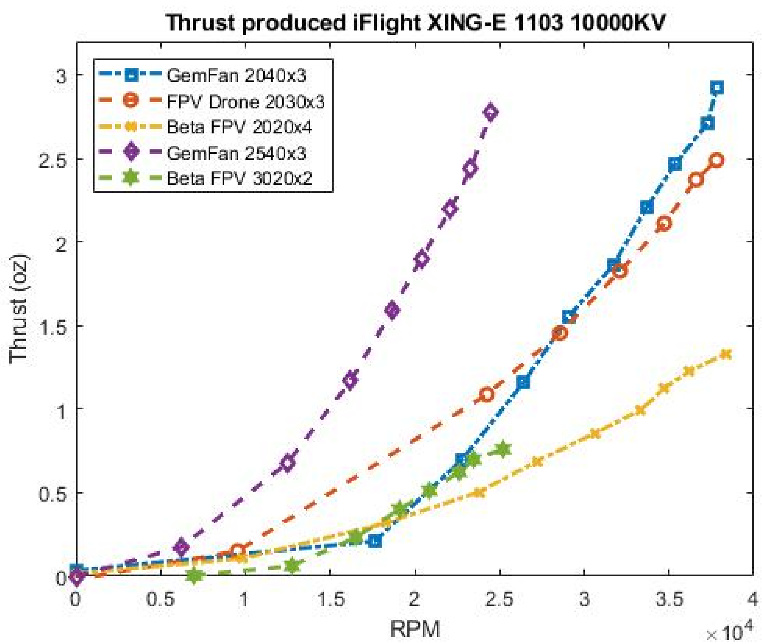

Figure 57: Thrust of different propellers for iflight 1103 10,000kv motor in static condition

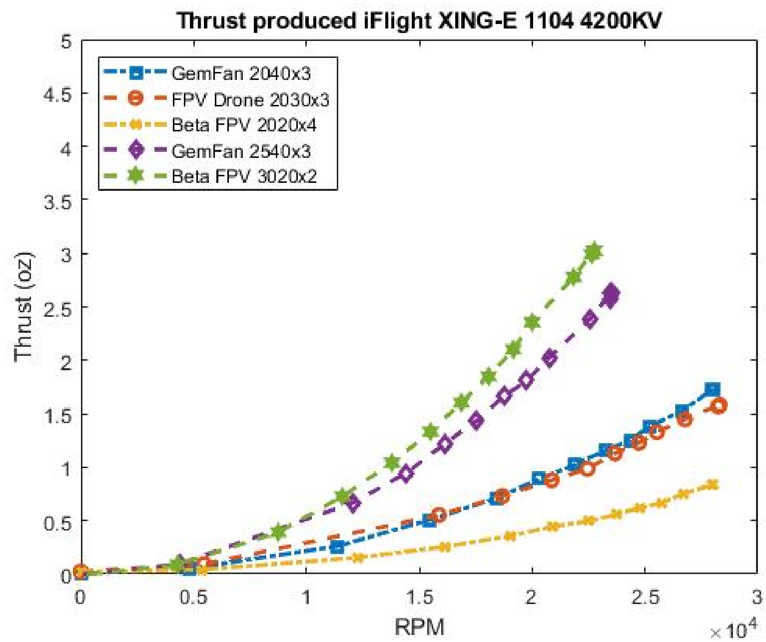

Figure 58: Thrust of different propellers for iflight 1104 4,200kv motor in static condition

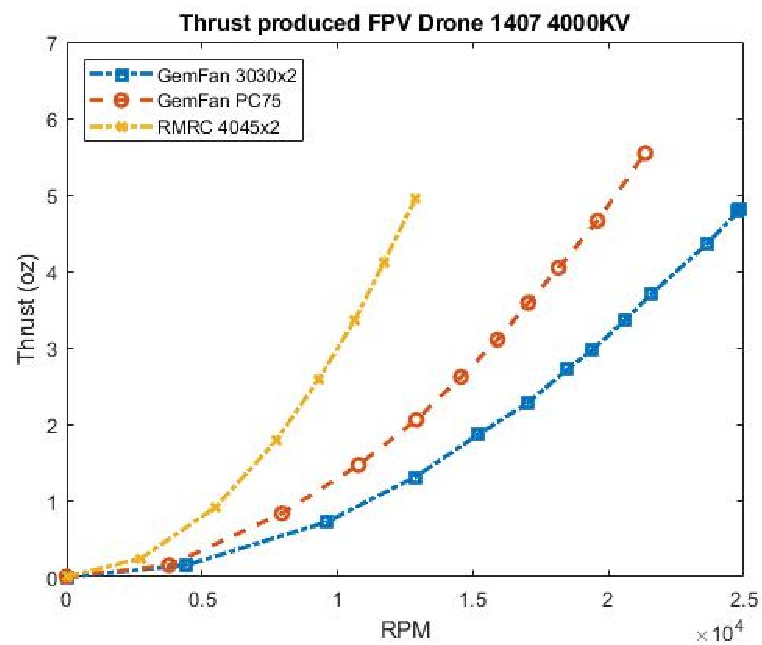

Figure 59: Thrust of different propellers for FPV Drone 4,000kv motor in static condition

The FPV Drone 1407 4000KV motor with the GemFan PC75 propeller was selected as the propulsion system for SPARROW due to its high amount of static thrust produced allowing the vehicle to be optionally hand launched.

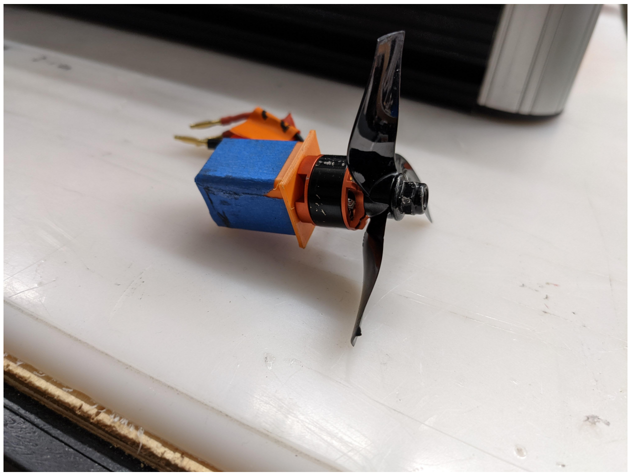

Figure 60: FPV Drone 1407 motor with GemFan PC75 as used on SPARROW

4.2.5 Structures

Load Estimates

Bending is the largest load in an unswept wing, followed by torsion. To ensure SPARROW can withstand these forces a simple loading analysis was done with a loading factor n = 2.5. The lift distributions seen below in figs. 61 and 63 shows elliptical, trapezoidal, and averaged approximations of lift experienced at each point on the chord. Figs. 62 and 64 shows the shear and moment forces experienced by SPARROW. Since the vehicle is so small, the forces experienced are not significant.

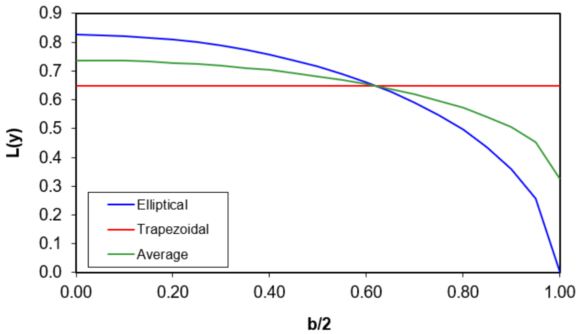

Figure 61: Elliptical, trapezoidal, and averaged wing lift distribution for wing 1

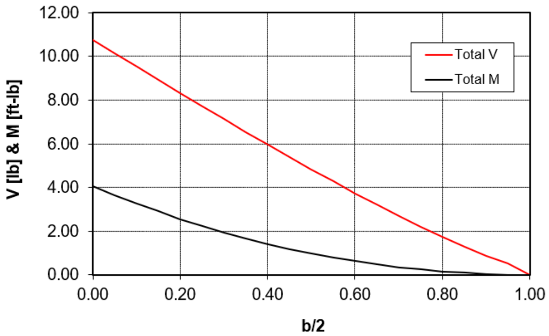

Figure 62: Wing shear and moment chordwise distribution

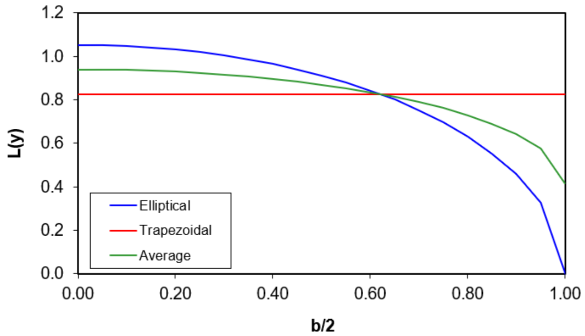

Figure 63: Elliptical, trapezoidal, and averaged wing lift distribution for wing 2

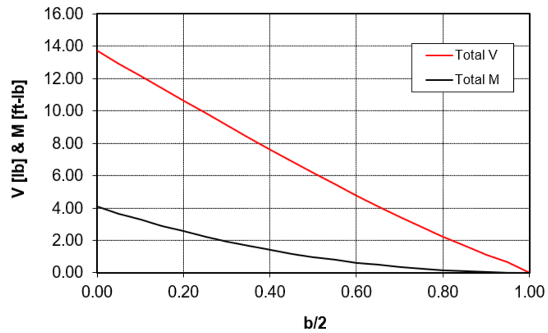

Figure 64: Wing shear and moment chord-wise distribution

Load Testing

Based on the above load estimates, the bending moment was approximated to be a single 0.55 lb point load on the wing tip. A roll of tape was used as it matched this weight. The wing was secured from its center on the edge of a table and the tape roll was placed on the wing tip. It was noted that the maximum deflection from the loading was approximately 0.75 in on the rear wing and 0.25 in on the forward wing. This was deemed sufficient to move forward with flight testing.

Figure 65: Load test for foreword wing with 0.55 lb weight at tip

Figure 66: Load test for rear wing with 0.55 lb weight at tip

Component Weight Breakdown

The component weight breakdowns for SPARROW MkVI and MkVII can be seen below. The main difference between the two is the additional weight in MkVII due to the change from a foam fuselage to the plastic shipping tube fuselage.

Table 20: Weight breakdown of all components on MkVI SPARROW

Category	Item	Weight (oz)	Totals (oz)
Airframe	Fuselage + Wings	1.738	
Airframe	Nose	0.506	
Airframe	Motor Mount	0.465	
Airframe			2.71
Avionics	Control Zero	0.494	
Avionics	Wiring Harness 1	0.211	
Avionics	Wiring Harness 2	0.06	
Avionics	Servo Adapter	0.142	
Avionics	GPS	0.294	
Avionics	Radio	0.566	
Avionics	Receiver	0.124	
Avionics	ESC/BEC	0.33	
Avionics	Servo x2	0.4	
Avionics	Battery (850mAh)	2.358	
Avionics	Battery cable	0.184	
Avionics	Motor+Prop	0.738	
Avionics			5.9
Total Amount			8.61

Table 21: Weight breakdown of all components on MkVII SPARROW

Category	Item	Weight (oz)	Totals (oz)
Airframe	Fuselage + Wings	4	
Airframe	Nose	0.6	
Airframe	Motor Mount	0.134	
Airframe			4.73
Avionics	Control Zero	0.494	
Avionics	Wiring Harness 1	0.211	
Avionics	Wiring Harness 2	0.06	
Avionics	Servo Adapter	0.142	
Avionics	GPS	0.294	
Avionics	Radio	0.566	
Avionics	Receiver	0.124	
Avionics	ESC/BEC	0.33	
Avionics	Servo x2	0.4	
Avionics	Battery (850mAh)	2.358	
Avionics	Battery cable	0.184	
Avionics	Motor+Prop	0.738	
Avionics			5.9
Total Amount			10.63

Materials Weight Breakdown

The main goals of SPARROW were to be both lightweight and low cost which created quite a challenge when designing it. Initially 3D printed was used for prototyping different components, but it quickly became apparent that it weighed too much to actually be used in the final version of SPARROW. The avionics alone weigh 0.45lbs leaving only 0.1lbs available for the fuselage and wings. Numerous different materials were explored as seen in table 22

Table 22: Weight of materials per unit length

Material	Weight
FliteTest Foam Board 2"x2"	0.052 oz/in^2
Hobby Lobby Foam Board 2"x2"	0.12 oz/in^2
Walmart Foam Board 2"x2"	0.06 oz/in^2
Carbon fiber wing	0.0285 oz/in^2
Plastic Shipping Tube 3"	0.17 oz/in
Plastic Shipping Tube 2.5"	0.16 oz/in
Plastic Shipping Tube 2"	0.14 oz/in
Plastic Shipping Tube 1.82"	0.09 oz/in
3D Printed Tube 1.82" ID 0.05" wall	0.13 oz/in
Staples Cardboard Shipping Tube 2"	0.213 oz/in

The SPARROW MkVI fuselage was entirely made of flite test foam board in order to keep the wight as low as possible. This worked for rapid prototyping, but it was noted that the foam had a tendency to break and bend during hard landings. Ultimately it was found that shipping tube was the ideal material for the fuselage. It did weigh more than the foam, but the extra strength it provided eliminated the need to repair the SPARROW fuselage in all but the most catastrophic crashes. Similarly, the SPARROW MKVI wings were made from foam board for prototyping purposes, but they were the component most likely to break during a landing or crash. To mitigate this carbon fiber wings were manufactured for SPARROW MkVII that were both stronger and lighter which completely eliminated the issues of wings breaking. Complex and relatively small materials such as the SPARROW nose and end cap were still chosen to be 3D printed due to their complex nature.

4.2.6 Hinge Mechanism

The hinge mechanism for the wings consists of a spring sandwiched between the wing mounts that rotate around a central axle. In initial prototyping this was a fully 3d printed mechanism, but after testing it was found that the central axle was prone to breaking so it was changed to be a # 8 screw. This was found to be sufficient. A major challenge for the hinge mechanism was getting the wings reliably aligned and held in place for flight. This was solved by creating a stopper which the wing mounts are forced to clamp onto as the spring rotates. The hinge was not able to be integrated onto SPARROW MkVII as tested, but it will be included in future versions.

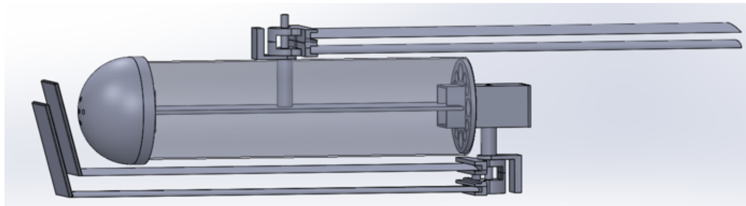

Figure 67: CAD model showing a design for the SPARROW MkVII hinge

4.3 Avionics

4.3.1 Configuration

The testing avionics package SPARROW used is powered by an omnibus flight controller. This does not offer autonomous capabilities, but exceeds in being a simple rate assisted flight controller giving the vehicle the best chance of flying. No telemetry radio or GPS were utilized for the initial avionics testing setup. This simplified setup was crucial in getting SPARROW to fly by simplifying the system in a way that made it easier to diagnose if flight issues were caused by the vehicle or avionics. It also allowed a human pilot to be part of the testing process which allowed for immediate feedback on flight characteristics enabling rapid prototyping.

Table 23: Detailed list of Sparrow's testing configuration of avionics

Function	Brand
Flight Controller	Omnibus F4
Telemetry Radio	None
Receiver	FrSKY X4R
BEC/ESC	ZTW Mantis Slim Brushless ESC 15A
GPS	None
Servo	Hitech HS-35HD Ultra Nano Servo
Battery	Venom 450mAh LiPo 3s Battery

The operational avionics package SPARROW is using is run off a mRo Control Zero F7 with Arduplane installed for its autopilot. This is paired with a ground station running mission planner to communicate with the SPARROW and monitor its activity. A pair of mRo air SiK Telemetry Radios are used to communicate between the SPARROW and ground station allowing for long range operation. The avionics package is powered by an 850mAh 3s battery to provide a balance between operational time and endurance. A table of this configuration can be seen below in 24 along with a block diagram and photo of this configuration in figs. 68, 69, and 70. Once fully operational, the SPARROW will be able to fly autonomously with the ground station being optional. Work is currently being done at USRI to enable multiple vehicles running off of Pixhawk flight controllers to communicate with each other, and is a feature being explored for implementation.

Table 24: Detailed list of Sparrow's operational configuration of avionics

Function	Brand
Flight Controller	mRo Control Zero F7
Telemetry Radio	mRo air SiK Telemetry Radio V2 915Mhz
Receiver	FrSKY R-XSR Ultra
BEC/ESC	ZTW Mantis Slim Brushless ESC 15A
GPS	mRo SAM GPS + IST8308
Servo	Hitech HS-35HD Ultra Nano Servo
Battery	CNHL MiniStar LiPo Battery 3s 650mAh

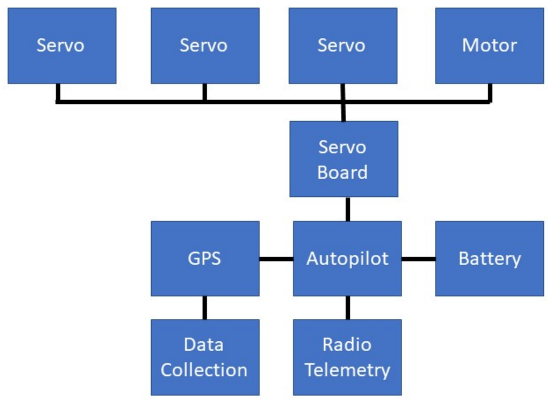

Figure 68: Avionics block Diagram

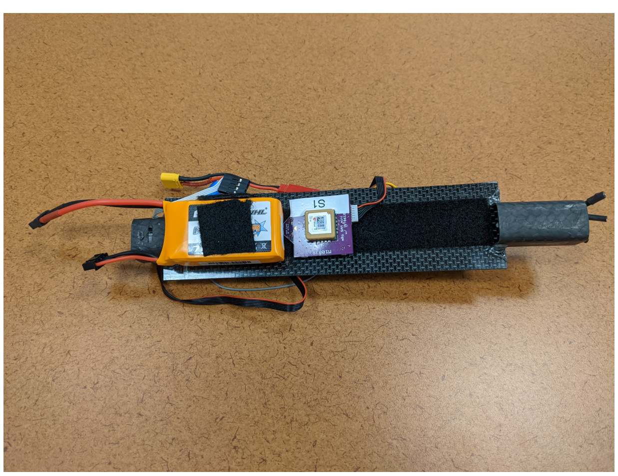

Figure 69: Top view of the SPARROW avionics

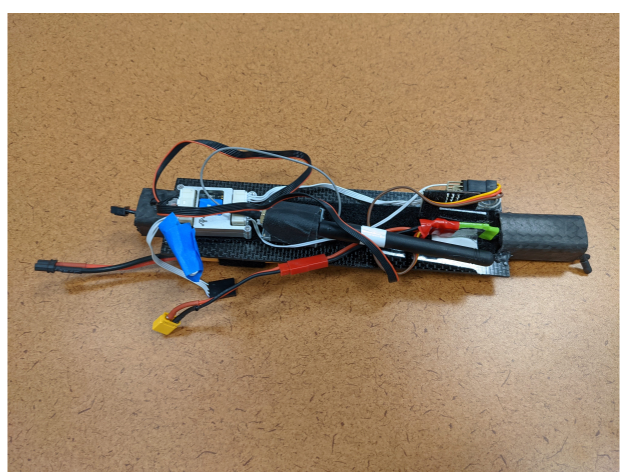

Figure 70: Bottom view of the SPARROW avionics

4.4 Weather Sensors

To accurately record the thermodynamic properties of the atmosphere, it is necessary to record pressure, temperature, humidity, and wind direction during flight. These sensors must be selected to collect accurate enough data for forecasting while also minimizing drift over time. USRI has previously done work with using UAS to collect atmospheric data and has already developed a sensor suite and data collection package which is comparable to a radiosonde. These sensors are shown below in table 25. Due to a shortage of pressure sensors across the world, only temperature and humidity sensors will be integrated into SPARROW. Of note is that the sensor package was originally designed to fly on a nimbus aircraft which has much more payload room than SPARROW. Changes were made to the USRI sensor package to reduce weight and size as much as possible.

Table 25: Sensors used to take temperature and humidity data in SPARROW

Parameter	Sensor
Temperature	IMET Primary NTC Thermistor
Humidity	HYT 271

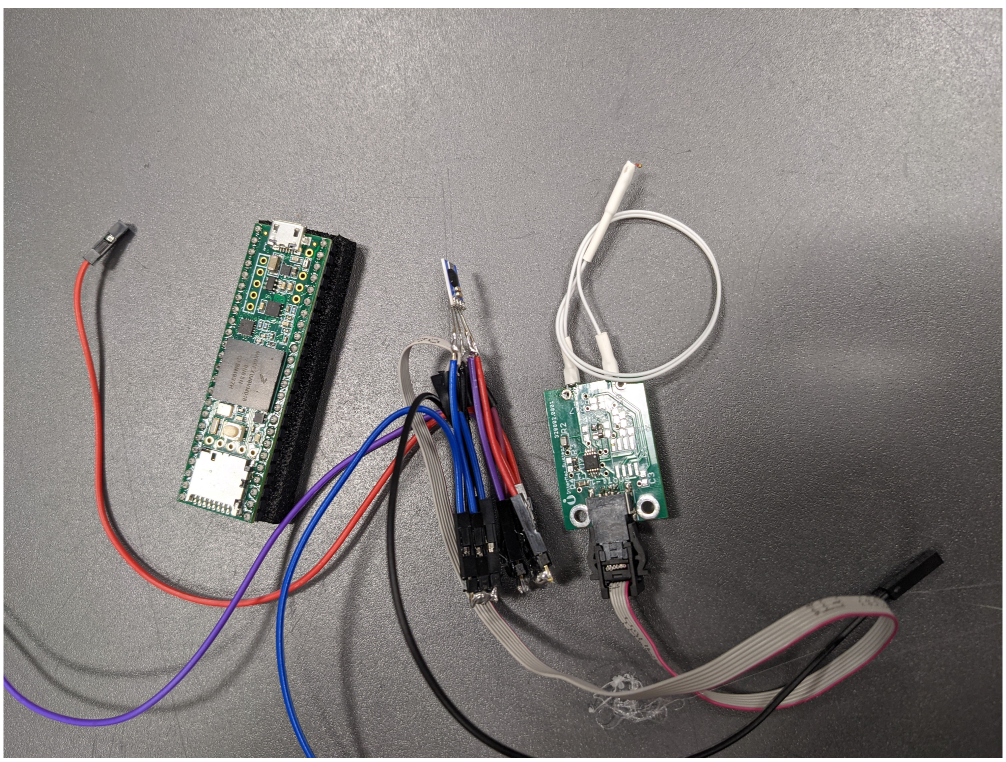

Figure 71: Sensors that are used in SPARROW to record temperature and humidity data

The data was collected and stored using a Teensy 3.6 running a custom firmware developed in house at USRI. This configuration allows for collection of data at up to 20Hz, and work is currently being done to allow this information to be transmitted back to the ground in real time.

4.4.1 Sensor Specifications

Humidity Sensor

The humidity sensor is an HYT 271 manufactured by Innovative Sensor Technology. It operates using a capacitive based humidity sensor which functions by using 2 metal plates separated by a nonconductive film. As the film is exposed to different levels of humidity, the capacitance changes which is then measured and correlated to humidity values based on calibration. These sensors are very fragile and must be handled with care. Typically, it is recommended that they are only handled with gloves on, and even then, only non-electrical points should be touched.

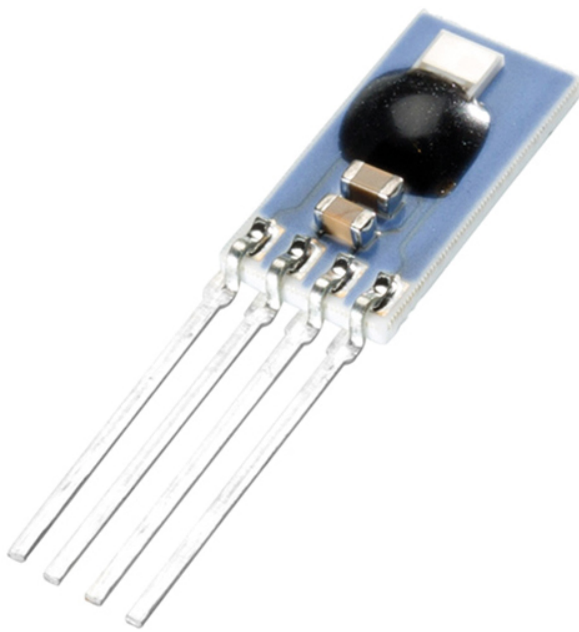

Figure 72: Innovative Sensor Technology's HYT 271 Humidity Sensor

Table 26: Sensor data for HYT 271 Humidity sensor used on SPARROW

Parameter	Value
Type	Capacitive polymer humidity sensor
Humidity Range	0-100% relative humidity
Max Dew Point	+80 C
Humidity Accuracy	+/- 1.8% rH
Humidity Resolution	0.02% rH
Temperature Measurement Range	-40 to 120 C
Temperature Accuracy	+/- 0.2 C
Temperature Resolution	0.01 C
Hysteresis	<+/- 1% rH
Response Time	<4s

Temperature Sensor

The temperature sensor used is the InterMet Primary NTC Thermistor. An NTC thermistor operates based on resistance characteristics of how a ceramic and metal composite interact with temperature changes. This change in resistance is then recorded and converted into a temperature value based on a predetermined calibration curve.

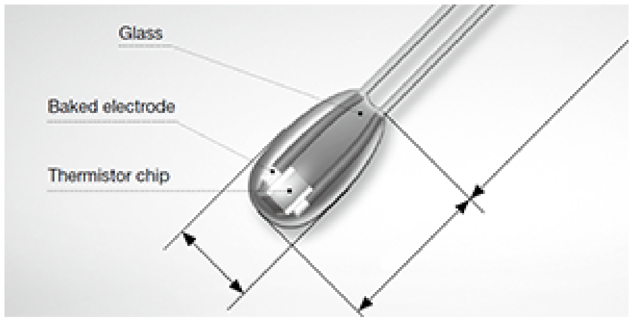

Figure 73: InterMet Primary NTC Thermistor

Table 27: Sensor data for InterMet Primary NTC Thermistor used on SPARROW

Parameter	Value
Type	Glass bead NTC thermistor
Temperature Range	-95 C to +50 C
Temperature Accuracy	0.3 C
Temperature Resolution	0.01 C
Response Time	1 s

4.4.2 Sensor Integration

Placement

The sensors used by SPARROW to collect atmospheric data are very sensitive, so careful placement is needed to ensure the data collected is valid. Previously at OSU three sensors in table 25 have been successfully used inside a Nimbus aircraft to collect weather data in conjunction with other universities. This was done by placing them inside an S duct with the inlet at the bottom of the aircraft and the outlet at the top pointing towards the back of the aircraft as seen in figs. 74, 75, and 76.

Figure 74: Side view of the Nimbus S duct

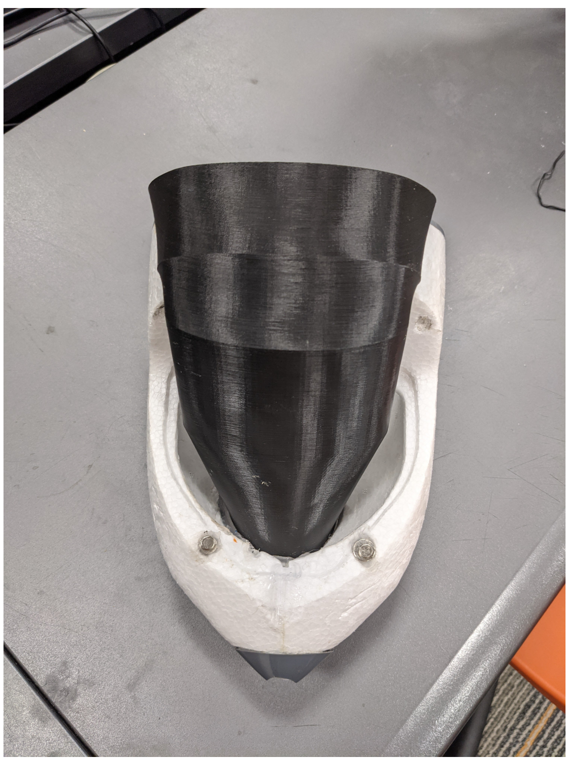

Figure 75: Top view of the Nimbus S duct

Figure 76: Rear view of the Nimbus S duct

The Nimbus S duct was made by 3D printing a large structure which is then integrated into the fuselage. The sensors are placed in the middle of the duct exposed to the inner air. This is done both to keep the sensors from being in direct airflow, and to isolate them from sources of potential heat contamination such as the sun or avionics.

Initially, attempts were made to replicate this configuration for SPARROW. The major challenge was finding a way to do this which is just as effective, but also much lighter weight. To accomplish this, an S duct was made using a 0.5” diameter straw which was cut to have a similar shape as the S duct in the Nimbus as seen in Figs. 77 and 78.

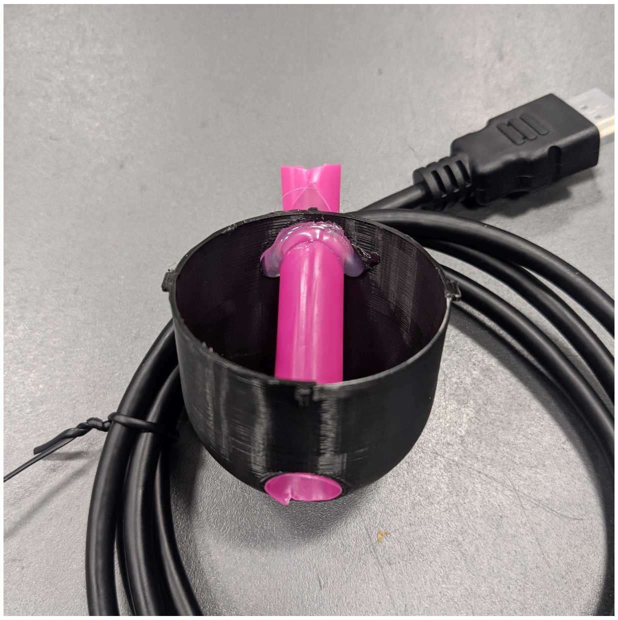

Figure 77: Modified S duct in SPARROW made from 0.5” diameter straw

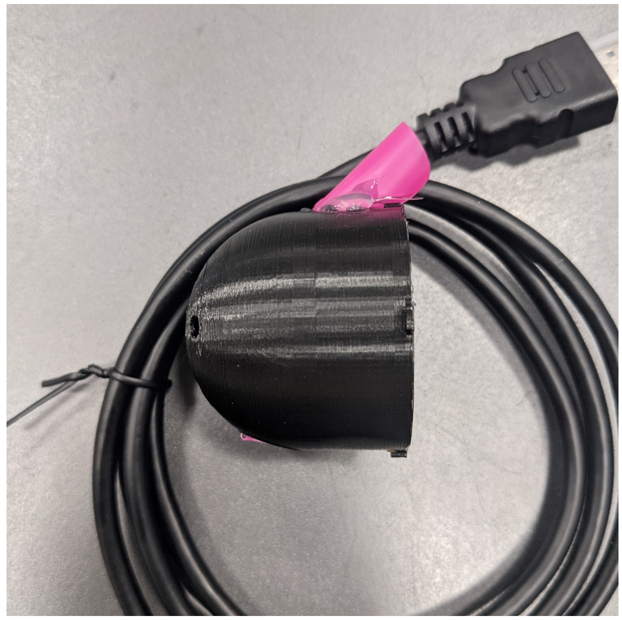

Figure 78: Modified S duct in SPARROW made from 0.5” diameter straw

Through testing, the s duct configuration was shown to not allow sufficient airflow over the sensors. Fig. 79 shows the resulting evolution of nose configurations for SPARROW that were tested following the s duct design. Once again, the major considerations were maximizing airflow over the sensors, minimizing heat contamination from avionics, and shielding the sensors from the sun.

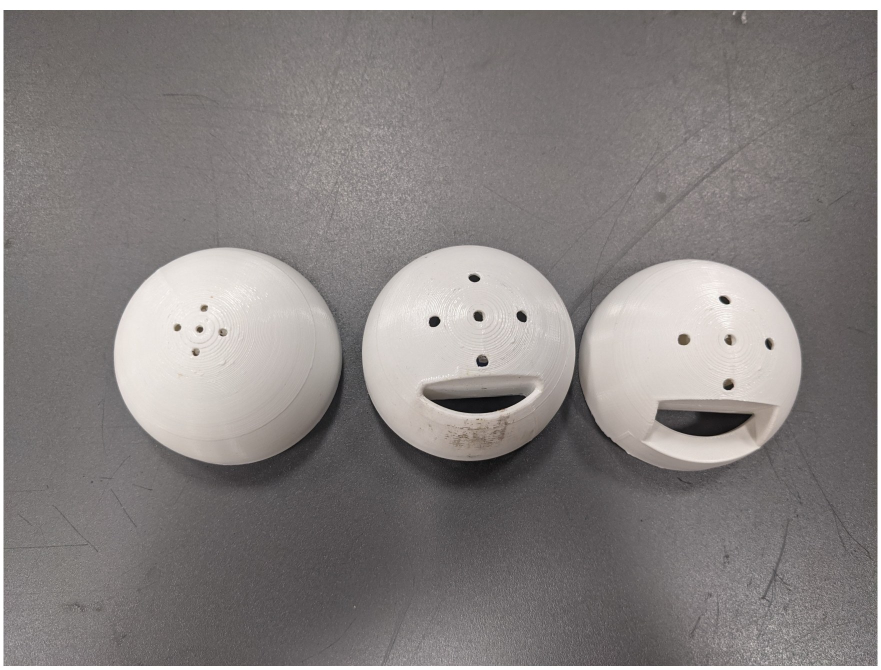

Figure 79: Evolution of SPARROW sensor mounts

4.5 Dropping Mechanism

In order to rapidly test the SPARROW vehicle, a dropping mechanism was constructed to allow for testing from a quadcopter. The major advantage to using a quadcopter for a drop testing platform is easily repeatable testing at different altitudes of interest. It is also significantly lower cost than rocket-based deployment. This mechanism was actuated using a separate FUTABA based controller and receiver than what was on the SPARROW. The dropper is essentially just a control rod attached to a servo that bridges the gap between two pieces of wood. As the servo actuates, the control rod is pulled back releasing the clip attached to the SPARROW vehicle allowing it to free fall before beginning flight.

Figure 80: Dropping mechanism integrated onto the USRI SKB 1000

Figure 81: Close view of servo for dropping mechanism

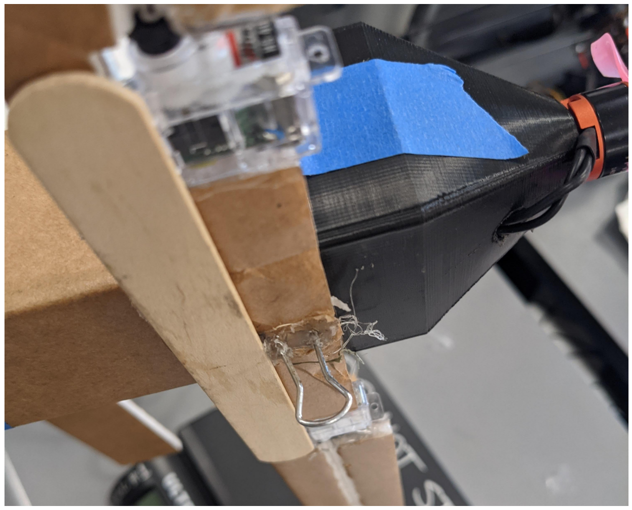

Figure 82: Clip on vehicle for dropping mechanism

CHAPTER V

Vehicle Construction

5.1 SPARROW MkVI

The wings for SPARROW are cut from foam board using a laser cutter as seen in fig. 83. This allows for precise cuts and repeatable manufacturing. The laser cutter used was a Jamieson CM-1080 set to 18% max power and 1% min power with 40 $\frac{mm}{s}$ travel speed. With these setting the foam board cutouts stayed attached to the sheet in the corners preventing any movement during cuts. The foam board used was from Flite Test and was 24" x 30". An example of the cutouts produced by the machine can be seen in fig. 84.

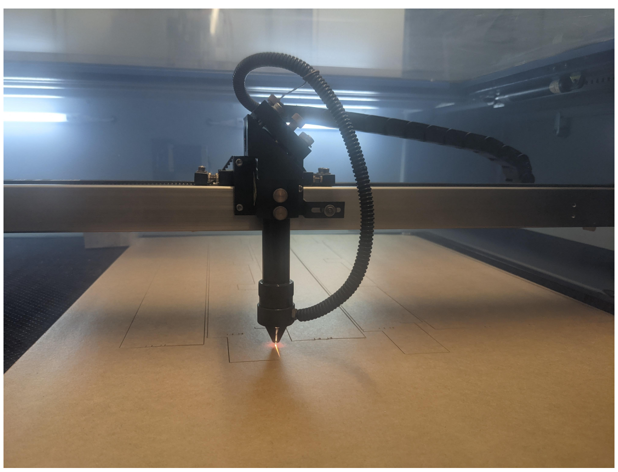

Figure 83: Laser cutting foam for SPARROW

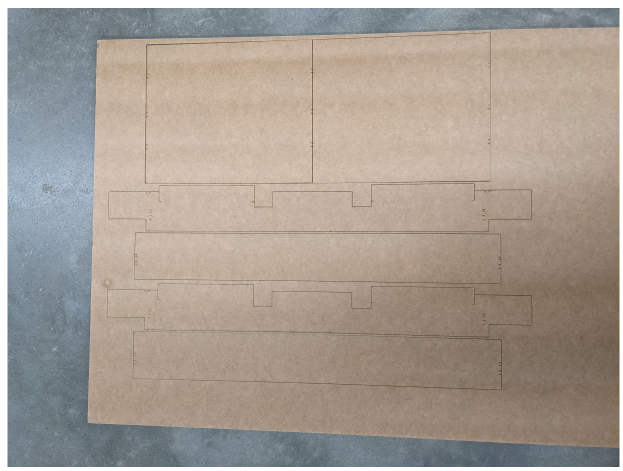

Figure 84: Foam board laser cut for SPARROW

5.1.1 Wing

All parts are cut in 2D and folded along themselves. Where folds are needed, grooves are cut such that only paper on one side of the foam board is left intact. The foam on each side of the groove is then chamfered with a knife to make it easier to fold. For control surfaces, a similar process is used with just a straight line cut instead of a groove.

To provide extra rigidity to the wing, a bamboo skewer was used as a spar. This was done by peeling back a strip of paper on the top side of the wing and pressing the foam board underneath down using a ruler. The foam is not cut out, but instead compressed to help facilitate rigidity. A strip of hot glue was then run down the channel and the bamboo skewer was pressed into place by a ruler with two 30 lb weights on top. The purpose of this was to ensure the skewer is level with the top of the wing and that the foam underneath is sufficiently compressed. This can be seen in figs. 85 & 86 Once the skewer has set for 2 minutes; the weights are taken off. The front part of the wing which will be folded over to make the airfoil step then has its paper removed to reduce weight and increase adhesion. A line of hot glue is then applied to the exposed foam, and it is folded over while using a ruler to apply even force. The ruler is then placed on top of the fold to protect the foam and 30lb weights are once again put on top to ensure good bonding.

Figure 85: Top view of crashed foam wing showing spar embedded into wing

Figure 86: Side view of foam wing

5.1.2 Fuselage

The fuselage was manufactured from simply folding a rectangular pattern of foamboard up and then epoxying the sides to form a rigid rectangular prism.

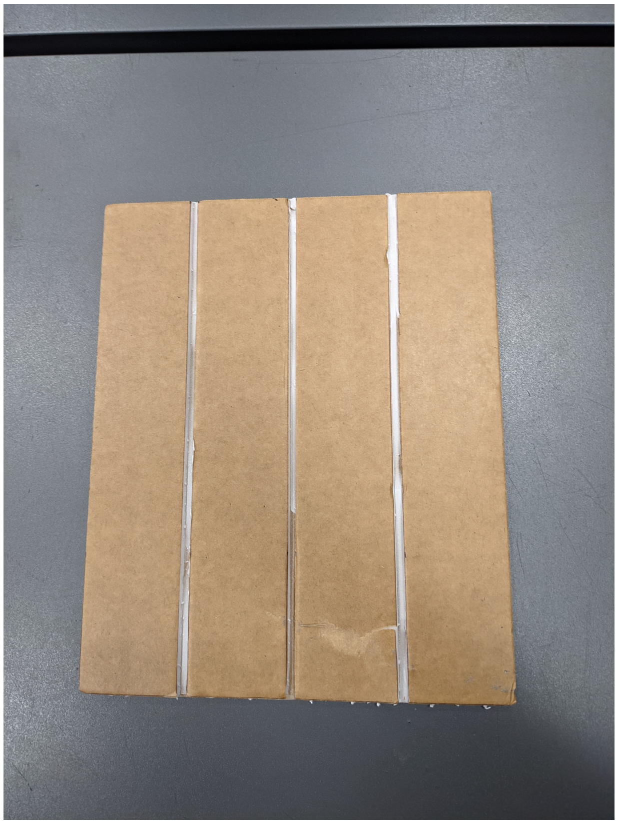

Figure 87: SPARROW MkVI foam fuselage unfolded before gluing

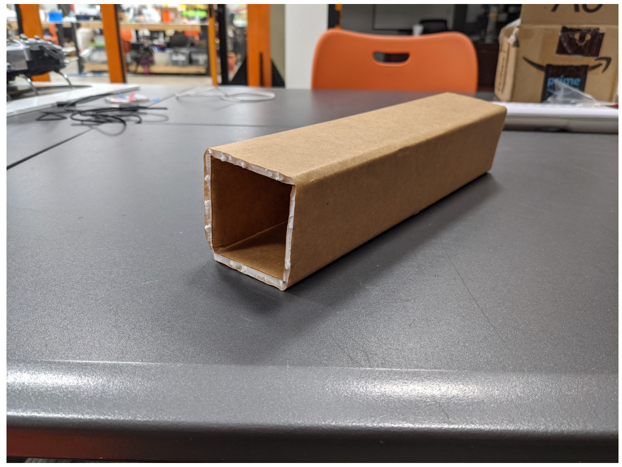

Figure 88: SPARROW MkVI foam fuselage folded and glued together

5.1.3 3D Printed Components

The nose and motor mount were 3D printed due to simplicity of manufacturing the complex geometries.

Figure 89: SPARROW MkVI 3D printed components

5.1.4 Assembly

The assembly of SPARROW MkVI involved the following steps.

1. Place avionics in fuselage
2. Fold up fuselage
3. Glue aft wing onto fuselage
4. Glue forward wing onto fuselage
5. Install nose and motor mount

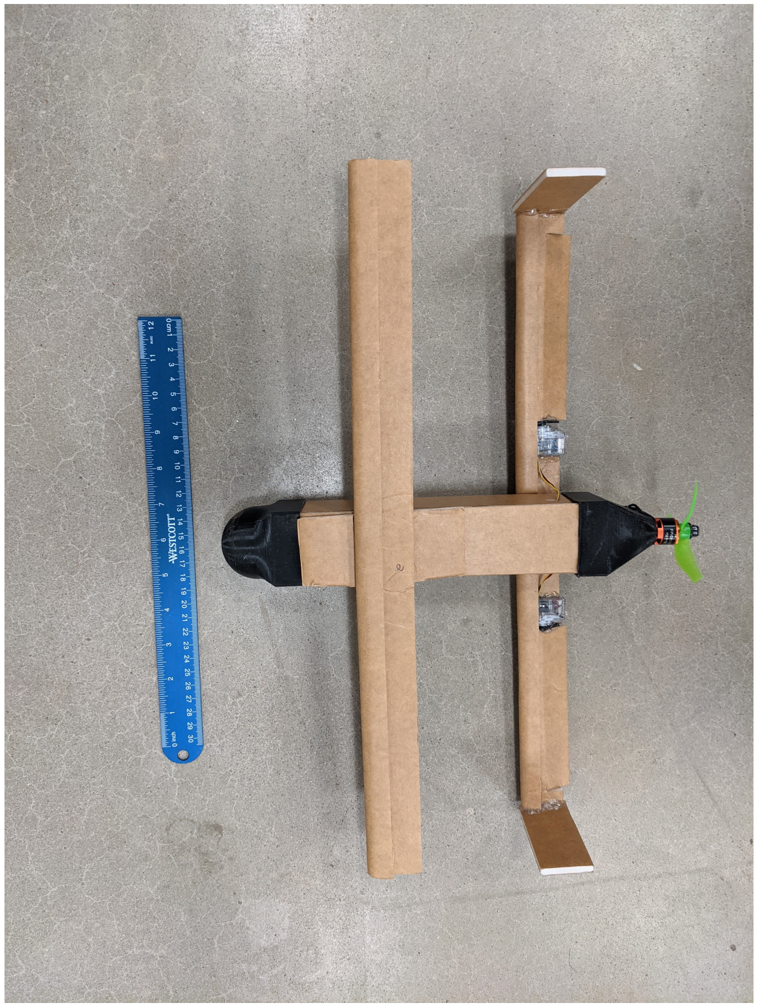

Figure 90: Assembled SPARROW MkVI vehicle

5.2 SPARROW MkVII

5.2.1 Fuselage Backbone

The fuselage backbone was constructed using carbon fiber components. The main portion of the backbone is a 2 mm carbon fiber plate cut to size. This is what all the avionics are mounted on. Each end of the plate has a square carbon fiber tube which is notched and epoxied on. The front tube acts as a mount to hold the nose of the vehicle in place. The aft tube acts as a mount for the motor.

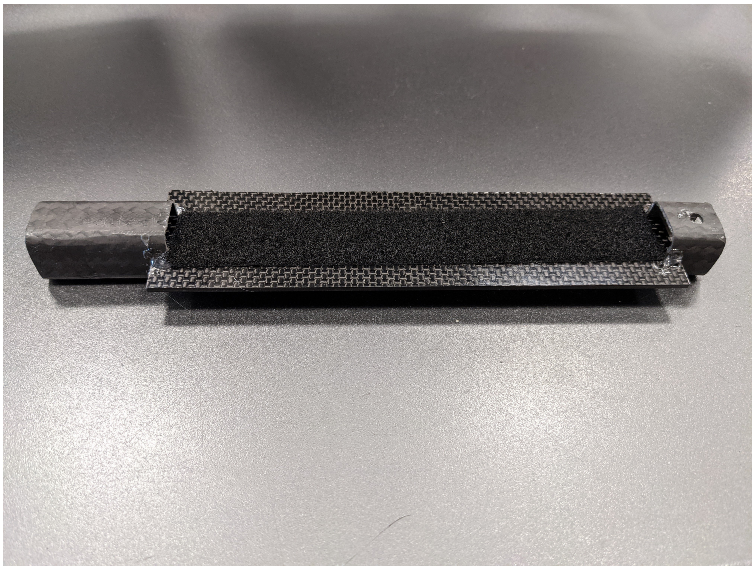

Figure 91: Backbone of the SPARROW vehicle

5.2.2 Composite Wings

Description of Layup

Both of the composite wings were manufactured using a standard layup process outlined below. Each wing consists of 4 layers of 6k carbon fiber and one layer of 1/32-inch balsa wood. The bottom layer was oriented at 45°, followed by a layer of 90°carbon fiber. Then a strip of balsa wood is added, followed by another layer of 90°carbon fiber and 45°. It is important that in this layup process the layers are symmetrical to maximize strength.

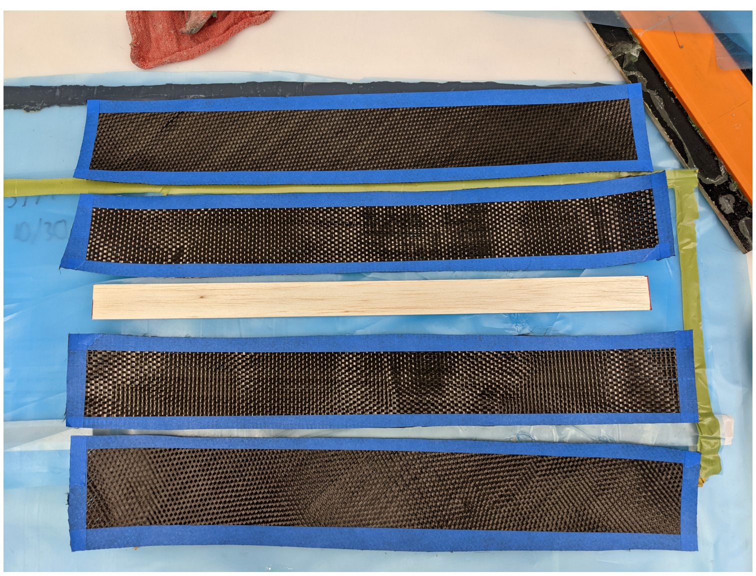

Figure 92: Layers trimmed and set in order to be used for the SPARROW wing layup

Mold Manufacturing Process

1. Design mold in CAD
2. 3D print mold
3. Epoxy mold together
4. Sand/epoxy mold
5. Epoxy layup surface
6. Sand Epoxy and repeat as needed

Figure 93: Allowing epoxy to dry on the layup surface of the mold

Layup process

1. Cut composite sheets to size of mold
2. Wax mold
3. Apply mold release
4. Stick gum tape around vacuum bag
5. Brush on initial epoxy
6. Put first layer of composite sheet in mold
7. Press sheet down to ensure it is flat against mold and absorb all epoxy. More epoxy is applied if needed to get rid of dry spots.

8. Additional layers of composite sheets are applied as described in the previous step until the final sheet has been placed down.
9. Perforated peel ply is placed on top of last composite layer
10. Cotton sheet is placed on top of perforated peel ply
11. Entire mold is wrapped in vacuum bag and vacuumed for 24 hours
12. After curing, part is carefully pried from mold

Figure 94: Vacuum bagged layup in the process of curing

Wing Prototypes

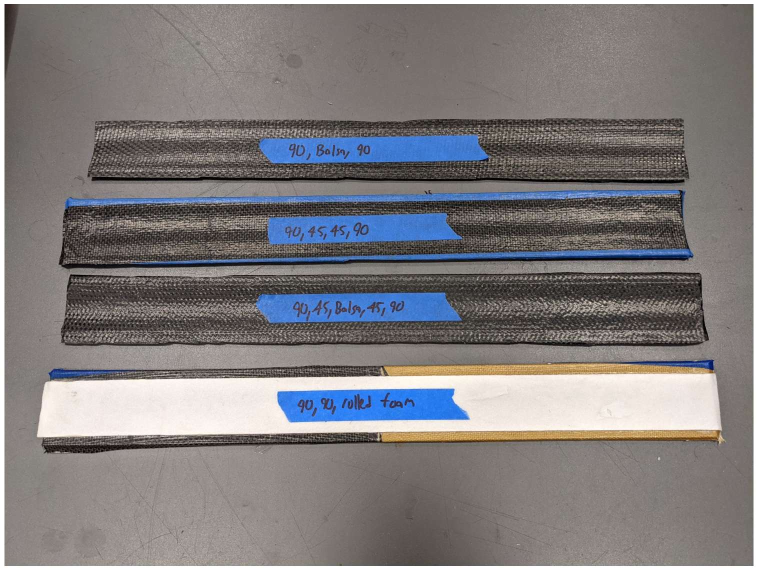

Figure 95: Iterations of SPARROW wing. Bottom is 2 layers half kevlar half carbon fiber arranged at 90, 90, with a rolled foam board on top. Next is 4 layers of carbon fiber arranged 90, 45, 45, 90. The 3rd wing is carbon fiber with balsa wood core arranged 90, balsa, 90. Top wing is also carbon fiber with balsa wood arranged 45, 90, balsa, 90, 45

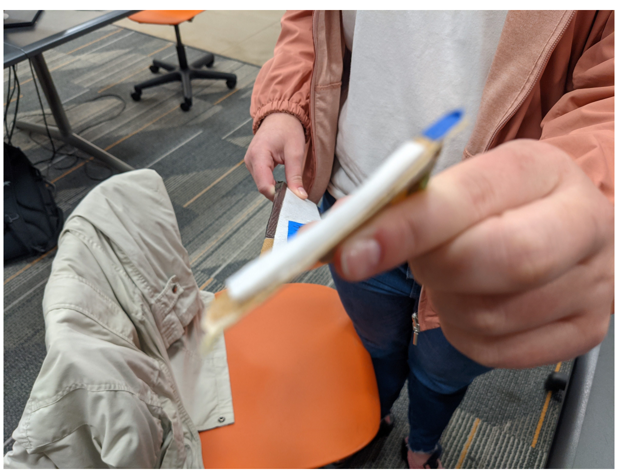

Figure 96: Torsion in the 90, 90, foam half kevlar half carbon fiber wing

Figure 97: Torsion in the 90, 45, 45, 90 carbon fiber wing

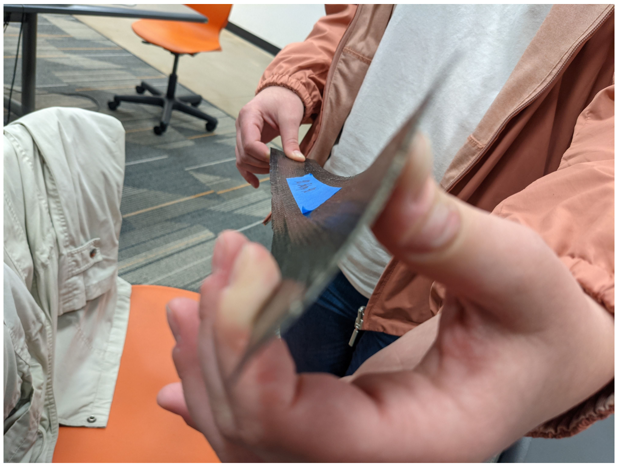

Figure 98: Torsion in the 90, balsa, 90 carbon fiber wing

Figure 99: Torsion in the 90, 45, balsa, 45, 90 carbon fiber wing. This is the final SPARROW wing

5.2.3 Control Surface Manufacturing and Integration

The control surfaces were cut from 0.5mm thick sheets of pre-made carbon fiber plate. Notches were then cut out of the rear wing using a pattern of the servo so that the point of rotation on the servo is just past the trailing edge of the wing. The servo is then epoxied in so that the servo horn rotates in plane with the wing. The elevon is then attached to the wing using gaffers tape such that it is touching the servo control horn. Finally, the control horn is epoxied to the elevon.

5.2.4 Fuselage

The fuselage is made from a cut down section of 2.55-inch outer diameter shipping tube with 0.028-inch thick walls.

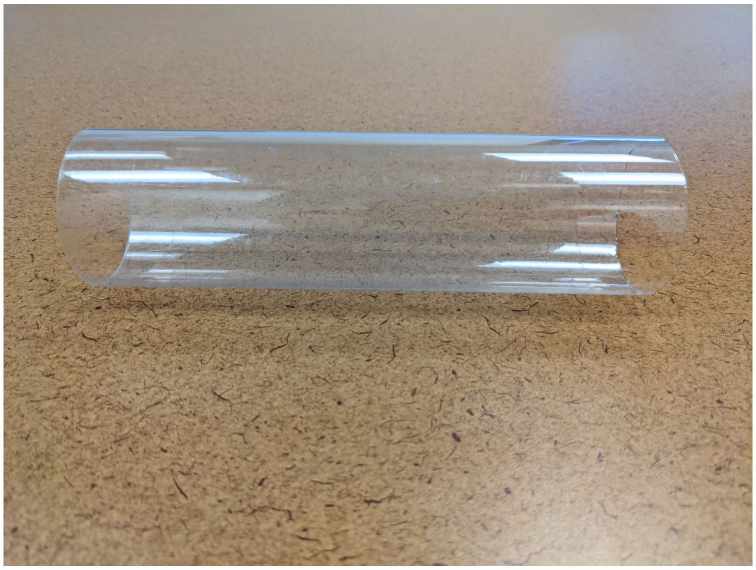

Figure 100: Fuselage of the SPARROW vehicle

5.2.5 3D Printed Components

For SPARROW MkVII the vertical stabilizers, nose, motor mount, and fuselage end cap were 3D printed. In most cases this was due to simplicity of rapidly manufacturing complex geometries. However, for the vertical stabilizers this proved to be useful in flight testing as it was noted that during a failed hand launch or hard landing the vertical stabilizers had a tendency to break. By being 3D printed, it was easy to simply glue on a new stabilizer to replace the broken one which allowed for increased pace of testing.

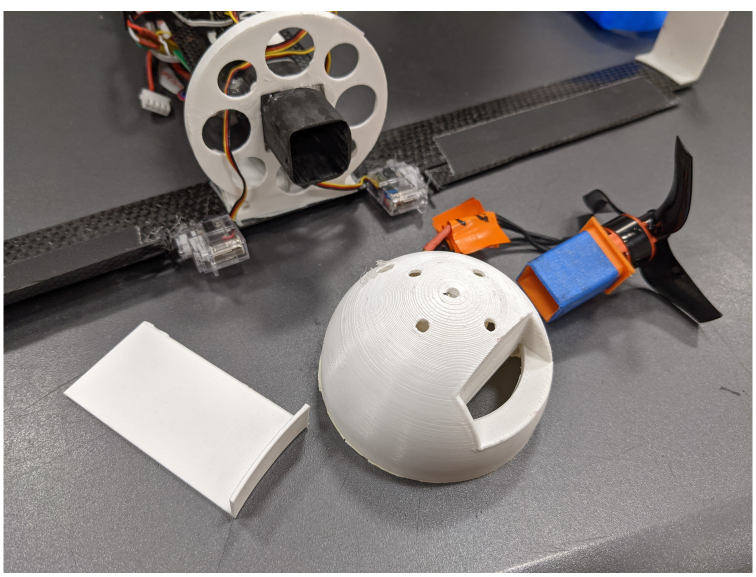

Figure 101: 3D printed components used for SPARROW

5.2.6 Assembly

The assembly of SPARROW MkVII as used for testing involved the following steps.

1. Place avionics on backbone
2. Place end cap onto backbone
3. Attach forward wing to fuselage with double sided tape. Attach rear wing to endcap with double sided tape
4. Install motor onto motor mount and insert into rear of fuselage backbone
5. Insert backbone into fuselage
6. Install weather sensors into nose
7. Install nose onto SPARROW and plug in sensors

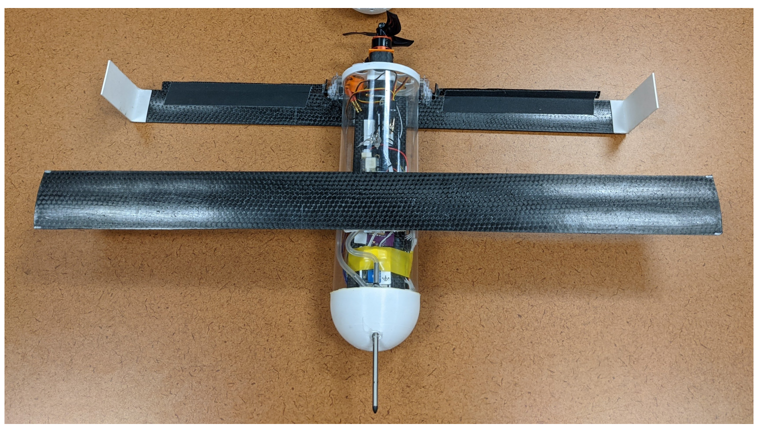

Figure 102: SPARROW Mk7 assembled

CHAPTER VI

Simulation, Testing, and Results

6.1 Test Sites

6.1.1 OSU Unmanned Airfield

Low altitude testing occurred at the Oklahoma State University Unmanned Aircraft flight station. It is located approximately 12 miles east of Stillwater and is equipped with a runway. The flight station has a persistent COA for 1500 ft AGL which is expandable to 3000 ft AGL as needed. The area directly around the flight field is relatively flat and grassy with no trees.

Figure 103: Oklahoma State University Unmanned Aircraft flight station

6.1.2 Choctaw

Medium altitude testing will occur at the Choctaw Nation FAA UAS IPP site. The Choctaw Nation owns a 44,000 acre ranch within 2 hours of the Dallas Metro area, and slightly more than one hour from both Oklahoma City and Tulsa. The property has very diverse terrain conditions over its roughly 27 mile length (southwest corner to northeast corner). There are many unique features to the property, including the perimeter boundary shape, proximity to transportation and communications infrastructure, and the general pristine conditions. At the core of the CNO research consortium plans is a unique advanced test range capability for emerging aviation technologies such as UAM. The CNO was selected as one of ten unmanned aircraft systems (UAS) Integration Pilot Program (IPP) lead entities in May 2018 by U.S. Department of Transportation (DoT) Secretary Elaine Chao. The CNO was the only Native American tribal government selected as a UAS IPP lead entity. The CNO research consortium will leverage existing successful programs – such as the UAS IPP – to further the capabilities of the CNO research consortium and provide access to unique research and development test environments. The ongoing activities reflect the strong commitment of the CNO tribal leadership to support forward-looking technology initiatives. This is being developed as part of the ongoing CNO UAS IPP and includes a +44,000 acre tribally-owned site in southeastern Oklahoma, as shown below. The CNO research consortium already has ongoing research efforts underway with OSU as part of the UAS IPP.

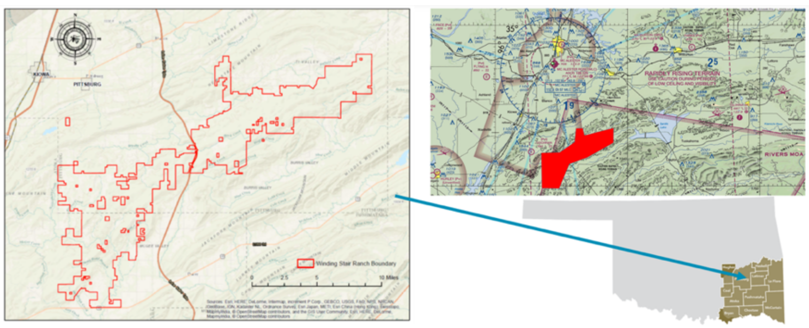

Figure 104: CNO FAA UASS IPP test range.

Figure 105: 40 foot Choctaw tower used for hand launch

Once FAA approvals are in place, solar balloons will be utilized for high altitude tests. Due to the high altitude drop height (around 70,000 ft) and long duration drift tendencies, these make an ideal platform for testing and will have the ability to carry aloft a dozen or more flight vehicles. Both solar and helium assisted solar balloon test launches have been performed to evaluate platform feasibility (Fig. 106).

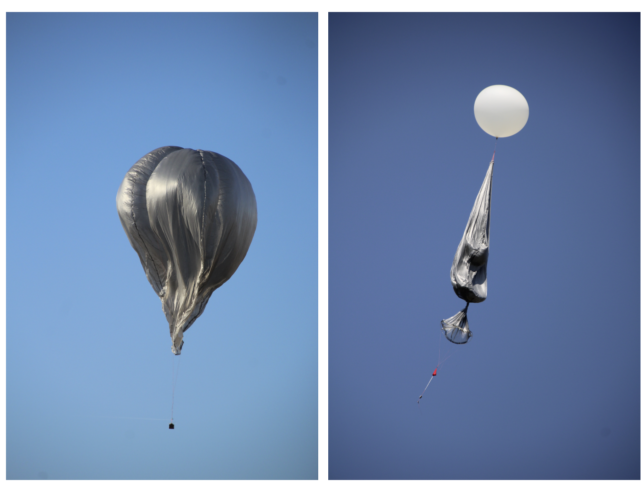

Figure 106: Solar balloon test launches with tracking payload

6.2 Testing Overview

Table 28: Test configuration matrix showing which tests were performed on SPARROW MkVI and SPARROW MkVII

	SPARROW MkVI	SPARROW MkVII
Gimbal test	yes	no
Ground hand launch test	yes	yes
Tower hand launch test	yes	no
Aerial drop test	yes	no

6.2.1 Sensor Ground Testing

Setup

The SPARROW temperature and humidity sensors were tested on the ground using the setup shown below. A large fan was placed in front of the sensors allowing for flight conditions to be better simulated. The entire setup was placed on top of a moving dolly to allow it to be easily rolled inside and outside without disrupting orientation or airflow over the sensors.

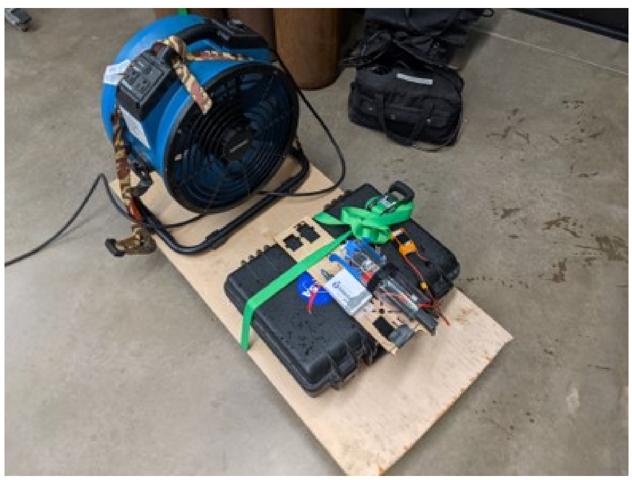

Figure 107: Configuration used for sensor ground testing

Nose V1

The first set of sensor testing was designed to evaluate the sensors themselves as well as their integration into SPARROW. To accomplish this, 2 iMet sensors were placed next to SPARROW for data comparison. 4 tests were conducted in total. For the first 2 tests the sensors were left outside of SPARROW exposed to the atmosphere directly. For the last 2 tests the sensors were integrated into SPARROW as shown in fig. 108. The first test in each set of tests were conducted with no fan on to check ambient response, while the second test in each set was conducted with a fan on blowing approximately 12 mph to better simulate flight conditions.

Figure 108: Temperature and humidity sensor integrated into SPARROW nose V1

Table 29: Nose V1 test matrix

Test number	Fan on	Sparrow sensors integrated into nose V1
1	No	No
2	Yes	No
3	No	Yes
4	Yes	Yes

6.2.2 SPARROW MkVI Ground Testing

Unpowered Flight Testing

Before putting avionics in the vehicle, an unpowered flight simulation was performed to test vehicle stability. The CG location and weight was simulated using lead weight and a gimbal device was secured to the CG location on the vehicle as seen in figs. 109 and 110. The gimbal was then held outside the window of a car traveling at predicted flight speeds. During these testes the SPARROW was able to maintain a pitch angle passively with no control input. This showed validated a few different things: the vehicle was stable in pitch, and the wings were strong enough to withstand flight speeds.

Figure 109: SPARROW MkVI prototype attached to gimbal

Figure 110: Side view of SPARROW MkVI attached to gimbal

Hand Launch Testing

Hand launching was the next step in flight testing to see if the vehicle could sustain flight. At first this was attempted using the full avionics layout that included the mRo control Zero with little success. To simplify things, an omnibus controller was instead used with only a smaller 2s battery and receiver on board. Instead of using an auto mission a human pilot assisted by a rate mode on the omnibus was used. The SPARROW almost flew but didn't seem to have enough power. Since the particular motor chosen supported 2s and 3s batteries, a 3s 450mAh battery was installed in the SPARROW and it finally achieved flight on its own! For these tests the motor on SPARROW was set to 75% throttle and thrown into the air in a steady level orientation. SPARROW was controllable, but due to its small size and high speed it was hard for the pilot on the ground to determine vehicle orientation. Attempts were also made at flying with higher capacity batteries in , however there was difficulty in hand launching with the configuration due to the lower thrust to weight ratio

Figure 111: SPARROW being thrown from the ground

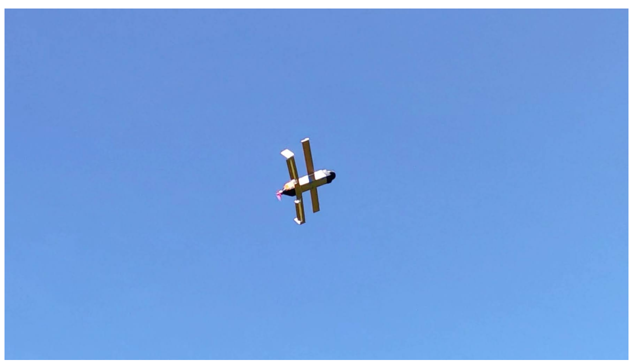

Figure 112: SPARROW in flight after being hand launched

Choctaw Tower Hand Launch testing

After establishing SPARROW could reliably fly using a basic RC setup with a lightweight battery, the next step was to see if SPARROW was capable of flying with more weight on board. As previously mentioned, there were issues hand launching using higher capacity (heavier) batteries, so the towers at the Choctaw Daisy ranch airfield were utilized to hand launch the vehicle. This was done before drop testing from a quadcopter due to its relative simplicity and greater control of deployment. When dropping the vehicle from a quadcopter there are issues such as rotor downwash and limited control of release orientation which have both negatively impacted previous tests. For this test the motor on SPARROW was set to 75% throttle and was thrown forward off the tower into the wind in a steady level orientation. SPARROW was once again able to achieve flight.

Figure 113: SPARROW MkVII before being thrown from Choctaw tower

Figure 114: SPARROW MkVII after being thrown from Choctaw tower

Figure 115: SPARROW MkVII in flight at Choctaw

6.2.3 SPARROW MkVI Drop Testing

Medium altitude flight testing was conducted at the Oklahoma State University Unmanned Aircraft Flight Station (UAFS). The UAFS has sufficient vehicle monitoring stations, support, landing areas, and personnel to support testing of the SPARROW. For the drop tests, the operational avionics configuration which includes the mRo Control Zero autopilot. This was necessary to do the vehicle being dropped from altitudes where a human pilot on the ground would struggle to determine vehicle orientation.

Initially a DJI Phantom was planned to be used as the dropping vehicle. This was due to its smaller size and the hope that there would be less effects from prop downwash on the SPARROW. To facilitate this, stilts were added to the phantom to raise it off the ground allowing the SPARROW and dropping mechanism to be attached to the side as seen in figs. 116 & 117. It turned out to be difficult to takeoff from the ground with roughly 0.7lbs. of weight on one side of the Phantom and roughly half the takeoff attempts resulted in the Phantom immediately flipping. The successful takeoffs were accomplished by taking off with full up throttle and full roll compensation to the opposite side from where the vehicle was mounted. Once in the air the Phantom had trouble gaining altitude due to the weight of its payload and also struggled to remain stable. For all but 1 test the SPARROW had to be released early to ensure the safety of the Phantom.

Figure 116: SPARROW dropping system installed on a DJI Phantom before drop testing

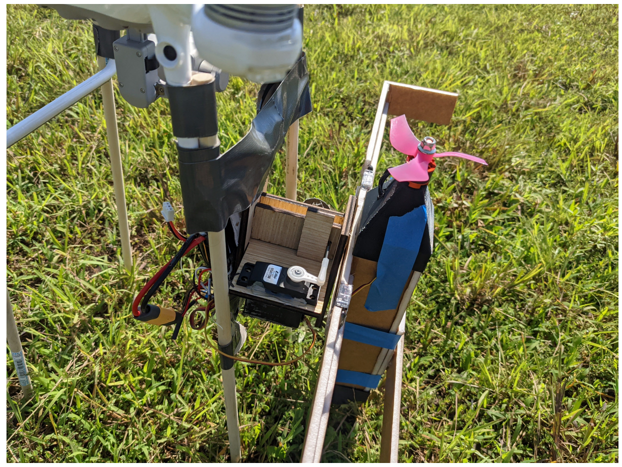

Figure 117: SPARROW prototype loaded on a DJI Phantom before drop testing

With only 1 semi successful drop test from the Phantom, the dropping mechanism was moved over to the USRI SKB1000 as seen in figs. 118 & 119. There was concern the larger props would cause damaging downwash to the vehicle, but it did not end up being an issue. The SKB1000 had the added advantage of being an extremely stable quadcopter designed to carry significantly heavier payload than just the SPARROW. This allowed for a controlled and slow ascent further keeping the vehicle from unnecessary swinging.

Figure 118: SPARROW dropping system installed on an USRI SKB1000 quadcopter before drop testing

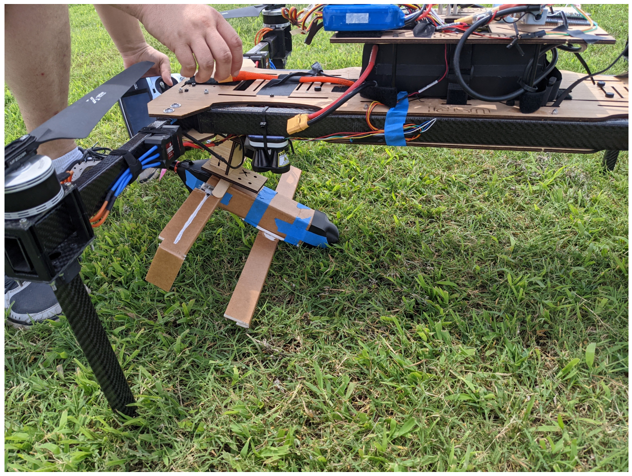

Figure 119: SPARROW loaded into dropping system on an USRI SKB1000 quadcopter before drop testing

6.2.4 SPARROW MkVII Testing

Based on testing of the SPARROW MkVI and its inability to be hand launched at a weight of 0.55 lbs., it was assumed that the 0.8 lb. SPARROW MkVII would have to be drop tested. However, it was found that SPARROW MkVII was perfectly capable of being hand launched which is likely due to using a more efficient airfoil. The process of doing this consisted of the thrower achieving a balancing between throwing the SPARROW forward to get an initial velocity and also lofting the SPARROW upwards to get separation from the ground. The pilot would engage full throttle as soon as the vehicle cleared the hand and typically SPARROW would begin flight immediately. In some instances when the pilot was slow to react, or the thrower did not give SPARROW enough velocity it would drop down close to the ground but quickly recover with full throttle. In some cases, with a bad throw SPARROW immediately crashed in the ground. Even with 5 crashes during testing SPARROW never sustained any more damage than a broken vertical stabilizer. Due to being 3D printed and only glued on, this was easy to switch out and be flight ready again in under 5 minutes.

Figure 120: SPARROW MkVII right before hand launching

Figure 121: SPARROW MkVII right after hand launching

Figure 122: SPARROW MkVII in flight

6.3 Results

6.3.1 Sensor Ground Testing

Nose V1

Table 30: Nose V1 test matrix

Test number	Fan on	Sparrow sensors integrated into nose
1	No	No
2	Yes	No
3	No	Yes
4	Yes	Yes

The results from test 1 are shown in figs. 123 and 124. This test was done without the sensors integrated into SPARROW's nose and with no fan blowing. Of note is that the SPARROW sensors were approximately 1 inch from the fuselage and avionics for this test. It can be seen that for temperature and humidity the SPARROW sensors follow the same general trend as the iMet sensors, but there is an offset in the data. This is most likely due to ambient heating from the SPARROW avionics. Test 2 was configured in exactly the same way, but with the fan turned on and blowing air over the sensors. These results are shown in figs. 125 and 126. It can be seen that in these graphs the SPARROW sensors almost perfectly match what the iMet sensors are reading. Worth noting is that iMet recommends putting their sensors directly into airflow when integrating them onto UAS.

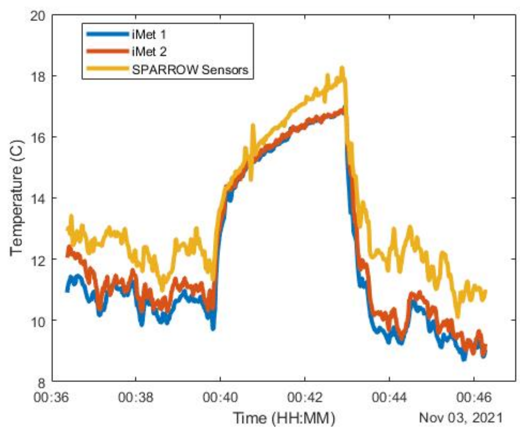

Figure 123: Test 1: Temperature sensor test in freestream with no fan blowing

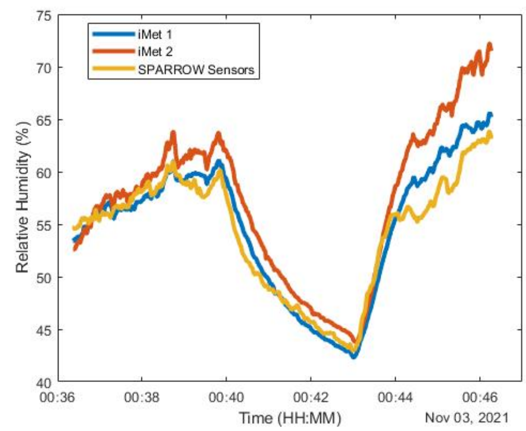

Figure 124: Test 1: Humidity sensor test in freestream with no fan blowing

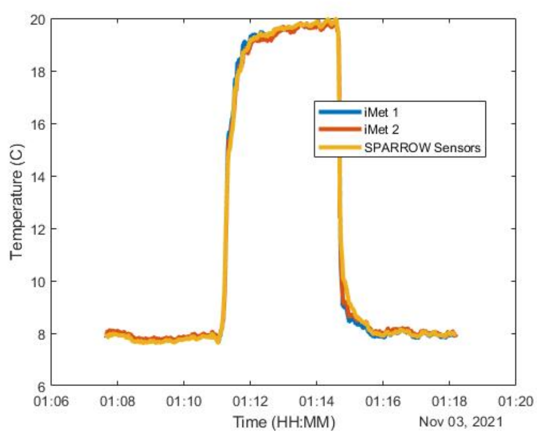

Figure 125: Test 2: Temperature sensor test in freestream with fan blowing

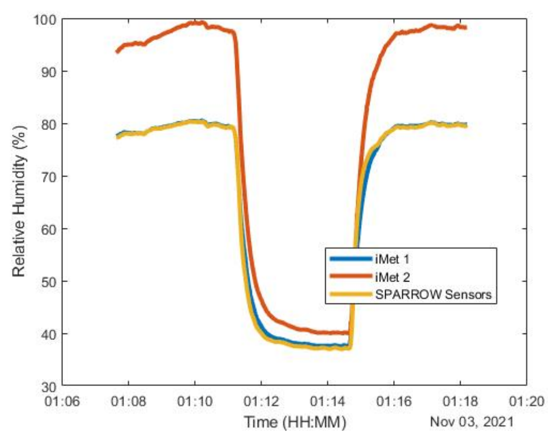

Figure 126: Test 2: Humidity sensor test in freestream with fan blowing

The results from test 3 are shown in figs. 127 and 128. These graphs highlight the lack of airflow over the sensors after they have been integrated into the nose. While the iMet sensors continue to respond as expected, the values for SPARROW stay near constant. However, as shown in figs. 129 and 130, with sufficient airflow over the sensors they are capable of following the same trends as the iMet values. Of interest is the longer response time for the SPARROW sensors in this test than in the 2nd test. This is believed to be due to the airflow being restricted due to recessing the sensors in a cavity. It is also believed that if this configuration flew the cavity could allow precipitation to collect and block it from escaping. To remedy this, a more open nose V2 was designed.

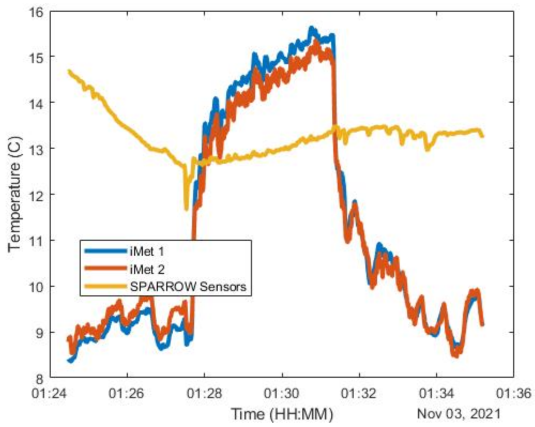

Figure 127: Test 3: Temperature sensor test in Nose V1 with no fan blowing

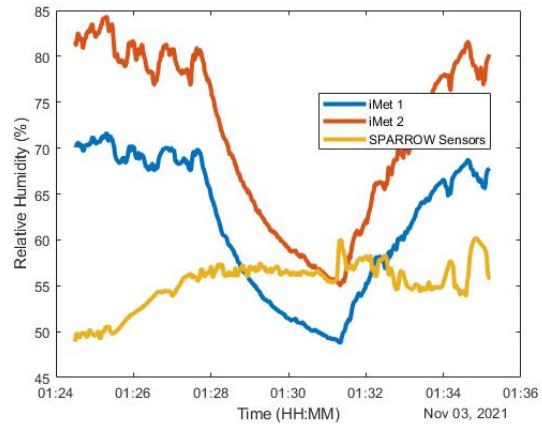

Figure 128: Test 3: Humidity sensor test in Nose v1 with no fan blowing

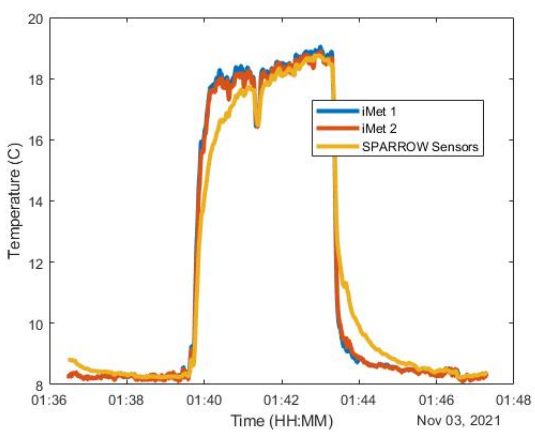

Figure 129: Test 4: Temperature sensor test in Nose V1 with fan blowing

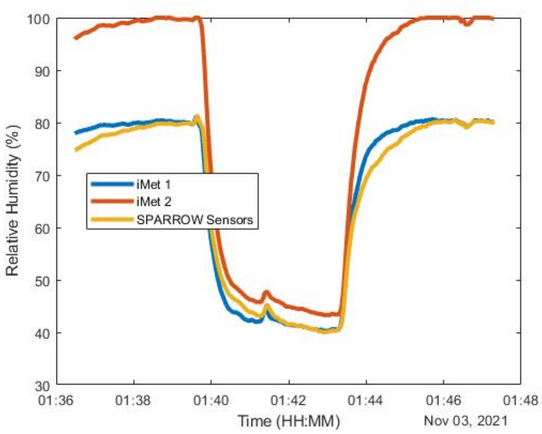

Figure 130: Test 4: Humidity sensor test in Nose V1 with fan blowing

The response times for the temperature sensors in tests 2 and 4 are compiled in table 31 below. For test 2 when both sets of sensors were in freestream with wind blowing the iMet and SPARROW sensors performed comparably. The response time seems high, but this is expected because of the large temperature gradient in which the test was performed in. In test 4 the SPARROW had almost twice the response time as the iMet sensor. This is believed to be related to the design of the Nose V1 in which the sensors were completely in cased by the 3D printed nose.

Table 31: Comparison of temperature sensor response time between SPARROW sensors and iMet sensors

Test	Parameter	SPARROW response time	iMet response time	Temperature difference
2 (freestream)	Temperature	23s	20s	12 C
4 (nose V1)	Temperature	27s	15s	10 C

Finally, a statistical analysis was performed on a 1 minute long steady state wind from tests 2 and 4 to compare the data collected from each sensor. Figs. 131 and 132 show a zoomed in view of the 1-minute window and the difference at each point between the temperature readings. There is a slight offset with the SPARROW sensors which could be corrected with calibration. As is, the SPARROW sensors in freestream read within +/- 1.6 C of the iMet sensor to a 95% confidence level as shown in fig. 135. The test 4 data is not as easy to compare due to the SPARROW sensors holding at more of an average temperate due to the previously mentioned integration issues. This data shows the importance of isolating the sensors from outside heat sources as much as possible. With the SPARROW sensors in the Nose V1 prototype the temperature readings were within +/- 6.9 C of the iMet values with 95% confidence.

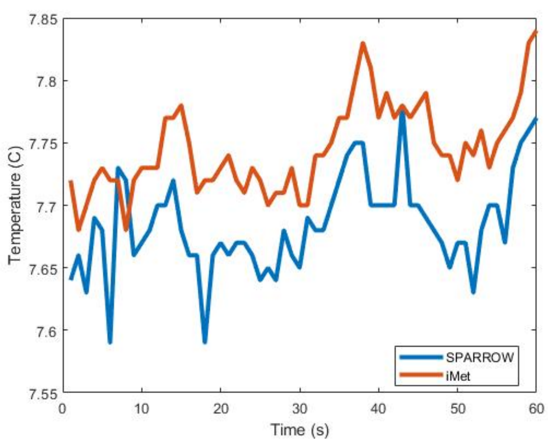

Figure 131: Test 2 temperatures for SPARROW and iMet with fan blowing over a steady state period

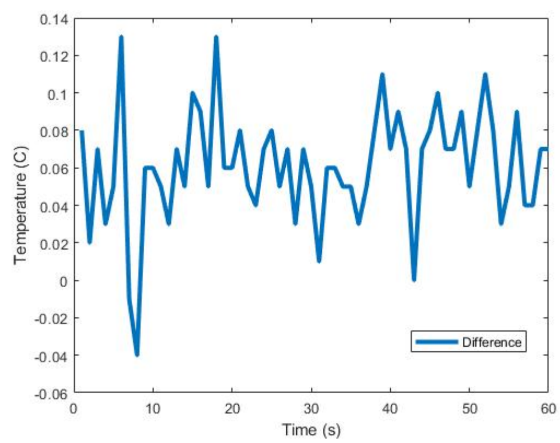

Figure 132: Test 2 temperature difference with fan blowing over a steady state period

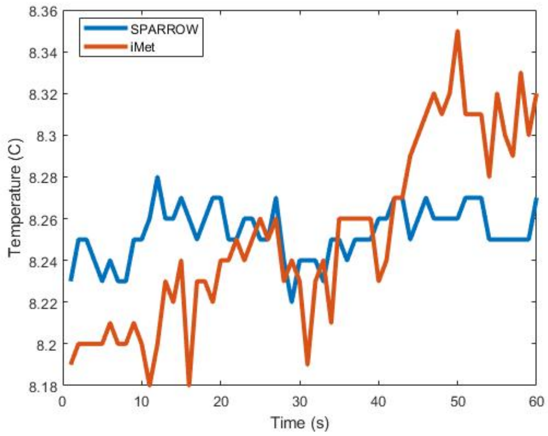

Figure 133: Test 4 temperatures for SPARROW and iMet with fan blowing over a steady state period

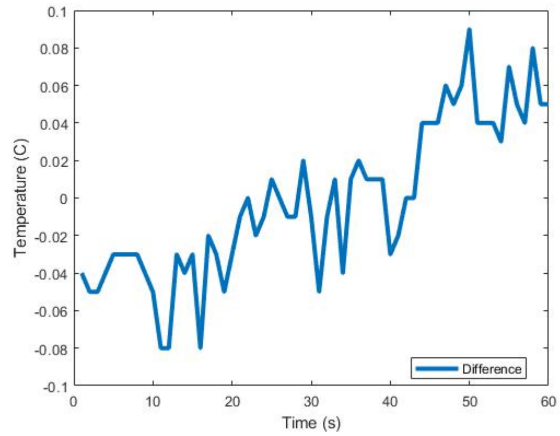

Figure 134: Test 4 temperature difference with fan blowing over a steady state period

SUMMARY OUTPUT								
Regression Statistics								
Multiple R	0.67669111							
R Square	0.45791086							
Adjusted R Square	0.44872291							
Standard Error	0.02901582							
Observations	61							
ANOVA								
	df	*SS*	*MS*	*F*	*Significance F*			
Regression	1	0.041959648	0.041959648	49.83819	2.14439E-09			
Residual	59	0.049673139	0.000841918					
Total	60	0.091632787						
	Coefficients	*Standard Error*	*t Stat*	*P-value*	*Lower 95%*	*Upper 95%*	*Lower 95.0%*	*Upper 95.0%*
Intercept	1.99323033	0.806077837	2.472751686	0.016309	0.380272305	3.606188358	0.380272305	3.606188358
X Variable 1	0.7347606	0.104079389	7.059616748	2.14E-09	0.526498222	0.943022976	0.526498222	0.943022976

Figure 135: Test 2 Excel regression analysis during 1 minute of steady state temperature data

SUMMARY OUTPUT

Regression Statistics	
Multiple R	0.365155987
R Square	0.133338895
Adjusted R Square	0.118396462
Standard Error	0.041289611
Observations	60

ANOVA

	df	SS	MS	F	Significance F
Regression	1	0.015213079	0.015213	8.923506	0.004120736
Residual	58	0.098880254	0.001705		
Total	59	0.114093333			

	Coefficients	Standard Error	t Stat	P-value	Lower 95%	Upper 95%	Lower 95.0%	Upper 95.0%
Intercept	-2.085335968	3.460296934	-0.60265	0.549093	-9.01187284	4.841200905	-9.011872842	4.841200905
X Variable 1	1.252448874	0.419268502	2.987224	0.004121	0.413191783	2.091705966	0.413191783	2.091705966

Figure 136: Test 4 Excel regression analysis during 1 minute of steady state temperature data

6.3.2 SPARROW MkVI Ground Testing

Hand Launch Testing

Hand launch testing was valuable for rapidly testing different configurations for SPARROW. Before the first successful flight there were approximately 15 failed attempts to get SPARROW airborne. Most of these involved bad throws, misconfigured avionics, and underpowered motor configurations. However, once a satisfactory configuration was obtained pilot feedback was collected and used to improve SPARROW's design. Towards the tail end of the failures, it was noted SPARROW was having trouble pulling up to gain altitude. While the control surfaces were sized appropriately based on both calculations and benchmarking, the flow disturbance due to the step on the airfoil was not accounted for. It was noted that while the elevons as originally designed were fully deflected up, they barely protruded above the top of the step. Due to the high aspect ratio of the wing the chord of the control surface was increased by extending the elevon back past the leading edge. This modification had a notable improvement in controllability and ultimately allowed for controlled flight to be possible.

SPARROW's first flight was a successful test. It was piloted entirely by a human with fly by wire assist and lasted roughly 45 seconds. No data was logged during this flight, but SPARROW demonstrated an ability to climb, cruise, turn, and land in a controlled manner. Pilot feedback from the flight noted that SPARROW was a little "squirrelly". To remedy this, the height of the vertical stabilizers was increased by 1" and handling notably improved.

Further flights were conducted with larger batteries in an attempt to get longer flight times. As an unintended consequence, different CG locations were also tested during these flights. This allowed for validation of neutral point locations and development of a CG envelope. Eventually in flight 4 a configuration was achieved which almost flew, but it was apparent that the limits of hand launching from the ground had been met for the given weight. During these tests each SPARROW airframe was able to attempt about 5 flights before fully breaking or gaining too much weight from hot glue repairs. These tests were by far the most destructive due to running into the ground at full throttle, often at an angle. However, only the airframes were ever damaged.

Table 32: CG location testing results for SPARROW MkVI aircraft

Flight	Weight (oz)	CG (in from TE)	Wind (mph)	Result
1	6.6	1/2	16	Flew well
2	7.3	1/4	16	Nosedive
3	8.1	1	16	Nose up
4	8.2	5/8	16	Almost flew

Choctaw Tower Hand Launch testing

The next step in the testing process involved tower launching from the Choctaw Daisy Ranch. Once again, these flights were done with a human pilot assisted by fly by wire. The first flight attempt immediately entered a flat spin and fell approximately 45 feet. This was most likely due to a bad throw. While spare airframes were available, the vehicle was undamaged and was immediately flown again for flight attempt #2. The 2nd flight was more of a pilot calibration flight. SPARROW was nearly pulled out before hitting the ground, but the throttle was cut out of caution to protect the airframe. SPARROW skidded for approximately 5 feet and was undamaged. Flight 3 was largely a success with SPARROW pulling out after dropping approximately 25 feet. SPARROW sustained flight for around 1 minute before the screws securing the motor vibrated out causing the motor to come loose and cut its own wires. The vehicle immediately fell from approximately 60 feet and landed undamaged minus the motor. This flight validated SPARROW's ability to fly in higher winds and in heavier configurations. Future SPARROWs had their motor screws secured using loctite to mitigate the risk of this happening again.

Table 33: Hand launch testing results for SPARROW MkVI aircraft

Flight	Weight (oz)	CG (in from TE)	Wind (mph)	Result
1	7.8	1/2	20	Flat spin/stall. Likely due to bad throw
2	7.8	1/2	20	Pulled up as hit ground
3	7.8	1/2	20	Pulled up after dropping 25 feet

6.3.3 SPARROW MkVI Drop Testing

Once SPARROW's flight ability was fully validated, the next step was configuring the autopilot. To accomplish this, a quadcopter was used to drop SPARROW from higher altitudes. The first successful drop test resulted in SPARROW showing severe oscillations in as seen in fig. 137. To compensate for this, the P gain was lowered. The second drop test exhibited significantly less oscillations and was much easier to control. However, it observed that it kept having a tendency to roll during flight. As a result, the I gain for roll was limited in the autopilot. Flight 3 as seen in fig. 138 show significant improvement in flight qualities, but it was noted the vehicle was unable to maintain altitude and had a tendency to randomly fall during flight before recovering itself. At the time it was assumed this was due to stalling. A fourth flight was then attempted in fly by wire mode and the pilot continued to have similar issues. After the flights it was noted that the motor made a squeaking noise when spinning along with a grinding feel. This motor was installed onto a thrust test stand, and it was observed that it produced less thrust and drew more current than expected. At some point during testing the motor had developed a bad bearing which negatively impacted performance. While further reviewing flight logs it was also noticed that the min and max speed and pitch limits for SPARROW were still set to the default values in the autopilot. These were also updated to match the predicted values.

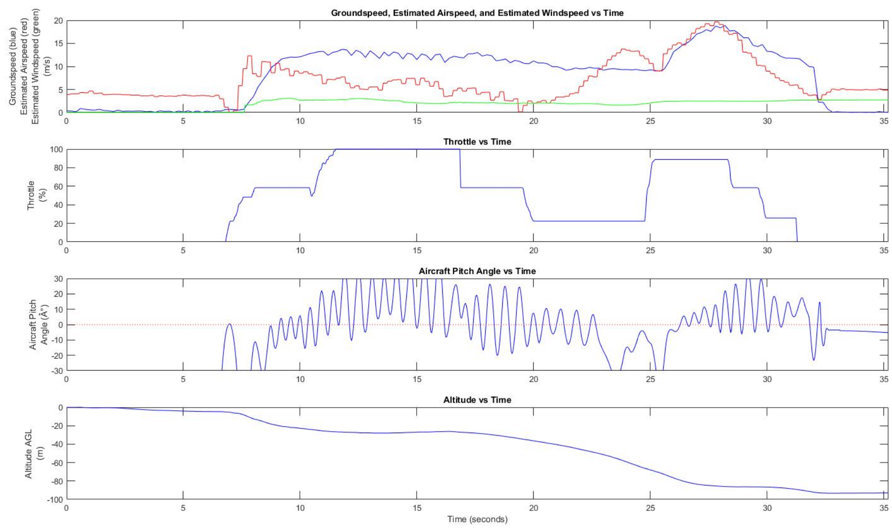

Figure 137: First drop test of SPARROW using autopilot

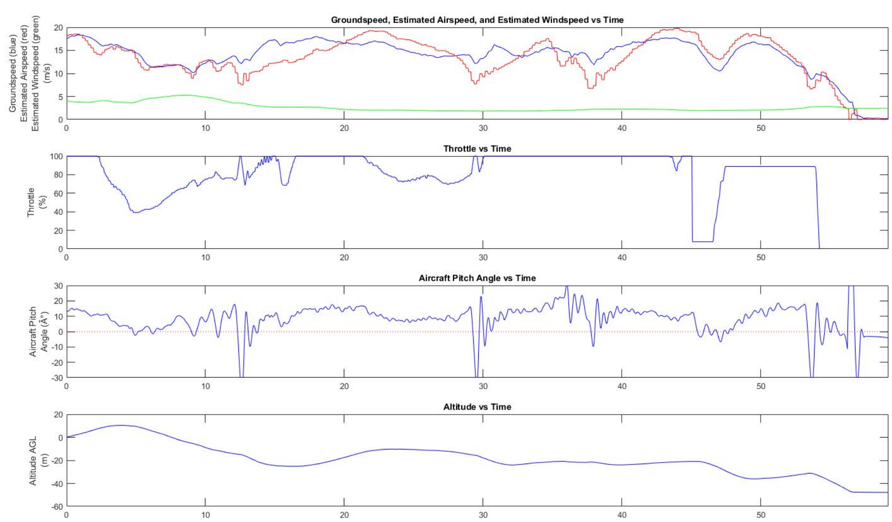

Figure 138: Third drop test of SPARROW using autopilot

Table 34: Drop testing results for SPARROW MkVI aircraft before tuning

Flight	Weight (oz)	CG (in from TE)	Wind (mph)	Result
1	8.6	1/2	2	Large oscillations in pitch
2	8.6	1/2	2	Had trouble maintaining altitude
3	8.6	1/2	2	Stalled but recovered
4	8.6	1/2	2	Had trouble maintaining altitude

With a new motor and updated autopilot limits, four more drop tests were performed 2 days later. These flights showed significant improvement from previous tests and demonstrated SPARROW was able to fly successfully in its current configuration. It also showed that SPARROW would be able to recover from being deployed in unexpected orientations which will occur while being deployed from the rocket.

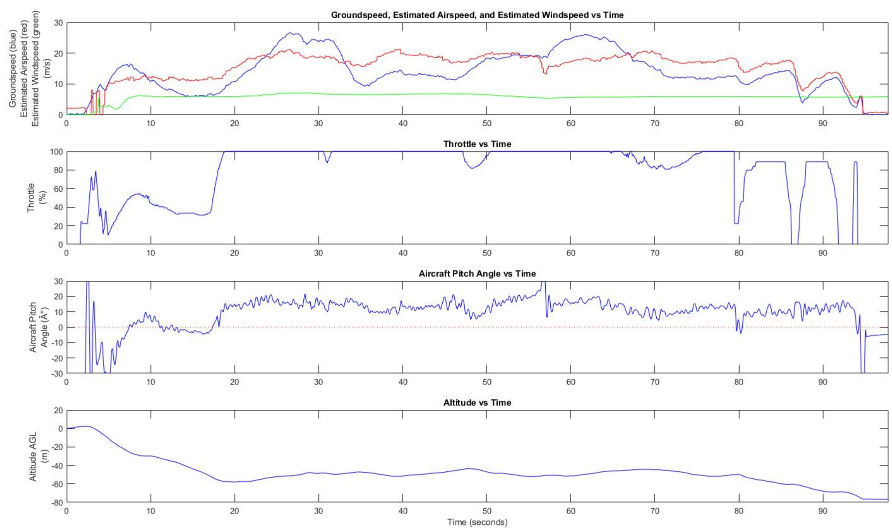

Figure 139: Fifth drop test of SPARROW using autopilot

Figure 140: View of SPARROW drop from SKB1000 before release

Figure 141: View of SPARROW drop from SKB1000 at release showing vehicle upside down

Figure 142: View of SPARROW drop from SKB1000 seconds after release showing vehicle already righted and flying

Table 35: Drop testing results for SPARROW MkVI aircraft after tuning

Flight	Weight (oz)	CG (in from TE)	Wind (mph)	Gusts (mph)	Result
5	8.6	1/2	9	12	Successful flight
6	8.6	1/2	8	17	Successfully flight
7	8.6	1/2	15	26	Stalled mid turn with gust
8	8.6	1/2	17	30	Successful Flight

6.3.4 SPARROW MkVII Testing

Discussion

During the initial SPARROW MkVII test flight it was noted that the vehicle exhibited a constant up and down pitching motion during flight. This behavior was fairly constant, although it alternated between being better or worse at all flight speeds. Based on this observation several changes were made in the field to mitigate the pitching motion. First the control surfaces were reinforced with extra tape the ensure there weren't any aeroelastic interactions occurring. This seemed to slightly improve the flight performance, but SPARROW still experienced oscillations in pitch during flight.

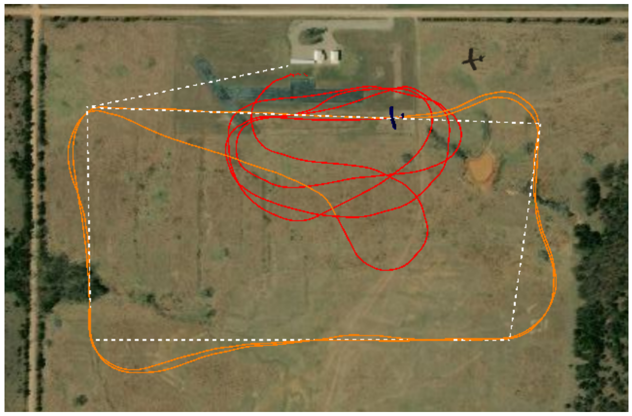

Figure 143: SPARROW MkVII flight test path before tuning

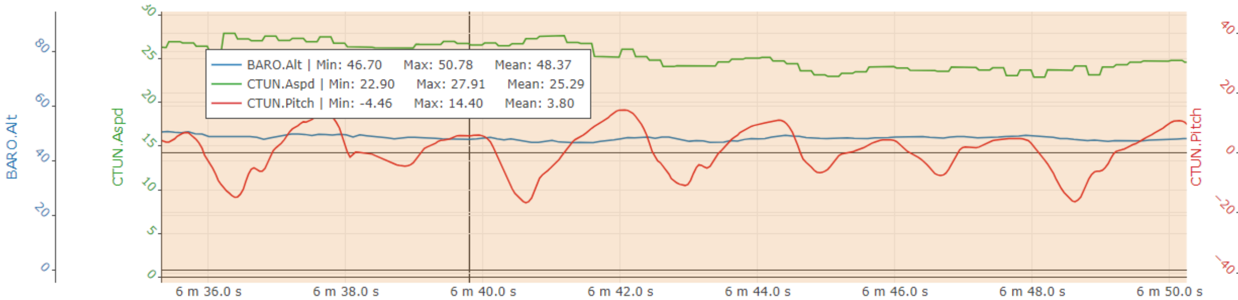

Figure 144: SPARROW MkVII attempt at steady level flight before tuning

Approximately 7 more test flights were performed in which PID tunings were adjusted along with parameters such as TRIM_PITCH_CD, TECS_SPDWEIGHT, and TECS_SINK_MIN. By monitoring the PID output graph in mission planner and adjusting these values during flight SPARROW was able to maintain steady level flight at speeds lower than approximately 50 ft/s as seen in fig. 146. At speeds above this SPARROW continued to experience significant oscillations in pitch, although it remained controllable. There are several potential reasons for this. It could be due to the way mission planner handles the scaling of control surface deflection with speed. Other aircraft at USRI have experienced similar issues in the past and needed a low speed tuning and a high speed tuning. It could also have been related to the wings simply being taped on for the test flights. At higher speeds the tape could have been more likely to shift in small amounts causing flutter. There could have also been an issue with cg location. Due to SPARROW being such a small aircraft there is only approximately 1/2 inch of margin for the CG to be located in and even being slightly off can cause unstable flight. Another possibility is it could be caused due to increased drag from the sensor inlet in the nose.

Figure 145: SPARROW MkVII flight test path after tuning

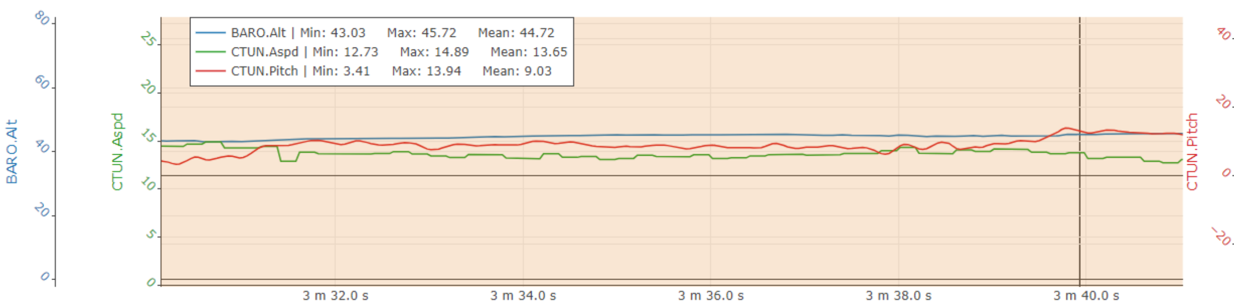

Figure 146: SPARROW MkVII steady level flight after tuning

Analysis

Based on the above test flights, SPARROW MkVII was reevaluated to see how it compared to its initial paper design and the results can be seen below in table 37. Stall velocity, max velocity, sink rate, and R/C max were obtained by analyzing flight logs. Endurance was calculated based on recording the battery used during the mission and extrapolating based on time of the mission.

In order to approximate a L/D value, the vehicle must be in steady level unaccelerated flight with the weight and thrust of the vehicle known. The weight of SPARROW is constant so that value was already given. To approximate thrust from partial throttle eqn. 6.3.1 was used where RPM is the speed at which the motor rotates, pitch is the propeller pitch in inches, and d is the propeller diameter in inches[22]. The results of this calculation can be seen below in fig. 36

$$F = 4.392399 * 10^{-8} * RPM * \frac{d^{3.5}}{\sqrt{pitch}} * (4.392399 * 10^{-8} * RPM * pitch - V0) \quad (6.3.1)$$

Table 36: Inputs and outputs used for dynamic thrust equation

Component	Value
V0	45 ft/s
RPM	17000
d	2.95
Pitch	3.6
Thrust	1.66 oz

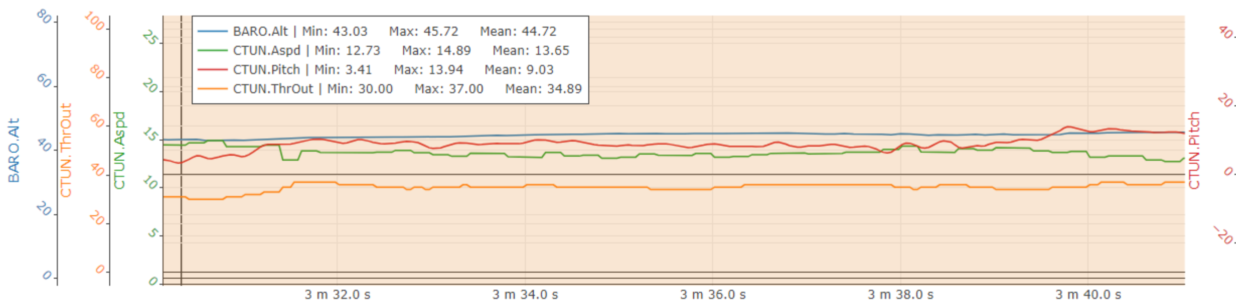

Figure 147: SPARROW MkVII during steady level flight with throttle percentage

Table 37: SPARROW's performance based on flight test data

Parameter	Flight Test Value	Calculated Value	Difference
Weight	0.8 lb.	0.55 lb.	45%
Aspect Ratio (front, rear)	11.6, 14.2	11.6, 14.2	NA
Wing Area (front, rear)	32.4 in^2, 21.25 in^2	32.4 in^2, 21.25 in^2	NA
Wing Span (front, rear)	18.5 in, 17 in	18.5 in, 17 in	NA
Vehicle L/D	7.7 (steady level)	9.3 (steady level)	13%
Cruise Velocity	45 ft/s	45 ft/s	NA
Stall Velocity	32 ft/s	36 ft/s	11%
Max Velocity	98 ft/s	125 ft/s	22%
Unpowered sink rate	6 ft/s	4 ft/s	50%
R/C (V = 65 ft/s)	12 ft/s	27 ft/s	55%
Endurance	15 min (30% throttle)	11.3 min (60% throttle)	33%

As seen in fig. 37, almost all of the predicted parameters were more optimistic than the actual performance experienced by SPARROW in flight. SPARROW MkVII was heavier than designed due to the decision to use 3d printed parts for complex geometries. This was particularly true for the wing attachment points. Even with low infill and thin walls on the prints, it proved difficult to keep the weight down. This could be improved by using different materials such as carbon fiber. The L/D value was also less than predicted, but the SPARROW used for the flight test had a cutout on the nose for sensor placement which created additional drag. The max velocity was 22% less than expected which is in part due to the pitching oscillations experienced by SPARROW at higher speeds. The unpowered sink rate was 2 ft/s higher than expected, but during this section of the flight SPARROW was being controlled by a human pilot so the trajectory wasn't optimized perfectly. The R/C is 55% less than expected, but this can be explained in part due to the pitch oscillations at higher speeds. Finally the endurance is better than expected due to SPARROW being able to maintain steady level flight at lower throttle than expected.

Meteorological Applications

Based the SPARROW sensor response time with the Nose V1 and the unpowered sink rate of 6 ft/s, SPARROW can resolve a temperature difference of 10 C in 162 feet of altitude. Practically this means that if SPARROW encountered a 10 C temperature differential in flight, the atmospheric layer must be at least 162 feet tall for SPARROW to capture it. The vertical resolution would be smaller with a lower temperature gradient, and would be also be improved with better sensor placement on SPARROW as described in section 6.3.4. For reference, if the iMet sensor were capable of flying the same as the SPARROW, the resolution for a 10 C temperature gradient would be 90 feet of altitude. However, if the iMet sensor was attached to a weather balloon ascending at 18 ft/s it would take 270 feet of altitude to resolve the 10 C difference. This shows that the SPARROW is capable of collecting higher resolution vertical data than a weather balloon. SPARROW also has the benefit of being able to maintain steady level flight for up to 14 minutes for additional observation of desired areas.

During flight testing it was noted that there is another potential mission for SPARROW due to its ability to be hand launched. If two separate batteries were used, one for the motor and one for the avionics, it would be possible to fly up to approximately 3,000 feet under the power of its motor until the battery dies. From this point it could glide down unpowered. This allows SPARROW to act as a rapidly deployable weather research system which can be easily transported in almost any vehicle due to its small size and weight. SPARROW can be transported fully assembled and can be easily hand launched from any terrain.

6.4 Mission Validation

SPARROW was flown on a simulated mission in which it completed orbits while collecting temperature and humidity data. This flight shows that SPARROW is capable of collecting in-situ atmospheric data during a mission. The flight lasted approximately 6 minutes. Of note is the sharp decline in values at the beginning of the flight. This is in line with what was experienced in ground testing and shows how the sensors need airflow to operate properly. Further work is needed to validate this data including an in vehicle calibration.

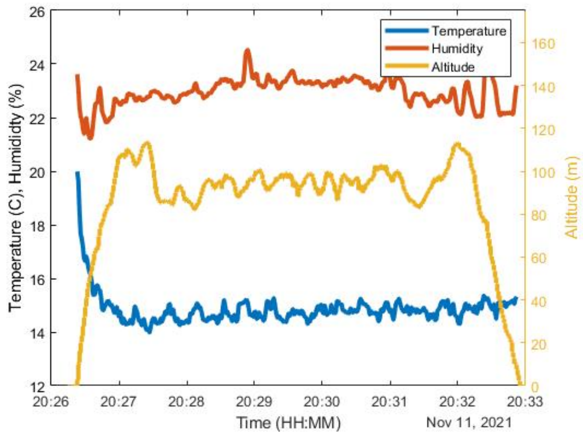

Figure 148: Temperature and humidity data collected during SPARROW flight

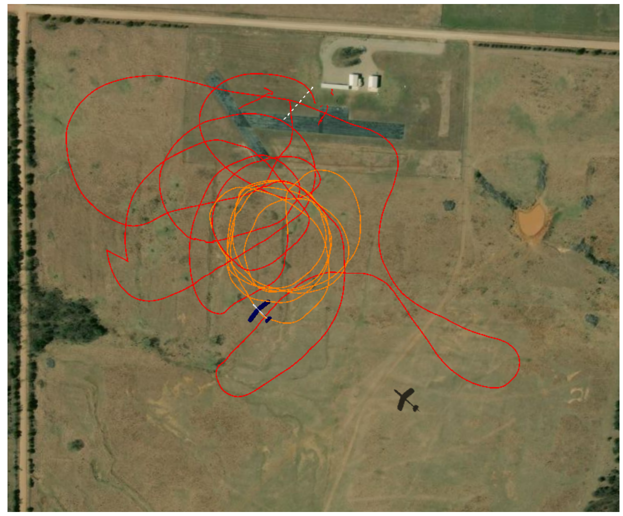

Figure 149: Flight path of SPARROW while collecting temperature and humidity data

CHAPTER VII

Conclusion

7.1 Summary

SPARROW was designed based around the highly constrained problem of functioning as a tube deployed micro air vehicle capable of collecting atmospheric data. To accomplish this, a set of design requirements were derived based on current methods of atmospheric profiling including radiosondes and dropsondes which are used by the national weather service. These requirements also used historical weather data as a baseline for vehicle capabilities to ensure effectiveness. A micro air vehicle was then designed based around these requirements to accomplish an atmospheric profiling mission which includes the collection of temperature and humidity data during flight. Next a suite of sensors were evaluated to determine their effectiveness while integrated into SPARROW, and multiple different locations for sensor integration were explored. Finally, SPARROW was test flown successfully both with sensors and its flight performance was then analyzed to evaluate how it would perform compared to existing atmospheric profiling methods. It was shown that SPARROW is capable of collecting higher resolution vertical data than a weather balloon even in a gliding configuration. In addition to having the capability of being deployed from a rocket or weather balloon, it was also shown SPARROW could complete a mission where it is hand launched from the ground where it then flies up under its own power and glides down from altitude. Such a mission would be valuable from a rapid sampling perspective due to the ease of transporting it. Based on the results of flight testing, SPARROW has been shown to complete all the objectives outlined for the vehicle.

7.2 Cost Analysis

The cost for each component of SPARROW can be seen below in table 38. These values only represent material cost and do not include cost of labor. Each SPARROW vehicle takes approximately 6 hours of labor from raw materials to flight testing.

Table 38: Cost breakdown by component for SPARROW MkVII

Category	Item	Cost ($)	Totals ($)
Airframe	Fuselage + Wings	30	
Airframe	Nose	1	
Airframe	Motor Mount	1	
Airframe			31
Avionics	Control Zero	350	
Avionics	GPS	70.9	
Avionics	Radio	38.9	
Avionics	Receiver	23.08	
Avionics	ESC/BEC	21.99	
Avionics	Servo x2	30	
Avionics	Battery	12.79	
Avionics	Motor+Prop	9.62	
Avionics			557.28
Payload	Meteorological Sensors	30	
Payload			30
Total Amount			$618.28

Based on raw materials cost, SPARROW is competitive to the radiosonde which is runs approximately $200. After 4 flights with reuse, the cost of materials can be completely recouped.

7.3 Future Work

Suggested future work for SPARROW is shown in the list below. While SPARROW has been shown to be capable of completing an atmospheric profiling mission, further testing and calibration would bring it to a finished product which can be used for meteorological work.

1. Calibrate sensors in atmospheric chamber
2. Deploy from rocket or weather balloon
3. Evaluate multiple SPARROWs flying at once
4. Integrate folding wing
5. Further integrate avionics into smaller package

REFERENCES

[1] Edward E. Adcock, B. D. Allen, James H. Neilan, Matthew P. Vaughn, Ralph A. Williams, Zachary R. Johns, Brian E. Duvall, and Nicholas H. Rymer, *Autonomous distributed atmospheric measurement acquisition (adama) – a multi-agent suas mission*, AIAA Scitech 2020 Forum, 2020.

[2] Roberto Albertani, Frank Boria, Scott Bowman, Dan Claxton, Peter Ifju, Baron Johnson, Kyu Lee, Mike Morton, and Mike Sytsma, *The university of florida autonomous micro air vehicle*, (2021).

[3] J.D. Anderson, *Aircraft performance & design*, McGraw-Hill international editions, McGraw-Hill Education, 1999.

[4] Jason Cantrell, Bradley LaCroix, and Peter Ifju, *Passive roll compensation on micro air vehicles with perimeter reinforced membrane wings.*

[5] Phillip B. Chilson, Tyler M. Bell, Keith A. Brewster, Gustavo Britto Hupsel de Azevedo, Frederick H. Carr, Kenneth Carson, William Doyle, Christopher A. Fiebrich, Brian R. Greene, James L. Grimsley, and et al., *Moving towards a network of autonomous uas atmospheric profiling stations for observations in the earth's lower atmosphere: The 3d mesonet concept*, Sensors **19** (2019), no. 12, 2720.

[6] Joseph J. Cione (ed.), *"noaa uas symposium"*, NOAA, October 2016.

[7] National Research Council, *Observing weather and climate from the ground up: A nationwide network of networks*, The National Academies Press, Washington, DC, 2009.

[8] eCalc, *propcalc - propeller calculator*, `https://ecalc.ch/motorcalc.php`, Accessed: 2021-11-25.

[9] Daniel J. Edwards, Aaron D. Kahn, Stearns B. Heinzen, Trenton Z. Young, Nicholas J. Arnold, Daniel Newton, Bob Eber, and Samuel V. Carter, *Cicada flying circuit board unmanned aerial vehicle*, 2018 AIAA Aerospace Sciences Meeting, 2018.

[10] Jack S. Elston, Jason Roadman, Maciej Stachura, Brian Argrow, Adam Houston, and Eric Frew, *The tempest unmanned aircraft system for in situ observations of tornadic supercells: Design and vortex2 flight results*, Journal of Field Robotics **28** (2011), no. 4, 461–483.

[11] Ioannis K. Erripis, *Prioria maverick, flexible wing uas*, `https://robohub.org/prioria-maverick-flexible-wing-uas/`, Accessed: 2021-11-25.

[12] Lauren Everett (ed.), *The future of atmospheric boundary layer observing, understanding, and modeling: Proceedings of a workshop*, Washington DC, National Academies of Sciences, Engineering, and Medicine, The National Academies Press, 2018.

[13] Shea D. Fehrenbach and Jamey D. Jacob, *Design of a rocketsonde launched uas*, Master's thesis, Oklahoma State University, 2016.

[14] Kyle T. Hickman, James C. Brenner, Andrew L. Ross, Jamey D. Jacob, and Victoria A. Natalie, *Development of low cost, rapid sampling atmospheric data collection system: Part 1 – fully additive-manufactured multi-hole prob*, AIAA Scitech 2021 Forum, 2021.

[15] iMet, *imet-1-abxn radiosonde 403 mhz gps with pressure sensor*, `https://www.intermetsystems.com/ee/pdf/202060_iMet-1-ABxn_Data_161006.pdf`, accessed October 10, 2021.

[16] A. Kräuchi and R. Philipona, *Return glider radiosonde for in situ upper-air research measurements*, Atmospheric Measurement Techniques **9** (2016), no. 6, 2535–2544.

[17] Jeffrey K. Lazo, Megan Lawson, Peter H. Larsen, and Donald M. Waldman, *U.s. economic sensitivity to weather variability*, Bulletin of the American Meteorological Society **92** (2011), no. 6, 709–720.

[18] Robert C. Nelson, *Flight stability and automatic control*, 2 ed., McGraw-Hill, New York, 1998.

[19] D.P. Raymer, American Institute of Aeronautics, and Astronautics, *Aircraft design: A conceptual approach*, AIAA Textbook Series, American Institute of Aeronautics and Astronautics, 1989.

[20] John Rogers, Bong Hoon Kim, Kan Li, Jin-Tae Kim, Yoonseok Park, Hokyung Jang, Xueju Wang, Zhaoqian Xie, Sang Won, Woo Jang, Kun Lee, Ted Chung, Yei Hwan Jung, Seung Heo, Yechan Lee, Juyun Kim, Cai Tengfei, Yeonha Kim, Poom Prasopsukh, and Yihui Zhang, *Three-dimensional electronic microfliers with designs inspired by wind-dispersed seeds*, (2021).

[21] National Weather Service, *Radiosonde observation*, `https://www.weather.gov/upperair/factsheet`, accessed October 10, 2021.

[22] Gabriel Staples, *Propeller static & dynamic thrust calculation - part 1 of 2*, `https://www.electricrcaircraftguy.com/2013/09/propeller-static-dynamic-thrust-equation.html`, Accessed: 2021-11-25.

[23] Black Swift, *Black swift s0 uas*, `https://bst.aero/black-swift-s0-vtol-uas/`, Accessed: 2021-11-25.

[24] Lance W. Traub and Cory Coffman, *Efficient low-reynolds-number airfoils*, Journal of Aircraft **56** (2019), no. 5, 1987–2003.

[25] Vaisala, *Dropsonde rd41*, https://www.vaisala.com/sites/default/files/documents/RD41-Datasheet-B211706EN.pdf, accessed October 10, 2021.

[26] ———, *Vaisala radiosonde rs92-sgp*, https://www.vaisala.com/sites/default/files/documents/RS92SGP-Datasheet-B210358EN-F-LOW.pdf, accessed October 10, 2021.

[27] XFLR5, *Xflr5*, http://www.xflr5.tech/xflr5.htm, Accessed: 2021-11-25.

APPENDICES

Thrust and Power Curve Code

```
rho5k = 0.066135672;
rho0k = 0.0765;
rho20k = 0.0408;
rho30k = 0.0287;
rho10k = 0.0565;
S = 0.35;
AR = 12.584;
e = 0.9;
pi = 3.14159;
W = 0.77;

%Thrust = [2.5,3.4,4.4,5.6,6.9,8.4,9.9,11.7,11.7];
%VT = [27,50,57,64,72,79,86,93,93];
%V =
    [5.44,10.87,16.31,21.74,27.18,32.61,38.05,43.48,48.92,54.35,59.79,65.22,70
%CD0 =
    [0.048,0.042,0.039,0.037,0.035,0.034,0.033,0.0326,0.032,0.031,0.0309,0.03,


V =
    [10.87,16.31,21.74,27.18,32.61,38.05,43.48,48.92,54.35,59.79,65.22,70.66,76
%CD0 =
    [0.0329,0.0344,0.0355,0.0364,0.0371,0.0378,0.0384,0.0389,0.0394,0.0398,0.0
CD00k = 0.039;
CD05k = 0.039;
CD010k = 0.043;
CD020k = 0.048;
CD030k = 0.055;
%Thrust5k = [5.3,5.3,5.3,5.4,5.4,5.4,5.4,5.1,4.3,3.5,2.7,];
VT = [0,10,20,30,40,50,60,70,80,90,100];
Thrust0k = [8,8,8.1,8.1,8.1,8.2,8.2,8.3,7.4,6.4,5.3];
```

```
Thrust5k = [7.2,7.2,7.3,7.3,7.3,7.4,7.4,7.4,6.8,5.9,4.9];
Thrust10k = [7.1,7.1,7.2,7.2,7.2,7.2,7.3,7.3,6.9,6,5];
Thrust20k = [4.9,4.9,4.9,5,5,5.1,5.1,5.1,5,4.4,3.8];
Thrust30k = [3.7,3.7,3.7,3.7,3.8,3.8,3.8,3.8,3.7,3.7,3.7];


VTf = VT.*1.467; %convert to ft/s


Thrustlb0k = (Thrust0k1).*0.0625; %convert to lbs
Thrustlb5k = (Thrust5k1).*0.0625; %convert to lbs
Thrustlb10k = (Thrust10k1).*0.0625; %convert to lbs
Thrustlb20k = (Thrust20k1).*0.0625; %convert to lbs
Thrustlb30k = (Thrust30k1).*0.0625; %convert to lbs




% q5k = V5k.^2 .* (0.5 * rho5k / 32.2) ;
% D05k = q5k * CD05k * S ;
% CL5k = W ./ (q5k*S);
% CDi5k = CL5k.^2 ./ (pi*e*AR);
% Di5k = CDi5k .* (q5k * S);
% D5k = Di5k + D05k;

[D00k,Di0k,D0k] = aero(rho0k,V,CD00k,W,S,e,AR);
[D05k,Di5k,D5k] = aero(rho5k,V,CD05k,W,S,e,AR);
[D010k,Di10k,D10k] = aero(rho10k,V,CD010k,W,S,e,AR);
[D020k,Di20k,D20k] = aero(rho20k,V,CD020k,W,S,e,AR);
[D030k,Di30k,D30k] = aero(rho30k,V,CD030k,W,S,e,AR);

[PA0k,PR0k,EP0k,Vep0k] = powerr(VTf,V,Thrustlb0k,D0k);
[PA10k,PR10k,EP10k,Vep10k] = powerr(VTf,V,Thrustlb10k,D10k);
[PA20k,PR20k,Ep20k,Vep20k] = powerr(VTf,V,Thrustlb20k,D20k);
[PA30k,PR30k,Ep30k,Vep30k] = powerr(VTf,V,Thrustlb30k,D30k);


%plot(V,D00k,V,Di0k,V,D0k,VTf,Thrustlb0k)

%%TR 0k 10k 20k 30k
plot(V,D0k,VTf,Thrustlb0k,V,D10k,VTf,Thrustlb10k,V,D20k,VTf,
    Thrustlb20k,V,D30k,VTf,Thrustlb30k)
legend('Thrust Required 0k ft','Thrust Avalaible 0k ft','Thrust
    Required 10k ft','Thrust Avalaible 10k ft','Thrust Required 20k
```

```
    ft','Thrust Avalaible 20k ft','Thrust Required 30k ft','Thrust
    Avalaible 30k ft')
xlim([15 150])
xlabel('Velocity (ft/s)')
ylabel('Thrust (lbf)')
figure

%%PR
plot(V,PR0k,VTf,PA0k,V,PR10k,VTf,PA10k,V,PR20k,VTf,PA20k,V,PR30k,
    VTf,PA30k)
legend('Power Required 0k ft','Power Avalaible 0k ft','Power
    Required 10k ft','Power Avalaible 10k ft','Power Required 20k
    ft','Power Avalaible 20k ft','Power Required 30k ft','Power
    Avalaible 30k ft')
xlim([15 150])
xlabel('Velocity (ft/s)')
ylabel('Power (lb ft/s)')


%plot(V,D020k,V,Di20k,V,D20k,VTf,Thrustlb20k)

%xline(36)
%xline(44)
%yline(2.5/16)
%xlim([15 150])
%ylim([0 0.2])
%legend('Profile Drag 0k ft','Induced Drag 0k ft','Total Drag 0k
    ft','Thrust Available 0k ft')%,'Stall Velocity','Cruise
    Velocity')
%xlabel('Velocity (ft/s)')
%ylabel('Drag (lbf)')

function [D0,Di,D] = aero(rho,V,CD0,W,S,e,AR)

q = V.^2 .* (0.5 * rho / 32.2) ;
D0 = q * CD0 * S ;
CL = W ./ (q*S);
CDi = CL.^2 ./ (pi*e*AR);
Di = CDi .* (q * S);
D = Di + D0;

end

function [PA,PR,EP,Vep] = powerr(V1,V2,TA,TR)
```

```
PA = V1 .* TA;
PR = V2 .* TR;
j = 0;
EP =1;
Vep = 1;


% for i = 0:9
%
%       if PA(i) > PR(i)
%           Vep(j) = V(i);
%           EP(j) = PA - PR;
%           j = j+1;
%       end

%end
end
```

Glide Analysis Code

```
function paperplane

clear all

%       Example 1.3-1 Paper Airplane Flight Path
%       Copyright 2005 by Robert Stengel
%       August 23, 2005

        global CL CD S m g rho
        S               =   0.24;               % Reference Area, ft^2
        AR              =       11.57;          % Wing Aspect Ratio
        e               =       0.9;            % Oswald Efficiency Factor;
    W       =     0.8;           % Airplane Weight, lbf
        g               =       32.2;           % Gravitational acceleration, ft/s^2
    m           =       W./g;                   % Airplane Mass, slug (lbs

        rho             =       0.002;          % Air density at Sea Level, slug/ft^3
        CLa             =       0.107%3.141592 * AR/(1 + sqrt(1 +
```

```
(AR / 2)^2));
                                                % Lift-Coefficient Slope, per rad
        CDo         =       0.039;              % Zero-Lift Drag Coefficient
        epsilon =       1 / (3.141592 * e * AR);% Induced Drag Factor
        CL          =       sqrt(CDo / epsilon);    % CL for Maximum Lift/Drag Ratio
        CD          =       CDo + epsilon * CL^2;   % Corresponding CD
        LDmax   =       CL / CD;                % Maximum Lift/Drag Ratio
        Gam         =       -atan(1 / LDmax);       % Corresponding Flight Path Angle, rad
        V           =       sqrt(2 * m * g /(rho * S * (CL * cos(Gam) - CD * sin(Gam))))
                                                % Corresponding Velocity, m/s

        Alpha   =       CL / CLa                % Corresponding Angle of Attack, rad

    % x(:,1) velocity
    % x(:,2) flight path angle
    % x(:,3) altitude
    % x(:,4) range

    %initial speed (fps)
    %V=50;

%       a) Equilibrium Glide at Maximum Lift/Drag Ratio
        H           =       300;                % Initial Height, ft
        R           =       0;                  % Initial Range, ft
        to          =       0;                  % Initial Time, sec
```

```
        tf                  =         H/3.9;                    % Final
          Time, sec
        tspan    =        [to tf];
        xo                  =         [V;Gam;H;R];
        [ta,xa] =         ode23(@EqMotion,tspan,xo);

%       b) 10 percent velocity increase
        xo                  =         [1.25*V;Gam;H;R];
        [tb,xb] =         ode23(@EqMotion,tspan,xo);

%       c) 5 percent velocity increase
        xo                  =         [0.5*V;Gam;H;R];
        [tc,xc] =         ode23(@EqMotion,tspan,xo);

%       d) 5 percent velocity decrease
        xo                  =         [0.5*V;0;H;R];
        [td,xd] =         ode23(@EqMotion,tspan,xo);

        figure
        plot(ta,xa(:,3))%,xb(:,4),xb(:,3),xc(:,4),xc(:,3),xd(:,4),
          xd(:,3))
        xlabel('Time, s'), ylabel('Height, ft'), grid

    legend('SPARROW glide path')%,'1.1V_o','1.05V_o','0.95V_o')

%       figure
%       subplot(2,2,1)
%       plot(ta,xa(:,1),tb,xb(:,1),tc,xc(:,1),td,xd(:,1))
%       xlabel('Time, s'), ylabel('Velocity, ft/s'), grid
%       subplot(2,2,2)
%       plot(ta,xa(:,2),tb,xb(:,2),tc,xc(:,2),td,xd(:,2))
%       xlabel('Time, s'), ylabel('Flight Path Angle, rad'), grid
%       subplot(2,2,3)
%       plot(ta,xa(:,3),tb,xb(:,3),tc,xc(:,3),td,xd(:,3))
%       xlabel('Time, s'), ylabel('Altitude, ft'), grid
%       subplot(2,2,4)
%       plot(ta,xa(:,4),tb,xb(:,4),tc,xc(:,4),td,xd(:,4))
%       xlabel('Time, s'), ylabel('Range, ft'), grid

    return

        function xdot = EqMotion(t,x)
%       Fourth-Order Equations of Aircraft Motion

```

```
global CL CD S m g rho

V       =       x(1);
Gam     =       x(2);
q       =       0.5 * rho * V^2;        % Dynamic Pressure, psf

xdot    =       [(-CD * q * S - m * g * sin(Gam)) / m
                    (CL * q * S - m * g * cos(Gam)) / (m * V)
                    V * sin(Gam)
                    V * cos(Gam)];
```

Analysis Equations

Wing Geometry

$\Lambda_{LE} := 0$

$b_{wing1} := 20.25in = 1.687 \cdot ft$	18.5	Current	20.25
$b_{wing2} := 17.75in = 1.479 \cdot ft$	17		17.75

$c_{wing1} := 1.75in = 0.146 \cdot ft$

$c_{wing2} := 1.25in = 0.104 \cdot ft$

$Sweep_{wing1} := 0deg = 0 \cdot rad$

$Sweep_{wing2} := 0deg = 0 \cdot rad$

Weights

$W_{ControlZero} := 0.494oz$

$W_{WH1} := 0.211oz$

$W_{WH2} := 0.06oz$

$W_{ServoBoard} := 0.142oz$

$W_{GPS} := 0.294oz$

$W_{Radio} := 0.566oz$

$W_{Receiver} := 0.124oz$

$W_{ESC} := 0.33oz$

$W_{Servox2} := 0.4oz$

$W_{BatteryCable} := 0.184oz$

$W_{Battery} := 2.358oz$

$W_{MotorProp} := 0.738oz$

$W_{Nose} := 0.506oz$

$W_{MM} := 0.465oz$

$W_{FuselageWings} := 1.738oz$

$W_{PTH} := 0.5oz$

$W_{Payload} := W_{ControlZero} + W_{WH1} + W_{WH2} + W_{ServoBoard} + W_{GPS} + W_{GPS} + W_{Radio} + W_{Rec}$

$W_{Propulsion} := W_{ESC} + W_{MotorProp}$

$W_{Airframe} := W_{Nose} + W_{MM} + W_{FuselageWings}$

$W := W_{Airframe} + W_{Battery} + W_{Payload} + W_{Propulsion} = 0.588\,lb$

$W := 0.77lb$

$W_{corr} := 32.2 \frac{ft}{s^2}$

Constants

$\rho_{5k} := 20.48 \cdot 10^{-4} \frac{slug}{ft^3}$

$\mu_{5k} := 3.637 \cdot 10^{-7} \frac{slug}{ft \cdot s}$

Assumptions

$C_{l\_\alpha\_assumed} := 0.107$ from circ airfoil data

from circ airfoil data

$C_{l\_max\_assumed} := 1.26$

$\alpha_{stall\_assumed} := 11$

$V_{assumed} := 55 \frac{ft}{s}$

$C_{D0\_assumed} := 0.039$

Simulation

$C_{l\_\alpha} := C_{l\_\alpha\_assumed}$

$C_{l\_max} := C_{l\_max\_assumed}$

$\alpha_{stall} := \alpha_{stall\_assumed}$

$C_{D0} := C_{D0\_assumed}$

$V_{cruise} := V_{assumed}$

$\rho := \rho_{5k}$

$\mu := \mu_{5k}$

$q := 0.5 \cdot \rho \cdot V_{cruise}{}^{2} = 99.662 \cdot \frac{lb}{ft \cdot s^2}$

Weight Fractions

$f_{airframe} := \frac{W_{Airframe}}{W} = 0.22$

$f_{propulsion} := \frac{W_{Propulsion}}{W} = 0.087$

$f_{battery} := \frac{W_{Battery}}{W} = 0.191$

$f_{payload} := \frac{W_{Payload}}{W} = 0.265$

Calculated Parameters

$RE := \frac{\rho \cdot V_{cruise} \cdot c_{wing1}}{\mu} = 4.517 \times 10^4$

$M := \frac{V_{cruise}}{340 \frac{m}{s}} = 0.049$

2 D Calculations

$AR_{wing1} := \frac{b_{wing1}}{c_{wing1}} = 11.571$

$AR_{wing2} := \frac{b_{wing2}}{c_{wing2}} = 14.2$

$S_{wing1} := b_{wing1} \cdot c_{wing1} = 0.246 \cdot ft^2$

$S_{wing2} := b_{wing2} \cdot c_{wing2} = 0.154 \cdot ft^2$

$S_{total} := S_{wing1} + S_{wing2} = 0.4 \cdot ft^2$

$$AR_{avg} := \frac{AR_{wing1} \cdot S_{wing1} + AR_{wing2} \cdot S_{wing2}}{S_{wing1} + S_{wing2}} = 12.584$$

$$e_{wing1} := \frac{2}{2 - AR_{wing1} + \left[4 + AR_{wing1}^{2} \cdot \left(1 + \tan\left(Sweep_{wing1}\right)^{2}\right)\right]^{0.5}} = 0.921$$

eqn4.15
Brandt

$$e_{wing2} := \frac{2}{2 - AR_{wing2} + \left[4 + AR_{wing2}^{2} \cdot \left(1 + \tan\left(Sweep_{wing2}\right)^{2}\right)\right]^{0.5}} = 0.935$$

$$Loading_{wing1} := \frac{W}{S_{wing1}} = 3.129 \frac{lb}{ft^2}$$

$$Loading_{wing2} := \frac{W}{S_{wing2}} = 4.997 \frac{lb}{ft^2}$$

$$e_{total} := \frac{S_{wing1} \cdot e_{wing1} + S_{wing2} \cdot e_{wing2}}{S_{wing1} + S_{wing2}} = 0.926$$

$$Cl_{required} := \frac{W \cdot W_{corr}}{q \cdot S_{total}} = 0.622$$

Old Stuff

3 D Calculations

$$e_{0\_wing1} := 4.61 \cdot \left(1 - 0.045 \cdot AR_{wing1}^{0.68}\right)\left(\cos\left(\Lambda_{LE}\right)\right)^{0.15} - 3.1 = 0.413$$

eqn 4.30 brandt

$$e_{0\_wing2} := 4.61 \cdot \left(1 - 0.045 \cdot AR_{wing2}^{0.68}\right)\left(\cos\left(\Lambda_{LE}\right)\right)^{0.15} - 3.1 = 0.25$$

$$k_{wing1} := \frac{1}{\pi \cdot e_{0\_wing1} \cdot AR_{wing1}} = 0.067$$

eqn 4.27 brandt

$$k_{wing2} := \frac{1}{\pi \cdot e_{0\_wing2} \cdot AR_{wing2}} = 0.09$$

$$k_{total} := \frac{k_{wing1} \cdot S_{wing1} + k_{wing2} \cdot S_{wing2}}{S_{wing1} + S_{wing2}} = 0.075$$

$$C_{L\_\alpha\_wing1} := \frac{C_{l\_\alpha}}{1 + \frac{57.3 \cdot C_{l\_\alpha}}{\pi \cdot AR_{wing1} \cdot e_{wing1}}} = 0.09$$

Brandt eqn 4.14

$$C_{L\_\alpha\_wing2} := \frac{C_{l\_\alpha}}{1 + \frac{57.3 \cdot C_{l\_\alpha}}{\pi \cdot AR_{wing2} \cdot e_{wing2}}} = 0.093$$

$$C_{L\_max\_wing1} := C_{L\_\alpha\_wing1} \cdot \alpha_{stall} = 0.995$$

$$C_{L\_max\_wing2} := C_{L\_\alpha\_wing2} \cdot \alpha_{stall} = 1.026$$

$$C_{L\_max\_total} := \frac{C_{L\_max\_wing1} \cdot S_{wing1} + C_{L\_max\_wing2} \cdot S_{wing2}}{S_{wing1} + S_{wing2}} = 1.007$$

$$C_{L\_MaxE\_wing1} := \sqrt{\frac{3C_{D0}}{k_{wing1}}} = 1.326$$

Minimum power required

$$C_{L\_MaxE\_wing2} := \sqrt{\frac{3C_{D0}}{k_{wing2}}} = 1.142$$

$$C_{L\_MaxE\_total} := \frac{C_{L\_MaxE\_wing1} \cdot S_{wing1} + C_{L\_MaxE\_wing2} \cdot S_{wing2}}{S_{wing1} + S_{wing2}} = 1.255$$

$$C_{D\_MaxE} := C_{D0} + k_{total} \cdot C_{L\_MaxE\_total}^{2} = 0.158$$

$$C_{L\_MaxR\_wing1} := \sqrt{\frac{C_{D0}}{k_{wing1}}} = 0.766$$

Assume parasite drag = induced drag for min total drag

$$C_{L\_MaxR\_wing2} := \sqrt{\frac{C_{D0}}{k_{wing2}}} = 0.659$$

$$C_{L\_MaxR\_total} := \frac{C_{L\_MaxR\_wing1} \cdot S_{wing1} + C_{L\_MaxR\_wing2} \cdot S_{wing2}}{S_{wing1} + S_{wing2}} = 0.725$$

$$C_{D\_MaxR} := C_{D0} + k_{total} \cdot C_{L\_MaxR\_total}^{2} = 0.079$$

$$C_D := C_{D0} + k_{total} \cdot C_{L\_max\_total}^{2} = 0.116$$

$$L\_D := \frac{Cl_{required}}{C_D} = 5.382$$

$$C_{l\_LDmax} := \sqrt{\frac{C_{D0}}{k_{wing1}}} = 0.766$$

2D

$$C_{D0} := 0.025$$

Performance

$$W_{max} := \frac{q \cdot S_{total} \cdot C_{L\_max\_total}}{W_{corr}} = 19.953 \cdot oz$$

$$V_{stall\_wing1} := \sqrt{\frac{W \cdot W_{corr}}{0.5 \cdot \rho \cdot S_{wing1} \cdot C_{L\_max\_wing1}}} = 55.443 \cdot \frac{ft}{s}$$

$$V_{stall\_wing2} := \sqrt{\frac{W \cdot W_{corr}}{0.5 \cdot \rho \cdot S_{wing2} \cdot C_{L\_max\_wing2}}} = 68.993 \cdot \frac{ft}{s}$$

$$V_{stall} := \sqrt{\frac{W \cdot W_{corr}}{0.5 \cdot \rho \cdot S_{total} \cdot C_{L\_max\_total}}} = 43.218 \frac{ft}{s}$$

$$L_{Dmax\_wing1} := \frac{1}{2\sqrt{k_{wing1} \cdot C_{D0}}} = 12.26$$

eqn 5.23 brandt

$$L_{Dmax\_wing2} := \frac{1}{2\sqrt{k_{wing2} \cdot C_{D0}}} = 10.555$$

$$L_{Dmax} := \frac{L_{Dmax\_wing1} \cdot S_{wing1} + L_{Dmax\_wing2} \cdot S_{wing2}}{S_{wing1} + S_{wing2}} = 11.603$$

$$V_{MaxE} := \sqrt{\frac{2 \cdot W \cdot W_{corr}}{\rho \cdot S_{total} \cdot C_{L\_MaxE\_total}}} = 38.709 \frac{ft}{s}$$

$$V_{MaxR} := \sqrt{\frac{2 \cdot W \cdot W_{corr}}{\rho \cdot S_{total} \cdot C_{L\_MaxR\_total}}} = 50.943 \frac{ft}{s}$$

$$q_{MaxE} := 0.5 \cdot \rho \cdot V_{MaxE}^{\ 2} = 0.011\,psi$$

$q_{MaxR} := 0.5 \cdot \rho \cdot V_{MaxR}^{2} = 0.018\,psi$

$D_{MaxE} := C_{D\_MaxE} \cdot q_{MaxE} \cdot S_{total} = 0.097\,lbf$

$D_{MaxR} := C_{D\_MaxR} \cdot q_{MaxR} \cdot S_{total} = 0.084\,lbf$

$SinkRate_{MaxE} := \frac{V_{MaxE} \cdot D_{MaxE}}{W \cdot W_{corr}} = 4.87\,\frac{ft}{s}$

$SinkRate_{MaxR} := \frac{V_{MaxR} \cdot D_{MaxR}}{W \cdot W_{corr}} = 5.528\,\frac{ft}{s}$ Brandt 5.4

$R_t := 1hr$

$n := 1.3$

$\eta_{tot} := 0.6$

$V_{Battery} := 11.1V$

$C_{Battery} := 450mA \cdot hr$

$$E_{max} := R_t^{1-1.3} \cdot \left[\frac{\eta_{tot} \cdot V_{Battery} \cdot C_{Battery}}{\frac{2}{\sqrt{\rho \cdot S_{total}}} \cdot C_{D0}^{\frac{1}{4}} \cdot \left(2 \cdot W \cdot W_{corr} \cdot \sqrt{\frac{k_{total}}{3}} \right)^{\frac{3}{2}}} \right]^{1.3} = 0.581 \cdot hr$$

$R_{Emax} := E_{max} \cdot V_{MaxE} = 15.326 \cdot mi$

$$R_{max} := R_t^{1-1.3} \cdot \left[\frac{\eta_{tot} \cdot V_{Battery} \cdot C_{Battery}}{\frac{1}{\sqrt{\rho \cdot S_{total}}} \cdot C_{D0}^{\frac{1}{4}} \cdot \left(2 \cdot W \cdot W_{corr} \cdot \sqrt{k_{total}} \right)^{\frac{3}{2}}} \right]^{1.3} \cdot V_{MaxR} = 17.016 \cdot mi$$

$E_{Rmax} := \frac{R_{max}}{V_{MaxR}} = 0.49 \cdot hr$

$E_{sb} := 192\,\frac{watt \cdot hr}{kg}$

$m_b := 0.08kg$

$\eta_p := 0.8$

$\eta_{b2s} := 0.9$

$g := 32.2\,\frac{ft}{s^2}$

$A_{motor} := 12A$

$P_{used} := 133watt$

$m_{aircraft} := 0.3kg$

$$E_{max2} := \frac{m_b \cdot E_{sb} \cdot \eta_{b2s}}{P_{used}} = 6.236 \cdot min$$

$$V_{cruise} = 16.764 \cdot \frac{m}{s}$$

$$V_{cruise} := 16.74 \frac{m}{s}$$

$$E_{level} := \frac{E_{sb} \cdot \eta_{b2s} \cdot \eta_p}{g \cdot V_{cruise}} \cdot \frac{m_b}{m_{aircraft}} \cdot L\_D = 72.452 \cdot min$$

$$R_{level} := \frac{E_{sb} \cdot \eta_{b2s} \cdot \eta_p}{g} \cdot \frac{m_b}{m_{aircraft}} \cdot L\_D = 45.218 \cdot mi$$

Stability

$$L_{nose} := \frac{2.74in}{2} - 0.25in$$

$$L_{fuse} := 7.5in$$

$$L_{motorMount} := 1.5in$$

$$SM := 0.15$$

$$c_{avg} := \frac{c_{wing1} + c_{wing2}}{2} = 1.5 \cdot in$$

$$X_{wing1LE\_fuseFront} := 1.25in$$

$$L_{vert} := 2.5in$$

$$S_v := L_{vert} \cdot c_{wing2} = 0.022\,ft^2$$

$$X_{CG\_wing1} := X_{wing1LE\_fuseFront} + L_{nose} + \frac{c_{wing1}}{2} = \blacksquare \cdot in$$

$$X_{CG\_wing2} := L_{nose} + L_{fuse} - \frac{c_{wing2}}{2} = 7.995 \cdot in$$

$$X_{wingOffsetCG} := 4.375in$$

$$X_{CG\_wing2} := X_{CG\_wing1} + X_{wingOffsetCG} = \blacksquare \cdot in$$

$$X_{CG\_vert} := X_{CG\_wing2}$$

$$X_{wingOffsetCG} := 4.5in$$

$$X_{CG\_wing1} := X_{CG\_wing2} - X_{wingOffsetCG} = 3.495 \cdot in$$

$$X_{AC\_wing1} := X_{CG\_wing1} - \frac{c_{wing1}}{4} = 3.058 \cdot in$$

$$X_{AC\_wing2} := X_{CG\_wing2} - \frac{c_{wing2}}{4} = 7.683 \cdot in$$

$$X_{wingOffsetAC} := X_{AC\_wing2} - X_{AC\_wing1} = 4.625 \cdot in$$

$$X_{NP} := \frac{X_{AC\_wing1} \cdot C_{L\_\alpha\_wing1} \cdot S_{wing1} + X_{AC\_wing2} \cdot C_{L\_\alpha\_wing2} \cdot S_{wing2}}{C_{L\_\alpha\_wing1} \cdot S_{wing1} + C_{L\_\alpha\_wing2} \cdot S_{wing2}} = 4.872 \cdot in$$ checks out

$$X_{TE\_wing1} := X_{CG\_wing1} + \frac{c_{wing1}}{2} = 4.37 \cdot in$$

$$L_{wing1TE\_NP} := X_{TE\_wing1} - X_{NP} = -0.502 \cdot in$$

$$X_{CG} := X_{NP} - SM \cdot c_{wing1} = 4.61 \cdot in$$

$$L_{Xcg\_Xnp} := X_{NP} - X_{CG} = 0.262 \cdot in$$

$$S_{avg} := \frac{S_{wing1} + S_{wing2}}{2}$$

$$L_v := X_{CG\_vert} - X_{CG} = 3.385 \cdot in$$

$$b_{avg} := \frac{b_{wing1} + b_{wing2}}{2}$$

$$L_t := X_{CG\_wing2} - X_{CG} = 3.385 \cdot in$$

$$V_v := \frac{L_v \cdot S_v}{S_{avg} \cdot b_{avg}} = 0.019$$ typically 0.02 for sailplane

$$V_H := \frac{L_t \cdot S_{wing2}}{S_{wing1} \cdot c_{wing2}} = 1.696$$ typically 0.5 for sailplane

$$X_{wing1} := X_{CG\_wing1} - \frac{L_{nose}}{2} = 2.935 \cdot in$$

$$X_{wing2} := X_{CG\_wing2} - \frac{L_{nose}}{2} = 7.435 \cdot in$$

$$X := X_{wing2} - X_{wing1} = 4.5 \cdot in$$

$$X_{AC\_wing1\_c} := 0.25$$

$$X_{AC\_wing2\_c} := 0.25$$

VITA

Andrew Walsh

Candidate for the Degree of

Master of Science

Thesis: DEVELOPMENT OF A MICRO AIR VEHICLE FOR METEOROLOGICAL SOUNDINGS

Major Field: Mechanical and Aerospace Engineering

Biographical:

Education:

Completed the requirements for the Master of Science in Mechanical and Aerospace Engineering at Oklahoma State University, Stillwater, Oklahoma in December, 2021.

Completed the requirements for the Bachelor of Science in Aerospace Engineering at Oklahoma State University, Stillwater, Oklahoma in December, 2018.

Completed the requirements for the Bachelor of Science in Mechanical Engineering at Oklahoma State University, Stillwater, Oklahoma in December, 2018.

Professional Membership:

Student Member of AIAA as of August, 2015